Implementation and Field Evaluation of Pretensioned Concrete Girder End Crack Control

Michael Oliva
Emre Kizilarslan
University of Wisconsin - Madison

Pinar Okumus
University at Buffalo

WisDOT ID no. 0092-15-01

May 2016

Research & Library Unit

Wisconsin Highway Research Program

WISCONSIN DOT
PUTTING RESEARCH TO WORK

Technical Report Documentation Page

1. Report No. WHRP 0092-15-01	2. Government Accession No	3. Recipient's Catalog No
4. Title and Subtitle Implementation and Field Evaluation of Prestensioned Concrete Girder End Crack Control Methods		5. Report Date May 2016 6. Performing Organization Code Wisconsin Highway Research Program
7. Authors Michael G. Oliva, Pinar Okumus, Emre Kizilarslan		8. Performing Organization Report No.
9. Performing Organization Name and Address University of Wisconsin-Madison 1415 Engineering Drive Madison, WI 53706		10. Work Unit No. (TRAIS) 11. Contract or Grant No. WisDOT SPR# 0092-15-01
12. Sponsoring Agency Name and Address Wisconsin Department of Transportation Research & Library Unit 4802 Sheboygan Ave. Rm 104 Madison, WI 53707		13. Type of Report and Period Covered Final Report, 2015-2016 14. Sponsoring Agency Code
15. Supplementary Notes		

16. Abstract

Wisconsin bulb tee pretensioned concrete girders are currently used for bridge construction. Their efficiency in load resistance has made them particularly desirable. To provide that efficiency, these girders are heavily prestressed. Cracking is evident, however, at the girder ends during de-tensioning. These cracks may create durability and capacity problems as cracks can lead corrosive water to the steel strands, endangering the structure. Cracks in the bottom flange, close to the strands, are the main concerns of this study. The primary focus was on proving the effectiveness of strand debonding at girder ends as a solution to cracking. This was accomplished through construction of prototype girders, monitoring their behavior, and using analytical techniques to understand the cause of the cracking A second goal was to provide the Wisconsin Department of Transportation with design recommendations for effectively using debonded strand in girders.

The construction of girders with debonded strand for two bridges proved that debonding was an effective solution for end crack control and elimination. Comparison of analytic predicted behavior and measured girder response data showed that the nonlinear analysis techniques used were accurate. Those techniques were then used to examine the behavior of Wisconsin 54W and 72W girders with various strand debonding patterns to provide the Department with recommendations for the best girder designs, in a range of strand contents, using debonded strand.

17. Key Words prestressed girders, bridge girders, girder cracking, prestress transfer, detensioning, debonding, bulb-tees, finite element models	18. Distribution Statement No restriction. This document is available to the public through the National Technical Information Service 5285 Port Royal Road Springfield VA 22161

18. Security Classif.(of this report) Unclassified	19. Security Classif. (of this page) Unclassified	20. No. of Pages 206	21. Price

Form DOT F 1700.7 (8-72) Reproduction of completed page authorized

DISCLAIMER

This research was funded through the Wisconsin Highway Research Program by the Wisconsin Department of Transportation and the Federal Highway Administration under Project 0092-15-01. The contents of this report reflect the views of the authors who are responsible for the facts and accuracy of the data presented herein. The contents do not necessarily reflect the official views of the Wisconsin Department of Transportation or the Federal Highway Administration at the time of publication.

This document is disseminated under the sponsorship of the Department of Transportation in the interest of information exchange. The United States Government assumes no liability for its contents or use thereof. This report does not constitute a standard, specification or regulation.

The United States Government does not endorse products or manufacturers. Trade and manufacturers' names appear in this report only because they are considered essential to the object of the document.

Implementation and Field Evaluation of Pretensioned Concrete Girder End Crack Control Methods

Wisconsin Highway Research Program

Project 0092-15-01

FINAL REPORT

by

Michael G. Oliva, Professor

Pinar Okumus, Professor

Emre Kizilarslan, MS Candidate

May – 2016

SUMMARY

Bulb-tee prestressed girders, used in Wisconsin for highway bridge construction, consistently exhibit cracking near the girder ends when under high prestress. The recommendation of a previous Wisconsin Highway Research Program analytic study was to efficiently eliminate girder end cracking by debonding prestressing strands near the girder ends.

The research program described here evaluates the strategy selected in the previous study through actual implementation, and provides recommendations for the design of the standard sets of Wisconsin 54W and 72W girders with debonded strands. The focus is primarily aimed at eliminating cracking in the bottom flange of the girders where cracks could allow moisture to reach prestressing strands and induce corrosion that migh affect the girder capacity.

Prestressed girders, 72 and 54 inches deep, were designed and built using three different debonded designs along with two standard designs to evaluate and prove the effectiveness of debonding. The girders were instrumented with various gages to record internal strains and detect cracking during the prestressing or detensioning process.

Then detailed analytical finite element models (FEM) of the girders were assembled using non-linear behavior to simulate the concrete cracking in the actual girders. The response predictions from the analytic models were compared with the measured response quantities from the actual girders to verify the accuracy of the analytic approach.

Finally, analytical modelling was employed to examine a wide range of possible 54 and 72 inch deep girder designs to select debonding patterns and the number of debonded strands that would best provide the desired uncracked performance in the girders. These studies resulted in a set of recommended girder designs that the Wisconsin Department of Transportation could use to create alternate standard girder designs in the WisDOT Bridge Manual.

MEASUREMENTS

Construction of a Wisconsin 72W girder, with 25% of the prestressing strands debonded for various lengths at the girder end, proved that debonding can significantly

reduce the concrete tension strains developed during detensioning. The tension strains measured in reinforcing bars of the debonded girder were at least 200με (micro strain) less than strains in a normal girder. In the critical bottom flange the strains in stirrups of the debonded beam were only 30% of the strains in a normal girder. Concrete gages measured tension strains in the bottom flange of the normal beam that were 21 times the strains in the debonded girder. The debonding was very effective in reducing concrete tension and cracking, but 25% debonding was found to be insufficient to prevent bottom flange cracking in a girder with high prestressing.

Two alternate debonding designs were used in the construction of Wisconsin 54W girders. One girder had 38% of its strands debonded for various distances at the end, the second had 62% of the strands debonded for only 8 inches. Both designs were successful in eliminating bottom flange cracking that was evident in normal 54W girders with high prestressing. The horizontal tension strain in the bottom flange concrete of the debonded girder was 45με while the normal girder showed 1050με. The total length of end cracks was 326in. in the normal girder, 56in. in the 38% girder, and 261in. in the 62%-8inch girder. While debonding for only 8 inches was effective in controlling bottom flange cracking, it may increase horizontal web cracking. This is not critical, however, since those cracks tend to close as addition dead and live load is carried by the girders.

RESULTS

Bottom flange Y cracking, that is detrimental to durability, can be eliminated by debonding the appropriate number of strands. When high amounts of prestressing are used, more than 26 strands, the AASHTO limit of 25% debonding is insufficient in eliminating flange cracking. Other states, such as Texas, build girders with as much as 50% debonding without detrimental bond effects. When a 72W girder has a full complement of 48 strands, debonding of 42% to 50% of the strands is necessary to eliminate flange cracking. A complete summary of the number of strands to debond, and best strand patterns, has been developed and they are provided as recommended designs in Chapter 8, and specifically in Table 8-1 (p173) and Figure 8-4.

The experimental and analytical investigations also identified other design suggestions to reduce concrete tension stresses and amounts of cracking, though they are insufficient to eliminate bottom flange cracking.

DESIGN SUGGESTIONS

1. Using staggered debonding or debonding all strand for 8 inches to 12 inches should be recommended in the WisDOT Bridge Manual to eliminate bottom flange Y cracking in Wisconsin 54W and 72W prestressed concrete girders, particularly when a large numbers of strand are used. *(see page 179)*

2. The quantities of debonded strands and debonding patterns shown in Figure 8-4 of this report should be considered for creating debonding alternates to Standards 19.16 and 19.18 in the WisDOT Bridge Manual. *(pages 174-75)*

3. The girder specifications should be changed to include a requirement that when precasters cut strands during detensioning the inner columns of strand should be cut before the outer columns, i.e. strand cutting should proceed from the inside of each row toward the outside. *(see pages 107& 160)*

4. The standard girder end design details that show five #6 sets of vertical web bars at the girder ends could be changed to show three sets since the strain results showed that the additional bars further from the girder end have low strains and are ineffective in crack control. *(see Figures 5.15&16, page 75, and Figures 6.15-17, page117)*

5. The bottom flange stirrups and banana stirrups, i.e. the short #3 bars placed horizontally near the top of the bottom flange, should either be eliminated from the standard details or they should be specified without epoxy coat. The epoxy coated bars in the test girders were ineffective as shown by very small strains, likely due to insufficient bond due to the epoxy coating. *(see Figure 5.20, page 79, and Figures 6.18-20, page 119)*

6. When multiple girders are cast in-line, the precaster should minimize the space between bulkheads at the end of adjacent girders. This will reduce the length of free strand at the girder ends. When the strand is flame cut the strand stored energy is released and causes dynamic loading of the end anchorage in the concrete and can increase end cracking. If the cut is made close to the girder end, then less energy is released and end cracking may be reduced. *(see pages 131-132)*

ABSTRACT

Wisconsin bulb tee pretensioned concrete girders are currently used for bridge construction. Their efficiency in load resistance has made them particularly desirable. To provide that efficiency, these girders are heavily prestressed. Cracking is evident, however, at the girder ends during de-tensioning. These cracks may create durability and capacity problems as cracks can lead corrosive water to the steel strands, endangering the structure. Cracks in the bottom flange, close to the strands, are the main concerns of this study. The primary focus was on proving the effectiveness of strand debonding at girder ends as a solution to cracking. This was accomplished through construction of prototype girders, monitoring their behavior, and using analytical techniques to understand the cause of the cracking A second goal was to provide the Wisconsin Department of Transportation with design recommendations for effectively using debonded strand in girders.

The construction of girders with debonded strand for two bridges proved that debonding was an effective solution for end crack control and elimination. Comparison of analytic predicted behavior and measured girder response data showed that the nonlinear analysis techniques used were accurate. Those techniques were then used to examine the behavior of Wisconsin 54W and 72W girders with various strand debonding patterns to provide the Wisconsin Department of Transportation with recommendations for the best girder designs, in a range of strand contents, using debonded strands.

Contents

1 INTRODUCTION 1
1.1 Definition of Problem 1
1.2 Objective 3
1.3 Scope of the Project 4
2 LITERATURE REVIEW 5
2.1 Codes for Anchorage Zones 5
2.1.1 AASHTO LRFD Bridge Design Specifications 5
2.1.2 International Federation for Structural Concrete 7
2.1.3 American Concrete Institute 318-14 (5) 10
2.2 Research on Anchorage Zone Cracking 10
2.2.1 Studies of Finite Element Analysis 10
3 PRESTRESSED GIRDERS 22
3.1 Pretensioning and Post-tensioning 22
3.2 Types and Properties of Pretensioned Highway Bridge Girders 23
3.3 Categorization of End Cracks 25
3.4 Splitting Resistance and Confinement Reinforcement at Anchorage Zone of Standard Girders 28
3.5 Summary 30
4 FINITE ELEMENT MODELLING 32
4.1 Geometry of the Girders 32
4.2 Review of Finite Element Models 33
4.3 Properties of Materials 34
4.3.1 Concrete Material Properties 35
4.3.2 Reinforcement Bar Material Properties 46
4.3.3 Strand Properties 46
4.4 Interactions 46
4.4.1 Bond Between Reinforcing Bar and Concrete Bond 46
4.4.2 Interaction Between Girder and Formwork 47

4.5 Boundary Conditions 47
4.6 Loading 48
4.7 Finite Elements 53
4.7.1 Concrete Elements 53
4.7.2 Steel Reinforcement Bar Elements 54
4.8 Meshing 54
4.9 Solution Method 55
4.10 Assumptions, Simplifications and Limitations 56
5 TEST AND FEM MODELS FOR 72W GIRDER 58
5.1 Girder Properties: 59
5.2 Instrumentation: 66
5.3 Test Data & Discossion 70
5.3.1 Gauges on Strands 70
5.3.2 Strains in Reinforcing Bars 74
5.3.3 Strains in Concrete: 79
5.4 Girder End Cracks 85
5.5 Comparison with Finite Element Model Results 89
5.5.1 Bonded Girder 90
5.5.2 25% De-bonded Girder With Strands Bonded in Staggered Lengths 94
5.6 Observations and Summary 98
5.7 Conclusion 100
6 TEST AND FEM MODELS FOR 54W GIRDERS 102
6.1 54W Girders Fabricated by County Materials Corporation 102
6.1.1 Properties of 54W Girders 102
6.1.2 Debonding of W54 Girders 108
6.1.3 Gauge Instrumentation 109
6.2 Cracks in Girders 126
6.3 Bonded Girder Comparison with the Results of Finite Element Models 133
6.3.1 Bonded Girder Crack Locations 133
6.3.2 Bonded Girder: Strain Results at Vibrating Wire Gauges 134

6.3.3 Bonded Girder: Strain Results at Strain Gauges 137
6.4 38% De-bonded Girder With Strands Bonded in Staggered Lengths 141
6.4.1 38% Debonding: Strain Results at Vbrating Wire Gauges 142
6.4.2 38% Debonded Girder: Strain Results at Strain Gauges 143
6.5 62% De-bonded Girder With Strands Bonded at 8in. From End 145
6.5.1 62% Debonded: Strain Results at Vibrating Wire Gauges 146
6.5.2 62% Debonded: Strain Results at Strain Gauges 148
6.6 Observations and Summary 151
6.7 Conclusion 152
7 CAUSE OF CRACKING & DESIGN OF GIRDERS 154
7.1 Concrete Response & Causes of Cracks 155
7.1.1 Cause of Inclined Crack & Horizontal Crack 157
7.1.2 Cause of Y Cracking 159
7.2 Steel Response 161
8 RECOMMENDED DEBONDING WITH DIFFERENT NUMBERS OF STRANDS IN WISCONSIN 54W AND 72W GIRDERS 165
8.1 Best Debonding Percentage for Each Girder 166
9 SUMMARY and CONCLUSIONS 178

LIST OF FIGURES

Figure 1-1. Cracks at the end of a Wisconsin 72W girder. 2
Figure 2-1. Three mechanism in FIB 2010 model code in anchorage zone (4)..... 7
Figure 2-2. The prism analogy for calculation of the bursting force (4). 8
Figure 2-3. Maximum spalling stresses (4)..... 9
Figure 2-4. Types of crack observed (6). 11
Figure 2-5. The FEA model created by Kannel et al. (6). 12
Figure 2-6. Nonlinear spring force-versus-displacement curve. (Note: A_{ps}: area of pre-stressing strand; f_{so}: stress in strand just after transfer; l_t: transfer length; L_{es}: end slip; and s: nonlinear spring spacing) (7). 14
Figure 2-7. Beam (top) and T beam (bottom) cross sections (7). 16
Figure 2-8. Comparison of experimental concrete surface strains and analytical concrete strains for a prism (left) and a typical T beam model (right) (7). 16
Figure 2-9.Typical cross sections of WF100G girder (9). 17
Figure 2-10. Constitutive model and theoretical stress-strain curve (9). 18
Figure 2-11. Principal stress distribution in concrete along anchorage zone (9). 20
Figure 3-1. Girder sizes: 54W and 72W. 24
Figure 3-2. The end details of girders. 25
Figure 3-3**.** Inclined, Horizontal Web, and Y cracks shown on 72W girder. 26
Figure 4-1. Model of Bonded 54W girder in Abaqus. 34
Figure 4-2. The graph of plastic constitutive behavior of concrete in compression. 38
Figure 4-3. Compression constitutive graph with the model of a bonded 72W girder..... 39
Figure 4-4. Post- Cracking Behavior Graph 42
Figure 4-5. Tension Model Used in Abaqus: top = before cracking, bottom = post cracking. (initial behavior depends on strain, ε; post cracking depends on crack width, w) 43
Figure 4-6. Yield surface in the deviatoric plane corresponding to different values of K 45
Figure 4-7. Boundary Conditions of models, mid-span section is at left, end at right. 48
Figure 4-8. Measured prestressing force in strand versus distance from end for 72W girder.50
Figure 4-9. Prestressing force in strand versus distance from end considering piecewise linear function for 72W girders. 51
Figure 4-10. Surface traction force applied to concrete elements in models for 72W Girder.51
Figure 4-11. 4 node tetrahedral and 6 node triangular prism elements 53
Figure 4-12. 2 Node linear Truss elements 54
Figure 4-13. Mesh example of 54W girder. 55
Figure 5-1. 72W cross section and reinforcement details of end zone. 60
Figure 5-2. Bonded girder strand pattern (top) and de-bonded girder strand pattern (bottom). 61
Figure 5-3. Concrete stress vs Distance from Ends for Bonded Girder..... 63

Figure 5-4. Concrete stress vs Distance from Ends for De-bonded Girder. 64
Figure 5-5. Plastic shield around strand for de-bonding. 65
Figure 5-6. Strand cutting order for bonded girder (left) and debonded girder (right). 66
Figure 5-7. Strain Gauge on re-bar (left), and after water-proof (right). 67
Figure 5-8. Locations of strain gauges at re-bars. 68
Figure 5-9. Location of strain gauges at strand. 68
Figure 5-10. Vibrating Wire Gauge Locations. 69
Figure 5-11. Strand test data for bonded girders. 71
Figure 5-12. Strand test data for de-bonded girders. 71
Figure 5-13. Bond Stress vs distance from ends of bonded girders. 73
Figure 5-14. Bond Stress vs distance from ends of debonded girders. 73
Figure 5-15. Bonded girder: Strain change of reinforcing bars in horizontal web crack region, most are 20” up from bottom (gauges, S2, S3, S4, S5 and S6). 75
Figure 5-16. Debonded girder: Strain change of reinforcing bars in horizontal web crack region, most are 20” up from bottom (gauges S2, S3, S4, S5 and S6). 75
Figure 5-17. Bonded girder: Strain change of reinforcing bars in inclined crack region, close to top of girder (gauges S7, and S8). *(Tension positive, compression negative)* 77
Figure 5-18. Debonded girder: Strain change of reinforcing bars in inclined crack region, close to top of girder (gauges S7, S8, and S9). *(Tension positive, compression negative)* 77
Figure 5-19. Bonded girder: Strain change of reinforcing bars in bottom flange 78
Figure 5-20. Debonded girder: Strain change of reinforcing bars in bottom flange 79
Figure 5-21. Strain change of vibrating wire gauges near the web and inclined cracking region. *(Tension positive, compression negative)* 80
Figure 5-22. Strain change of vibrating wire gauges near the Y cracking region. *(Tension positive, compression negative, V5 is vertical)* 81
Figure 5-23. Location of vibrating wire gauges VW1 and VW2 in both bonded (left) and de-bonded (right) girders. 82
Figure 5-24. Location of vibrating wire gauges in bonded (left) and de-bonded (right) girders. 85
Figure 5-25. Cracks at the ends of bonded and de-bonded girders. 86
Figure 5-26. Number of visible cracks found in each girder. 87
Figure 5-27. Average & maximum crack widths 87
Figure 5-28. Total length of cracks at girder ends. 88
Figure 5-29. The comparison of actual girder end cracking with Abaqus model strains for bonded girder. *(tension is negative)* 91
Figure 5-30. Concrete strain comparison for bonded girder. 91
Figure 5-31. Reinforcing bar strain comparison for bonded girder. 94
Figure 5-32. The comparison of actual girder end cracking with Abaqus model strains for the de-bonded girder. 95

Figure 5-33. Concrete strain comparison for de-bonded girder..... 96
Figure 5-34. Reinforcing bar strain comparison for de-bonded girder..... 98
Figure 6-1. End details of 54W girder. 103
Figure 6-2. Original strand pattern at the ends of girders..... 104
Figure 6-3. Bottom and top concrete stresses in bonded girder..... 105
Figure 6-4. Bottom and top concrete stresses in 38% de-bonded girder. 106
Figure 6-5. Bottom and top concrete stresses in 8in. de-bonded girder. 106
Figure 6-6. Strand Cutting Sequence..... 107
Figure 6-7. 38% debonded girder with staggered pattern (left with debonded lengths shown by symbols) and 62% debonded girder with 8in debond length (right). 108
Figure 6-8. At the left, strain gauge on strand and at the right, the gauge after protection. . 109
Figure 6-9. The location of Strain Gauges at Strand. Elevation view (right), and cross section view (left)..... 110
Figure 6-10. Location of Foil Strain Gauges. 111
Figure 6-11. The 2in. (left) and 6in. (right) vibrating wire gauges..... 112
Figure 6-12. Location of Vibrating Wire Gauges..... 113
Figure 6-13. The Change in strain at locations along strand of 38% debonded beam. 114
Figure 6-14. Bond Stress Variation Used in the Analytical Models..... 116
Figure 6-15. The test results of web bar strain gauges S1, S2, and S3 for bonded girder.... 117
Figure 6-16. The test results of web bar strain gauges S1, S2, and S3 for 38% debonded girder. *(positive is tension)*..... 117
Figure 6-17. The test results of web bar gauges S1, S2, and S3 for debonded 8in. girder... 118
Figure 6-18. The test strain results for S4 (on banana bar) and S5 (on chicken leg bar) stirrups for bonded girder. *(positive is tension)* 119
Figure 6-19. The test strain results for S4 (on banana bar) and S5 (on chicken leg bar) stirrups for 38% de-bonded girder. *(positive is tension)*..... 120
Figure 6-20. The test strain results for S4 (on banana bar) and S5 (on chicken leg bar) stirrups for 8in. de-bonded girder. *(positive is tension)*..... 120
Figure 6-21. Strain results for vibrating wire gauge VW1. *(positive = tension)*..... 123
Figure 6-22. Strain Results for Vibrating wire gauge VW2. *(positive = tension)*..... 123
Figure 6-23. Strain Results for Vibrating wire gauge VW3. *(positive = tension)*..... 124
Figure 6-24. Strain Results for Vibrating wire gauge VW4. *(positive = tension)*..... 124
Figure 6-25. The location of vibrating wire gauges in bonded (top left), 38% debonded (top right), and the girder that is debonded 8 in. from end (bottom)..... 127
Figure 6-26. Close-up picture of bottom flange for bonded (top), 38% de-bonded (middle), and 8in. debonded (bottom) girders..... 128
Figure 6-27. U bars beneath the top row of strands and above the bottom row of strands in side view (top) and in top view (bottom)..... 130
Figure 6-28. Total crack lengths of girders..... 131

Figure 6-29. Plan of de-bonded girders in the same formwork bed. 132
Figure 6-30. Other end of normal girder which was in the middle of the bed..... 133
Figure 6-31. The comparison of bonded girder ends in reality and in model..... 134
Figure 6-32. Concrete strain comparison between data obtained by VW gauge 1 and finite element model during prestress release for bonded girder. *(positive = tension)*..... 135
Figure 6-33. Concrete strains comparisons between data obtained by VW gauge 2 and finite element model during prestress release for bonded girder. *(positive = tension)*..... 135
Figure 6-34. Concrete strains comparisons between data obtained by VW gauge 3 and finite element model during prestress release for bonded girder. *(positive = tension)*..... 136
Figure 6-35. Re-bar strain comparisons between data obtained from strain gauge 1 and finite element model during prestress release for bonded girder. *(positive = tension)*..... 138
Figure 6-36. Re-bar strain comparisons between data obtained from strain gauge 2 and finite element model during prestress release for bonded girder. *(positive = tension)*..... 138
Figure 6-37. Re-bar strain comparisons between data obtained from strain gauge 3 and finite element model during prestress release for bonded girder. *(positive = tension)*..... 139
Figure 6-38. Re-bar strain comparisons between data obtained from strain gauge 4 and finite element model during prestress release for bonded girder. *(positive = tension)*..... 139
Figure 6-39. Re-bar strain comparisons between data obtained from strain gauge 5 and finite element model during prestress release for bonded girder. *(positive = tension)*..... 140
Figure 6-40. The comparison of 38% de-bonded girder ends in reality and in model. 141
Figure 6-41. Concrete strain comparison between data obtained by VW gauge 1 and finite element model during prestress release for 38% de-bonded girder. *(positive = tension)*..... 142
Figure 6-42. Concrete strain comparison between data obtained by VW gauge 3 and finite element model during prestress release for 38% de-bonded girder. *(positive = tension)*..... 142
Figure 6-43. Concrete strain comparison between data obtained by VW gauge 4 and finite element model during prestress release for 38% de-bonded girder. *(positive = tension)*..... 143
Figure 6-44. Re-bar strain comparisons between data obtained from strain gauge 2 and finite element model during prestress release for 38% de-bonded girder. *(positive = tension)*..... 144
Figure 6-45. Re-bar strain comparisons between data obtained from strain gauge 4 and finite element model during prestress release for 38% de-bonded girder. *(positive = tension)*..... 144
Figure 6-46. Re-bar strain comparisons between data obtained from strain gauge 5 and finite element model during prestress release for 38% de-bonded girder. *(positive = tension)*..... 145
Figure 6-47. The comparison of 62% de-bonded girder ends in reality and in model. 146
Figure 6-48. Concrete strains comparisons between data obtained via VW gauge 2 and finite element model during prestress release for 62% de-bonded girder. *(positive = tension)*..... 147
Figure 6-49. Concrete strains comparisons between data obtained via VW gauge 3 and finite element model during prestress release for 62% de-bonded girder. *(positive = tension)*..... 147
Figure 6-50. Concrete strains comparisons between data obtained via VW gauge 4 and finite element model during prestress release for 62% de-bonded girder. *(positive = tension)*..... 148

Figure 6-51. Re-bar strain comparisons between data obtained from strain gauge 1 and finite element model during prestress release for 62% de-bonded girder. *(positive = tension)*..... 148
Figure 6-52. Re-bar strain comparisons between data obtained from strain gauge 2 and finite element model during prestress release for 62% de-bonded girder. *(positive = tension)*..... 149
Figure 6-53. Re-bar strain comparisons between data obtained from strain gauge 3 and finite element model during prestress release for 62% de-bonded girder. *(positive = tension)*..... 149
Figure 6-54. Re-bar strain comparisons between data obtained from strain gauge 4 and finite element model during prestress release for 62% de-bonded girder. *(positive = tension)*..... 150
Figure 6-55. Re-bar strain comparisons between data obtained from strain gauge 5 and finite element model during prestress release for 62% de-bonded girder. *(positive = tension)*..... 150
Figure 7-1. Principal tensile strains in concrete, elevation view (left) and cross section view at the end (right). *(positive = tensile)*..... 156
Figure 7-2. Principal tensile strains directions – 0” is the girder end. 158
Figure 7-3. Principal tensile strains directions on the cross section of bottom flange at various distances in from the girder end. 160
Figure 7-4. Longitudinal stresses – S11 (psi) of reinforcing bars in 72W girder. 162
Figure 8-1. Strand patterns at the ends of girders. Distances denoted are locations where those strands start bonding. 168
Figure 8-2. Contour plots of bonded and debonded 72W girders with 48 strands. 171
Figure 8-3. Maximum principal strain at horizontal and Y crack region from each girder.. 172
Figure 8-4. Best debonding patterns for 72W and 54W girder with different number of strands. The designation “32DB31%” represents 32 total strands with 31% debonded. 175
Figure 9-1. Half of 72W girder with 48 strands..... 189

LIST OF TABLES

Table 2-1. Peak values of stresses at 6in. from the end of girders (6). 13

Table 3-1. The calculations on amount of bursting steel reinforcing in the anchorage zone for 72W girder. 29

Table 3-2. The calculations on amount of bursting steel reinforcing in the anchorage zone for 54W girder. 30

Table 4-1. Features of girders modelled in Abaqus. 33

Table 4-2. Plasticity input parameters for models. 45

Table 5-1. Crack control effectiveness of the methods that Okumus (1) examined for 54W girders. 59

Table 5-2. Concrete stresses in both bonded and de-bonded girders. 63

Table 5-3. Strain Changes at Designated Strain Gauge Locations 72

Table 5-4. Data from vibrating wire gauges in debonded and bonded girders. 84

Table 6-1. Concrete stresses at bottom and top fibers of the corresponding girders. 105

Table 6-2. Strain changes at locations along strand upon release. 114

Table 6-3. Total End Crack Lengths of each Girder. All measures are in inches. 130

Table 7-1. Maximum stresses observed in 54W and 72W models. 163

Table 8-1. Best debonding percentages for 72W and 54W girder with different number of strands and their maximum values in horizontal and Y crack cracking locations. 174

Table 9-1. Compression Behavior for bonded 72W girder..... 184

Table 9-2. Input for compression behavior for bonded 72W girder. 185

Table 9-3. Tensile behavior for bonded 72W girder..... 186

Table 9-2. Input for tensile behavior for bonded 72W girder. 187

Table 9-5. Debonding patterns tried on different girders. 188

Table 9-6. Description of debonding patterns tried on different girders. 191

1 INTRODUCTION

1.1 Definition of Problem

One of the reasons for using concrete as a construction material is because of its strength in compression. Concrete is weak in tension and can crack. With the invention of prestressed concrete, concrete tension forces are counteracted by stressing in advance, thereby inducing compressiuon and using concrete's strongest property. When combined with high strength concrete, cracking can be decreased, deflections can be reduced, and smaller sized members are possible resulting in lighter structures. This technology has gained popularity among designers, particularly for bridge structures.

Bridge designers currently use deep wide flanged pretensioned, bulb tee, concrete girders in many bridge projects. Their wide top flanges provide stability and carry the flexural compression block high in the girder for a longer moment arm. This provides improved efficiency resulting in small number of girders or longer span capabilities. High pretension force is often applied to those girders.

The ends of these girders are where the prestressing, from steel stressing tendons under initial tension, is applied to the concrete. The transfer is achieved by bond between tendons and concrete that develops when the tendons are released, from their initial tension state, and they try to shorten while connected to the concrete. Even though the tendon or strand pretension force is released gradually, tensile stresses or bursting stress develop in the concrete. These secondary stresses are often enough to create cracks in thin sectioned

pretensioned girders in the end zones. As girders are built deeper with more prestress force, the cracks tend to be larger (2) as in Figure 1-1.

Figure 1-1. Cracks at the end of a Wisconsin 72W girder.

Even though these girders are structurally efficient, the cracks cause potential problems for serviceability and capacity because these cracks may lead to aggressive water and salt infiltration. This is particularly likely when these end zones will be placed on bridge abutments which are prone to wetting from leaking deck joints. When water enters these cracks, corrosion and loss of strength in the steel strands could occur. Heavy concrete end diaphragms may protect the girder ends and reduce corrosion sensitivity. In other situations the strength reducing consequences of these cracks might be severe.

Many researchers have addressed the strength behavior of girder end zones by using empirical methods, simplified linear elastic concepts, or strut-and-tie methods. The empirical and strut-and-tie methods are focused on the ultimate strength condition and involve non-linear material behavior, but cannot be correctly used to predict service behavior. The linear material methods are only appropriate until initial concrete cracking occurs. Due to cracking, the true strain distribution is not correctly defined with linear analysis methods. Unfortunately nonlinear analysis of girder ends in the service condition has not been provided in most currently available literature. Aware of the lack of comprehensive nonlinear analysis work for the problem, this research selected the ABAQUS software program to examine the behavior of girder ends with the explicit use of nonlinear finite element analysis (FEA).

1.2 Objective

Two main objectives are involved in this project. The first is to prove, through physical testing and observation, that the use of debonded prestressing strands at the girder ends can reduce or eliminate the cracking problems. Assuming that debonding is proved effective, the second objective is to provide the Wisconsin Department of Transportation (WisDOT) with design recommendations for unbonded 54W and 72W prestressed girders.

Girder end behavior and factors of cracking need to be understood in order to control cracking. Therefore a secondary aim, needed to meet the objectives, is to investigate and then model how the strain and stress take shape in nonlinear girder ends with pretensioned forces. For this purpose, girders are modelled in ABAQUS 6.12 with nonlinear material properties.

1.3 Scope of the Project

54 in. and 72 in. deep concrete bulb tee girders will be analyzed and tested to examine and control cracking. Wisconsin standard wide flange girders are examined. This project only focusses on end cracking observed in WisDOT girders due to high forces during the prestress or detensioning process. Other types of cracks are not investigated. Shortly, this research will pursue the following items:

- Initially predicting end zone behavior of bulb tee girders through nonlinear models,
- Veirfying FEA methods by comparison with measured test results,
- Examining how the prinicipal strains and stresses occur in nonlinear girder ends with pretension forces,
- Finding the amount of strand debonding that should be used to prevent end cracks from occurring,
- And selecting the most efficient debonding method.

2 LITERATURE REVIEW

Girder anchorage zone cracking was observed as early as the 1960s, shortly after prestressing became an accepted practise. Now cracking is of greater concern because thinner and deeper sections than previously seen are used with higher amount of prestressing. In this chapter, code provisions for crack control in pretensioned members and recent studies about modelling anchorage zone cracking are discussed. Though there are other research reports available on prestressed girders, like analytical studies or empirical and semi-empirical studies, they are not mentioned here as they are not related to the current end cracking problem.

2.1 Codes for Anchorage Zones

2.1.1 AASHTO LRFD Bridge Design Specifications

The rules for pre-tensioned anchorage zones are given in 5.10.10 section of AASHTO LRFD Bridge Specification (3).

In the commentary on splitting reinforcement, AASHTO indicates that “Splitting resistance is of prime importance in relatively thin portions of pretensioned members that are tall or wide, such as the webs of I-girders and the webs and flanges of box and tub girders. Prestressing steel that is well distributed in such portions will reduce the splitting forces, while steel that is banded or concentrated at both ends of a member will require increased splitting resistance.”

The splitting resistance of pre-tensioned anchorage zones to be provided by reinforcement in the ends of pre-tensioned beams is given by Equation 2-1.

$$\mathbf{P_r = f_s * A_s} \qquad \text{Equation 2-1}$$

Where:

f_S= stress in steel not to exceed 20 ksi.

As =total area of reinforcement located within the distance h/4 from the end of the beam (in2)

h =overall dimension of precast member in the direction in which splitting resistance is being evaluated (in).

AASHTO specifies that the stress in reinforcing bars that are resisting splitting should not exceed 20ksi. The purpose of the choice of the 20 ksi stress limit in steel is to control crack size. Also, for pre-tensioned I-girders or bulb tees, the area of steel referred to is the total area of the vertical reinforcement placed within h/4 from the ends of members.

The code also states that “For the distance of 1.5d from the end of the beams other than box beams, reinforcement shall be placed to confine the prestressing steel in the bottom flange. The reinforcement shall not be less than No.3 deformed bars, with spacing not exceeding 6.0 in. and shaped to enclose the strands.” This reinforcement is generally assumed to control the cracks occurring around the perimeter of strands as they prevent the concrete bursting.

2.1.2 International Federation for Structural Concrete

In the case of prestressing with pretensioned tendons or wire, the FIB model code explains the cracking with three mechanisms as in 7.13.6.5.1 (Figure 2-1).

- Bursting is estimated to occur due to spreading forces over the cross-section,
- Spalling is identified to ensue in the case of thin webs.
- Splitting takes place along the transmission length as a result of the effect of internal pressure exerted by the prestressing steel during shortening (wedging effect).

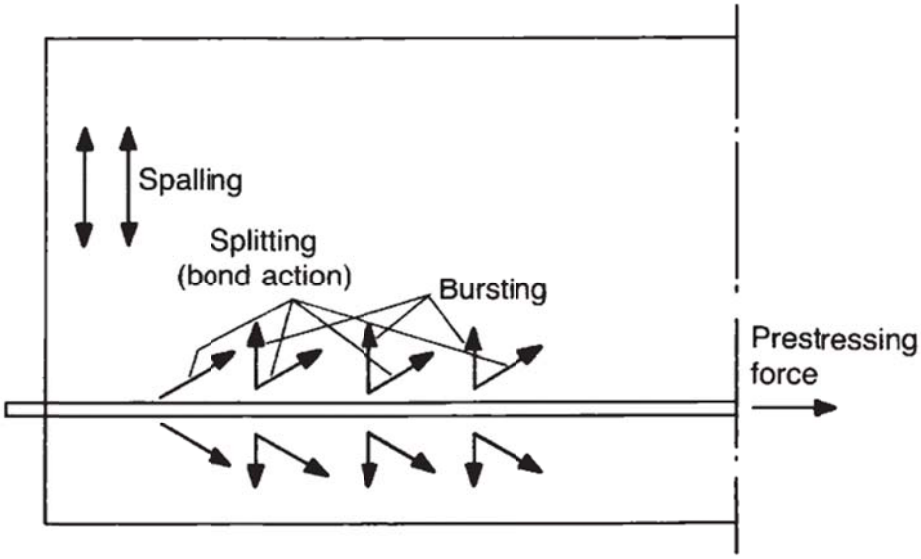

Figure 2-1. Three mechanism in FIB 2010 model code in anchorage zone (4).

To calculate the bursting force, the FIB code uses the symmetric prism analogy in Figure 2-2. The calculation is based on a virtual prismatic element, defined in order to describe the bursting forces. The prism is shown in Figure 2-2(a) (shaded area). The calculation of length of the prism (l_{bs}), the internal lever arm for the bursting force (z_{bs}), the bursting force (N_{bs}), and the maximum bursting stress (σ_{bs}) can be found in the code.

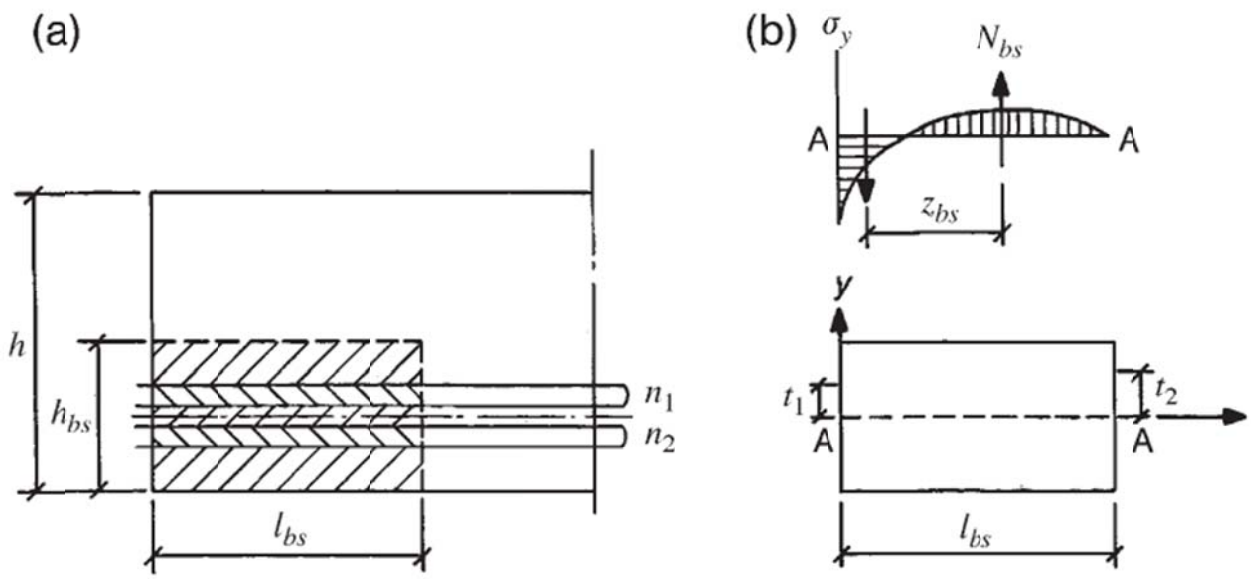

Figure 2-2. The prism analogy for calculation of the bursting force (4).

The FIB code gives a chart shown in Figure 2-3 (a) for the calculation of the spalling stress as a function of eccentricity and transmission length. This is based on linear elastic analysis for members with h smaller than 400mm (15.7 in.). If maximum bursting stress (σ_{spl}) is smaller than the design axial strength of concrete (f_{ctd}), no spalling reinforcement is necessary.

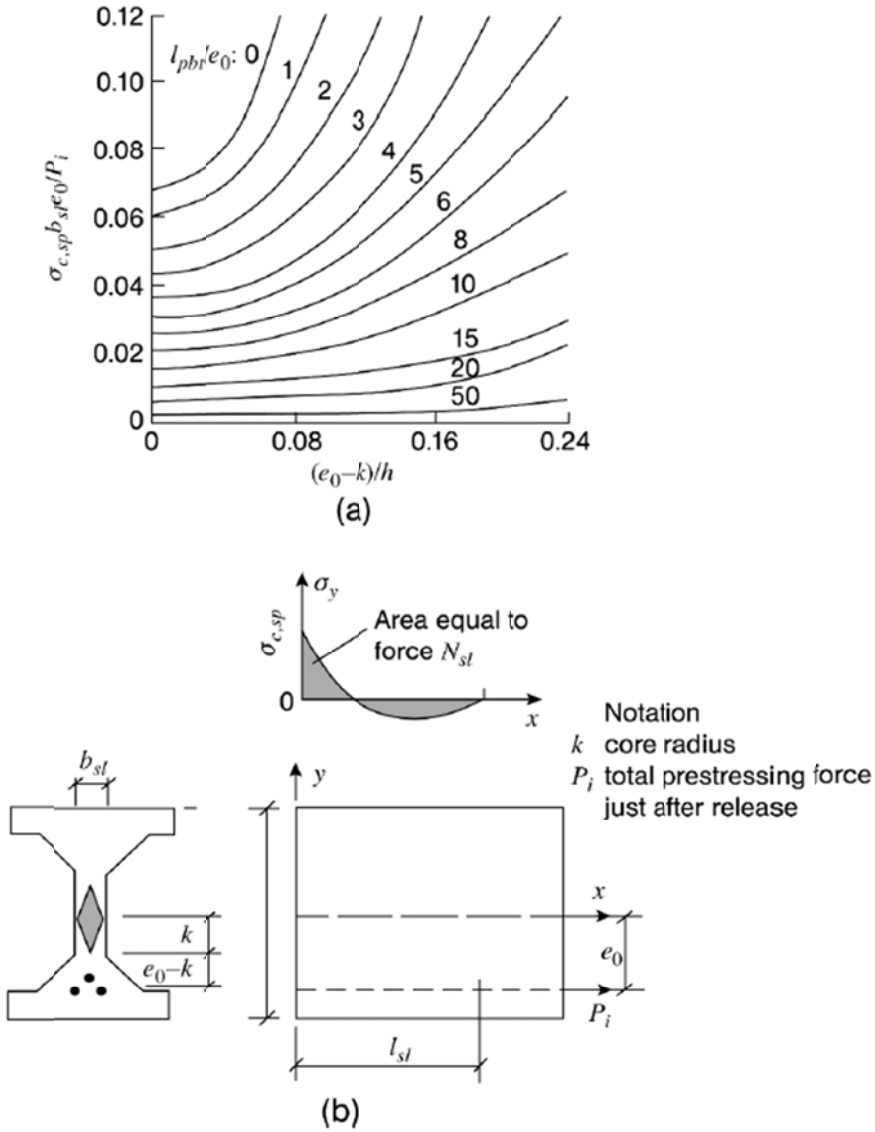

Figure 2-3. Maximum spalling stresses (4).

With enough concrete cover between strands or wires satisfying minimum cover values in the table of the FIB section, no reinforcement is required.

2.1.3 American Concrete Institute 318-14 (5)

This code is mainly concerned with post-tensioned anchorage zones and the code refers to the provisions in the AASHTO Standard Specifications for Highway Bridges (3).

2.2 Research on Anchorage Zone Cracking

2.2.1 Studies of Finite Element Analysis

Kannel et al. (6) examined the strand cutting order and debonding & strand cutting order together using FEA as a crack control method. They observed three different types of cracks in the girders they examined in Figure 2-4; cracking at the base of the web, and inclined and vertical cracks on the sides of the bottom flange. They built FEA models in ABAQUS to explore 3-D effects in the anchorage regions through the transfer length. The concrete and strands were modeled with 3D solid and truss elements respectively as shown in Figure 2-5. To lessen computational times, the remainder of the girder (after transfer length) was modeled with beam elements and girders were symmetrically cut in half both in the longitudinal and transverse directions. Lastly, the transfer of prestress from strands to concrete were modelled with two different cases: 1) assigning a varying area for the truss elements along the transfer length (ramped area method) and 2) utilizing springs to connect the truss to concrete elements, both of which gave close results.

They thought that changing strand release order would considerably decrease the stresses because they found out that the cause of cracks is mainly due to the concrete restraint of the uncut strands and shear stress initiated by the cutting order of strands. The study

suggested that some of the straight strands should be flame cut before all of the draped strands are released to prevent the vertical cracks at the bottom flange or to restrict their location to within the first foot. Moreover, release of the bottom straight strands should be in changing columns from the interior of the cross section toward the outside of the flange but the outer most strand column shall not be cut in the last step. This helps to get rid of angled cracks. Debonding also lessens cracking but a longer free length of debonded strands were needed so that less restriction from these strands was obtained. Moreover, the debonded strands were left bonded the first 2in.-4in. from the end to prevent water penetration into the plastic shielding.

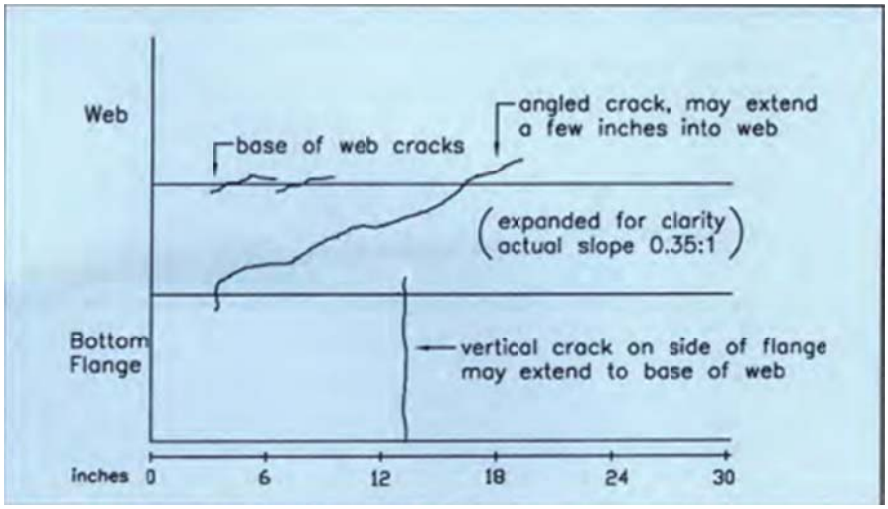

Figure 2-4. Types of crack observed (6).

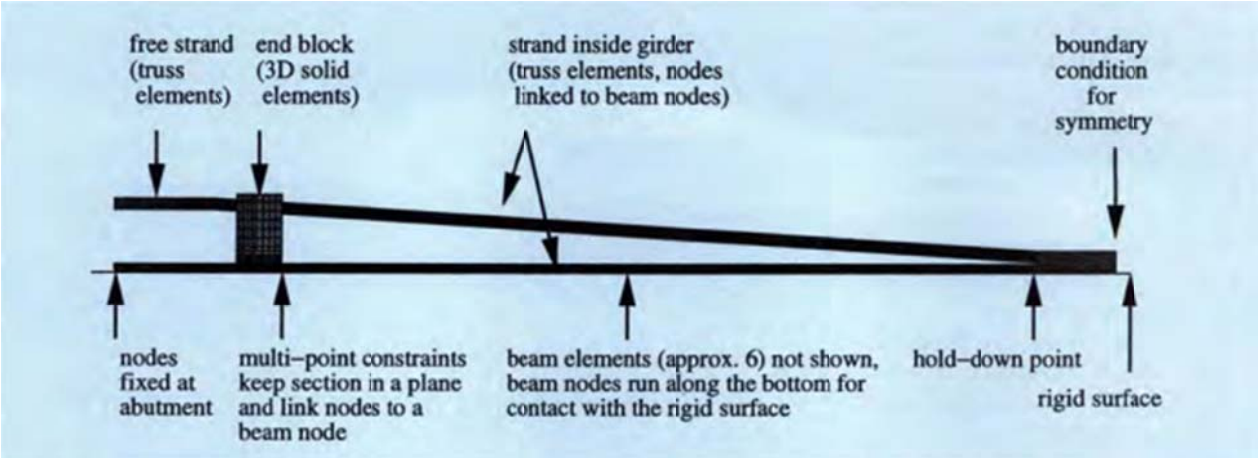

Figure 2-5. The FEA model created by Kannel et al. (6).

The model was built with fully linear elastic behavior because the aim of the study was to get rid of cracks and without cracks, concrete behaves in the elastic range. On the other hand, the maximum principal stresses in the cross section at 6in. from the end of girders are shown in Table 2-1 for three different girders. Even the girders designed to eliminate cracking exceeded the cracking limit of 490 psi so the assumption of fully elastic range for material behavior is invalid.

Step	Maximum principal stress, psi			Axial stress, psi			Shear in horizontal plane, psi		
	54A	54B	54C	54A	54B	54C	54A	54B	54C
2	127	220	220	126	105	59	10	209	204
3	282	311	230	280	272	161	21	217	201
4	535	455	304	463	427	271	364	232	209
5	771	543	397	559	486	279	538	347	302
6	746	573	348	329	408	184	626	331	285
7	673	320	295	105	119	133	678	374	373
8	685	496	459	-202	24	75	658	585	543
9	—	685	575	—	-202	-74	—	658	605

Note: 1 in. = 25.4 mm; 1 psi = 6.89 kPa.

Table 2-1. Peak values of stresses at 6in. from the end of girders (6).

Carroll et.al. (7) modeled the bond and slip between prestressing strand and the surrounding concrete based on the known relationship between end slip and transfer length and tried to develop a modeling technique to predict member behavior in a correct and efficient way, including end slip, strand force development, and concrete strains and stresses based on a specified transfer length. According to Carroll, the force from the pre-stressing strand to the surrounding concrete is transferred by adhesion and mechanical interlock between the two materials. However, as the strands retract during release, adhesion between the pre-stressing strands and surrounding concrete is broken. The strands expand laterally, causing circumferential stresses along their length. Mechanical interlock and friction due to the Hoyer effect (8) then produces bond stresses between the strand and the concrete surrounding it.

The analytical models were built utilizing GT STRUDL structural design and analysis software. Concrete was modelled as solid brick elements, with truss elements representing the pre-stressing strands and finally nonlinear spring elements explaining the interface between the pre-stressing strands and the surrounding concrete. The nonlinear springs have a bilinear force-versus-displacement relationship in Figure 2-6. The solid elements and truss elements are not directly attached. Instead, a series of duplicate joints is implemented along the line corresponding to the desired location of the pre-stressing strand(s), to which the truss elements are attached. However, the material behavior, other than the springs, was modelled with linear elastic properties.

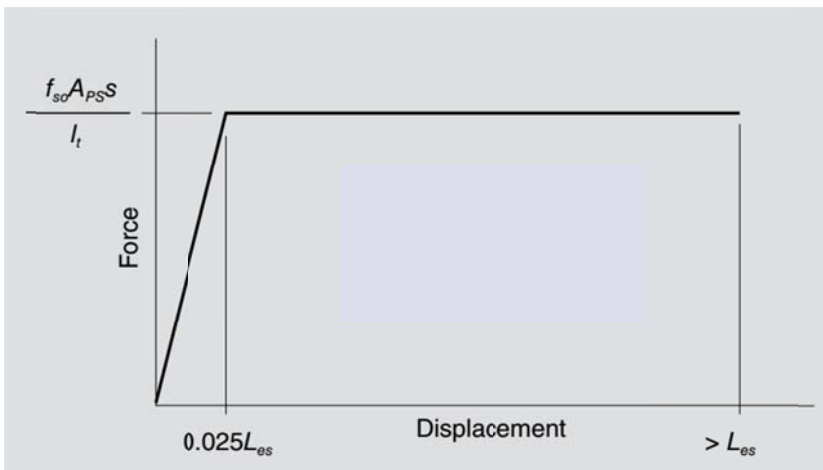

Figure 2-6. Nonlinear spring force-versus-displacement curve. (Note: A_{ps}: area of pre-stressing strand; f_{so}: stress in strand just after transfer; l_t: transfer length; L_{es}: end slip; and s: nonlinear spring spacing) (7).

There are two common practices used to apply the prestressing force to the members in the analytical software. The first method is to apply equivalent loads externally to the member, on the other hand, the second one uses steel segments perfectly bonded to the member combined with the application of initial strains. Since both fail to explain the slip

interaction, Carroll tried to simulate the pre-stressing force by a change in temperature applied to the truss elements, ensuring equivalent strain equal to that produced by pre-stress force.

To compare the analytic and experimenalt data (from gauges), 23 models (8 prisms and 15 T beams) were built. T beams had 17in., 19in. and 24in. depths and they all accommodated only 3 strands and prisms had a maximum of 5 strands in a 24in x 4in cross section shown in Figure 2-7.

Figure 2-8 shows the comparison of experimental concrete surface strains and analytical concrete strains for one prism and one typical T beam model. The maximum errors are 20% for prisms and approximately 40% for T beams. Even though the comparison has errors, the authors used linear elastic behavior without justification. They also made a conclusion that the comparisons confirm the practicality and accuracy of the models. The T beams are heavily pre-stressed and show some cracks around strands, so the results of beams having only 3 strands cannot be modelled with linear elastic material property and might not represent the case with larger amount of strands in deep girders.

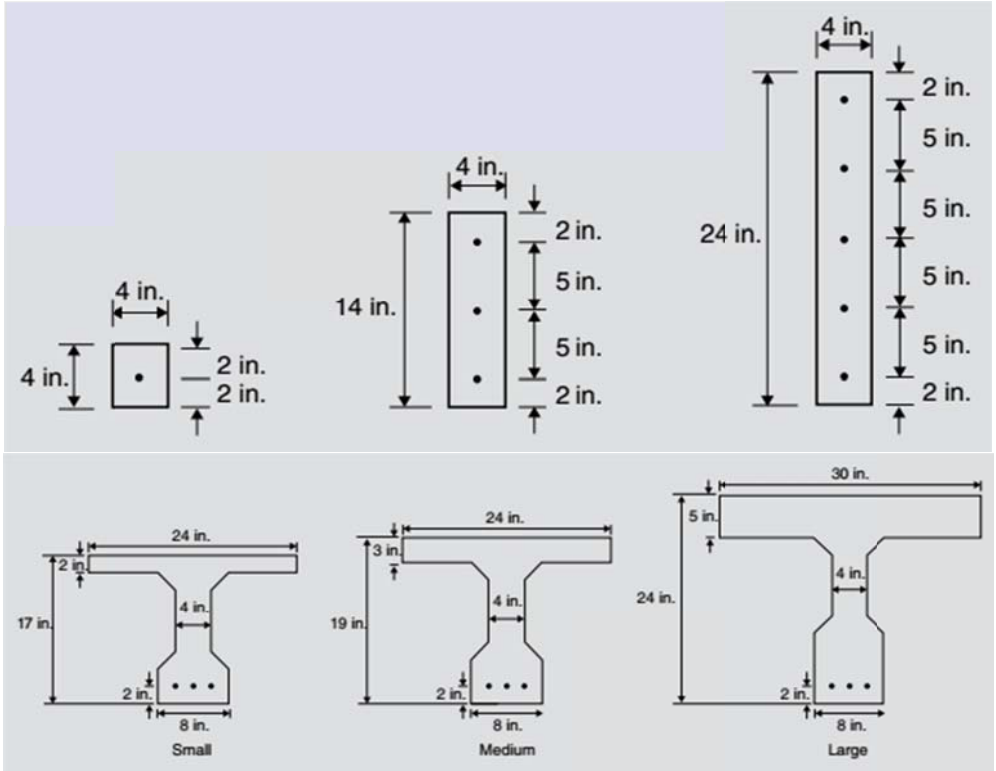

Figure 2-7. Beam (top) and T beam (bottom) cross sections (7).

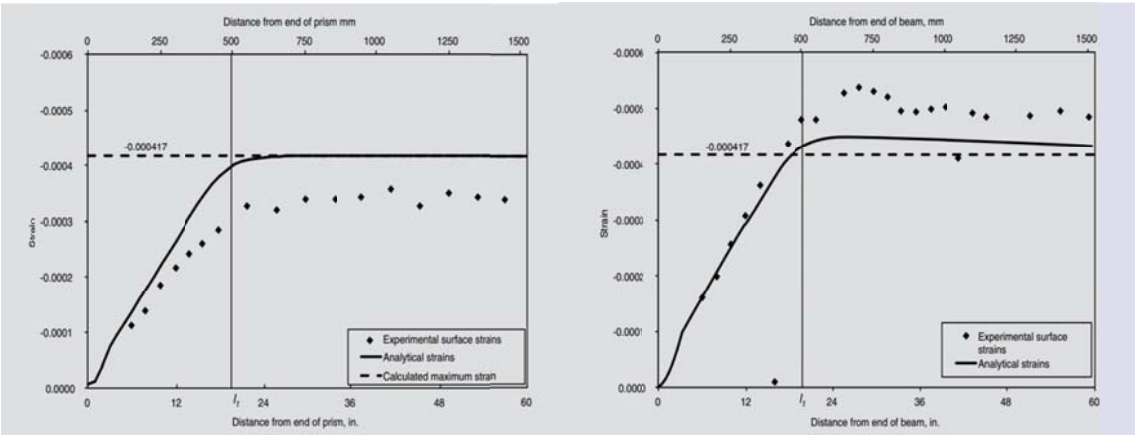

Figure 2-8. Comparison of experimental concrete surface strains and analytical concrete strains for a prism (left) and a typical T beam model (right) (7).

Arab et al. (9) examined the behavior of the end zone reinforcement of eight deep super girders used in construction of the Alaskan Way viaduct in Seattle, Washington. In their paper, the analysis of anchorage zone cracking of deep pre-tensioned concrete I-girders with nonlinear material properties was presented and they compared the results obtained from an elastic analyses as well as strength methods such as the Gergely-Sozen method (10) strut-and-tie method (11) and nonlinear finite element method.

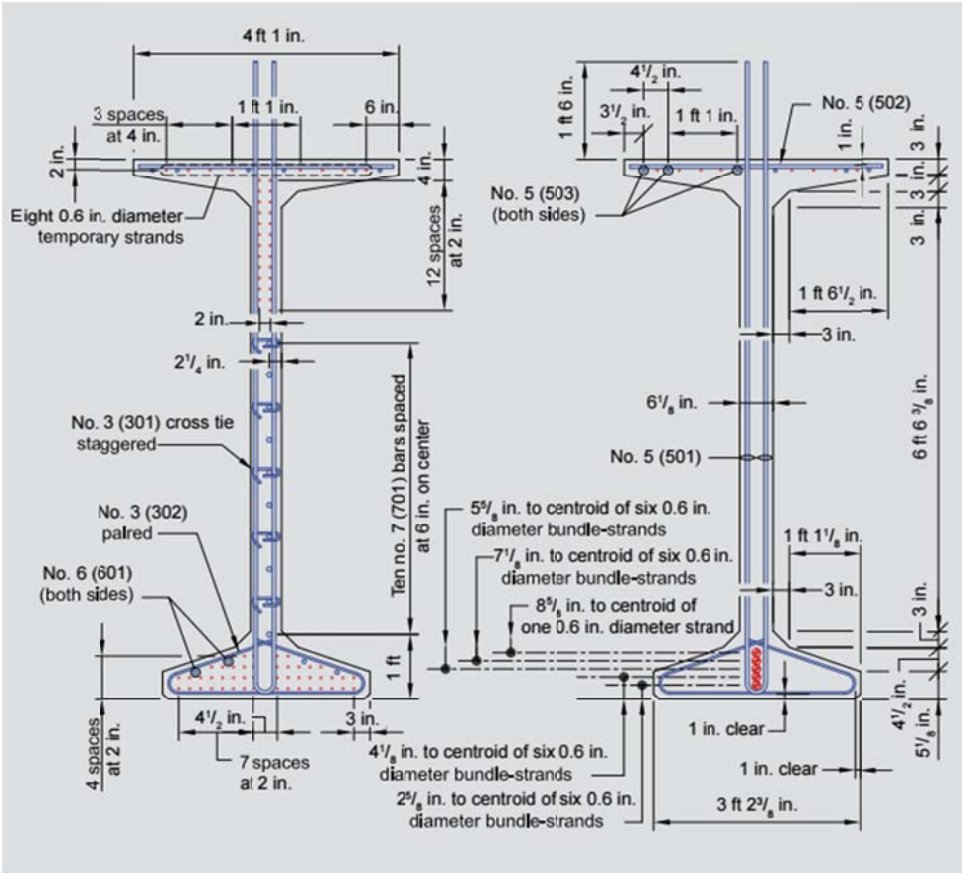

Figure 2-9.Typical cross sections of WF100G girder (9).

The girders that they investigated are WF100G girders, each of which are 205 ft. (62 m) long and 100 in. (2500 mm) deep. Each girder was pre-tensioned using eighty 0.6 in. (15 mm) diameter, 270 ksi (1860 MPa), low-relaxation seven-wire strands (Figure 2-9).

They used two finite element techniques to simulate pre-tensioned concrete girders immediately after the release of pre-stressing, which are extrusion and embedment. The embedment technique was preferred because of the other method's complexity. Data was input for the interaction of the released strands with the concrete within the transfer length. Concrete was modelled as three-dimensional continuum brick elements, and the pre-stressing strands were truss members. Mild reinforcement, such as end zone, shear, and confinement bars, were modeled using three-dimensional beam elements with shear stiffness. A concrete damage plasticity constitutive model was used for the simulation of the elasto-plastic response of the concrete by examining the response of a 2 × 8 in. prism to uniaxial compressive and tensile straining in Figure 2-10.

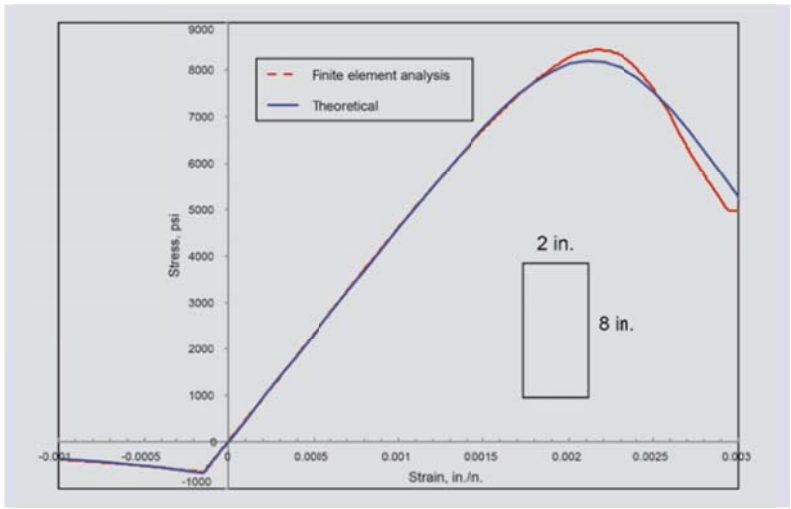

Figure 2-10. Constitutive model and theoretical stress-strain curve (9).

Monitoring end zone reinforcement, they found that strain gauge results in end zone reinforcement showed strains higher than the strain capacity of the concrete, so models should be built with nonlinear concrete properties. The Gergely-Sozen procedure (10), meant for an ultimate strength condition, did not predict the high tensile stresses observed at the web and bottom flange interface during de-tensioning. The bar stresses were about 85% higher than the 20 ksi limit (AASHTO). Also, the stress transfer of strands was Judged to vary in a parabolic fashion, rather than being linear as assumed by the AASHTO LRFD specifications. This woiuld mean that AASHTO significantly underestimates the tensile stresses in parts of the anchorage zone during release.

From the finite element analysis results with all girders, the authors observed that the stress distribution showed that the requirement of distributing the end zone reinforcement within a distance equal to h/4 from the girder end was needed, as noted in the AASHTO Specifications. However, the stress distribution shows that a relatively high stress concentration extends beyond h/4 to about h/2 (Figure 2-11), where no end zone reinforcement is needed according to the AASHTO LRFD specifications recommendation. They suggested the findings of Tuan et al. (12) that put 50% of the end zone reinforcement within h/8 and the remainder of the end zone reinforcement between h/8 and h/2 from the end. Also, the finite element analysis predicted the correct location of highest tensile stress, which was observed at the web and bottom flange interface but at a lower height than that suggested by the Gergely-Sozen (10) procedure.

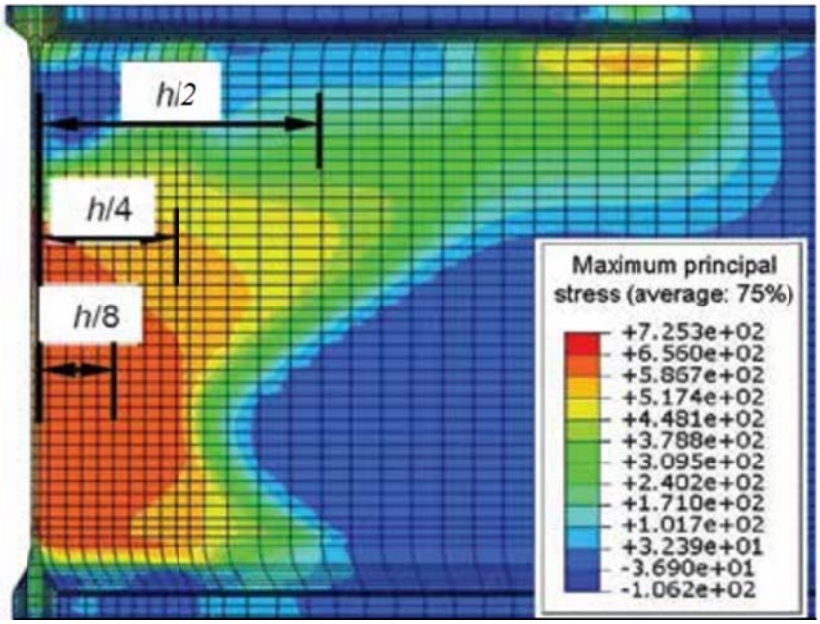

Figure 2-11. Principal stress distribution in concrete along anchorage zone (9).

Moreover, they claimed that the huge number of straight strands concentrated in the bottom flange in combination with the relatively narrow web caused shear lag at the web and bottom flange interface. Their model estimated this phenomena and the correct location of greatest shear stresses (i.e. cracks consistent with the cracks observed in the monitored girders), which started at about h/8 and extended to 0.7h from the end of the girder at a height of 14 in. from the bottom.

In their final comment, they said that the current AASHTO LRFD specifications requirement for splitting reinforcement does not account for the shear-lag phenomenon along the web and bottom flange interface. Hence, their own solution used a shear friction theory. This could be another alternative for estimating the tensile stresses in the end zone reinforcement along the web and bottom flange interface.

Ayoub et al. (13) presented methods to model pre-tensioned girders with nonlinear material properties. The model consists of three main components: a beam-column element for the behavior of concrete, a truss element for the pre-stressing tendons, and a bond element that describes the transfer of stresses between the pre-stressing tendons and the concrete. The model is primarily depending on a two-field mixed formulation, where forces and deformations are both approximated within the element. The nonlinear response of the concrete and tendon components are based on the section discretization into fibers with uniaxial hysteretic material models. The stress transfer mechanism was modeled with a distributed interface element with special bond stress-slip relation. They also presented a method for accurately simulating the pre-stressing operation. To test the accuracy of models, they conducted correlation studies with the proposed model and these studies confirmed the accuracy and efficiency of the model.

3 PRESTRESSED GIRDERS

3.1 Pretensioning and Post-tensioning

Concrete is a good structural material for carrying compressive loads but not for tension loads. Therefore, conventional concrete is combined with high strength steels, in order to avoid resisting tension in the concrete. In that way, steel reinforced concrete members will be strong both in tension and compression. Though this method eliminates the need to resist tensile stresses in the concrete, it should end up with small cracks in the concrete body. Fewer cracks provide a stiffer cross-section so large cross-sectioned concrete members are not needed. This allows designers and engineers to design lighter structures.

Prestressing is a special method for reinforcing concrete. Prestressed concrete can be divided into two categories: pretensioned and post-tensioned. In pretensioning, high strength strands, called tendons, are first tensioned inside molds, and then concrete is cast around them. After the concrete gains sufficient strength, the strands are cut and the force in steel, as it tries to shorten again, is transmitted to concrete by bond over a distance from the end of the members, a distance known as the transfer length. Energy stored, due to initial stretching of tendons, is also transferred to concrete through bond between concrete and tendon over that distance. An initial compression force is induced in the concrete.

Another method for prestressing is post-tensioning. In this method, hollow ducts and strands are threaded before concrete is cast, and after concrete reaches sufficient strength the strands are stressed by means of hydraulic jacks and then clamped at their ends. And finally, the duct is filled with grout to protect tendons from corrosion.

The main difference between the two methods is the way the prestressing force is transferred to the concrete body. In pretensioned members, the transfer gradually occurs through bond over a distance from member ends;, in post-tensioning, the force transfer is achieved by mechanical anchors at the end face of the members.

3.2 Types and Properties of Pretensioned Highway Bridge Girders

There are four standard types of deep wide flange prestressed girders that WisDOT has been generally using for bridges: 45W, 54W, 72W and 82W sections. The numbers indicate the depth of girders in inches. Currently Wisconsin is not using the 82W girders due to end cracking problems and shipping difficulties. Only 54W and 72W girders are investigated in this project due to their cracking problems. The letter “W” after the numbers denotes the “W”ideness of girders. Regardless of the girder’s height, all girders have the same top and bottom flange shapes, which are respectively 4 feet, and 2.5 feet in width (Figure 3-1). They have been proven efficient in resisting loads over long spans. The wide top flange provides a compression block with large area and the big bottom flange can accommodate numerous steel strands. These girders can be designed with up to 8 draped and a total of 40, 42, 48, and 50 strands for respectively 45in to 82in girders. Spans to 170ft can be reached.

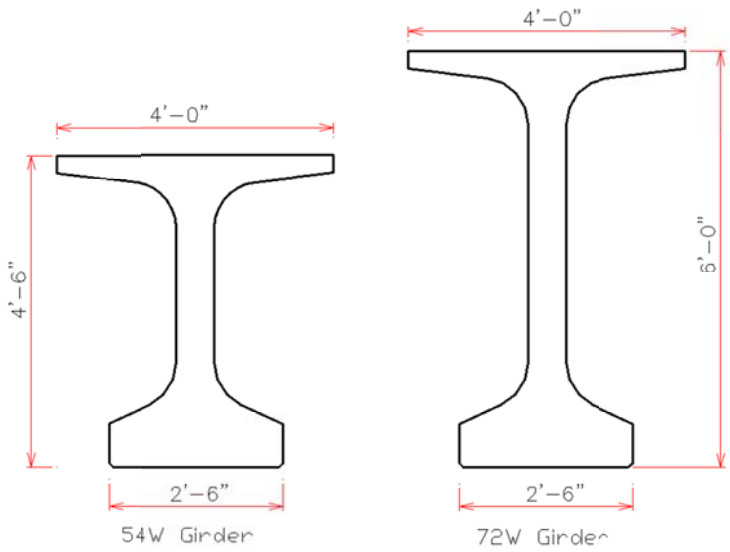

Figure 3-1. Girder sizes: 54W and 72W.

These girders also have the same general pattern for end zone reinforcement as in Figure 3-2, though in different quantities, since the top and bottom flange dimensions are the same. The only change in different girders is the length of web steel reinforcing bar. They are adjusted to fit in depths of girders. Additionally, there are five #4 U reinforcing bars along the web going 7ft inside of the 82W girder only. All mild reinforcement bars are ASTM A706, Grade 60 steel. The strands are 0.6in in diameter, and have 270 ksi ultimate strength with low relaxation. All bridge girder strands are uncoated, per American Association of State Transportation and Highway Official (AASHTO) requirements (3), and particularly subject to corrosion and deterioration if exposed to corrosive conditions by concrete cracks. The girders also have bottom steel stirrups that are epoxy coated to control corrosion. All other details are provided in the Standard Details of the WisDOT Bridge Manual (14). However, these details can be changed according to each project's needs.

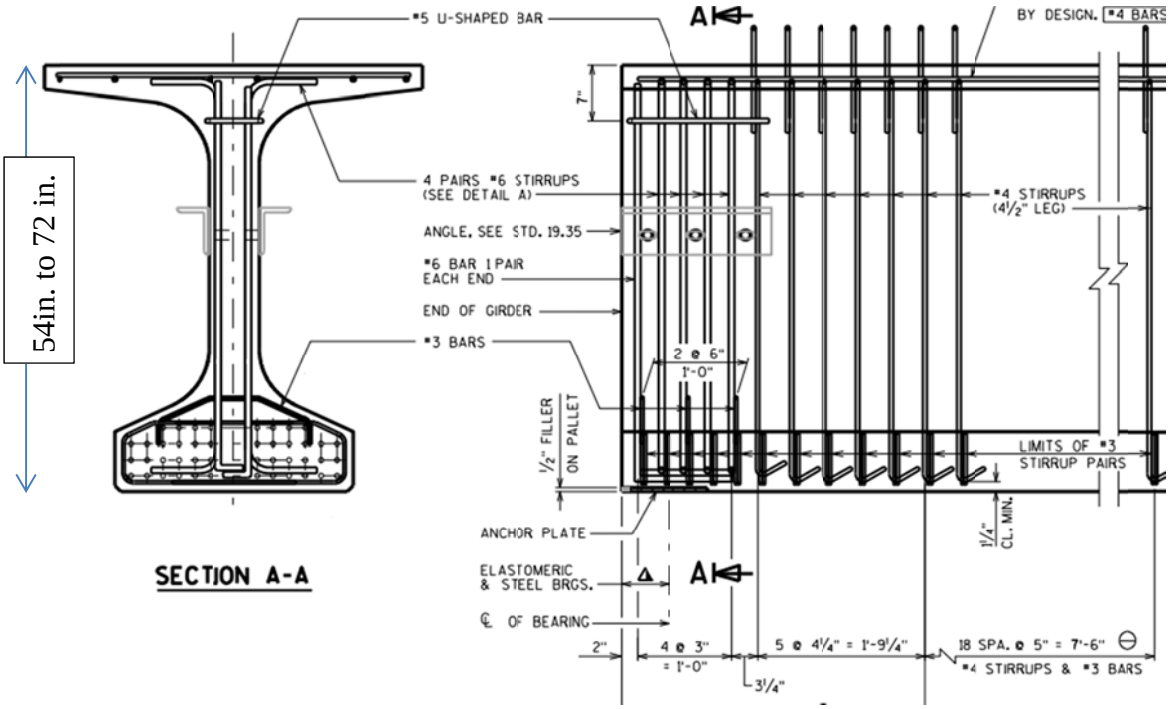

Figure 3-2. The end details of girders.

There are two other pretensioned girder types used by WisDOT: 28in and 36in “I” girders. They do not have wide flanges and from observations, they do not show as much critical cracking at the end.

3.3 Categorization of End Cracks

The number of strands needed in a girder is designed according to the maximum moment demand near mid-span, but the same amount of strand is not needed at the ends of girders because there the bending moments are minimal. With draped strands (strands lifted up from the bottom flange toward the beam top) to prevent high tension stresses in concrete at the upper fiber of girders, cracks are still observed in these deep girders. The cracks are

located at different positions over the girder depth and induced by different effects. According to their directions and locations; the girder cracks of concern in this study can be categorized in three groups: inclined cracks, horizontal web cracks, and Y-cracks (1) (Figure 3-3).

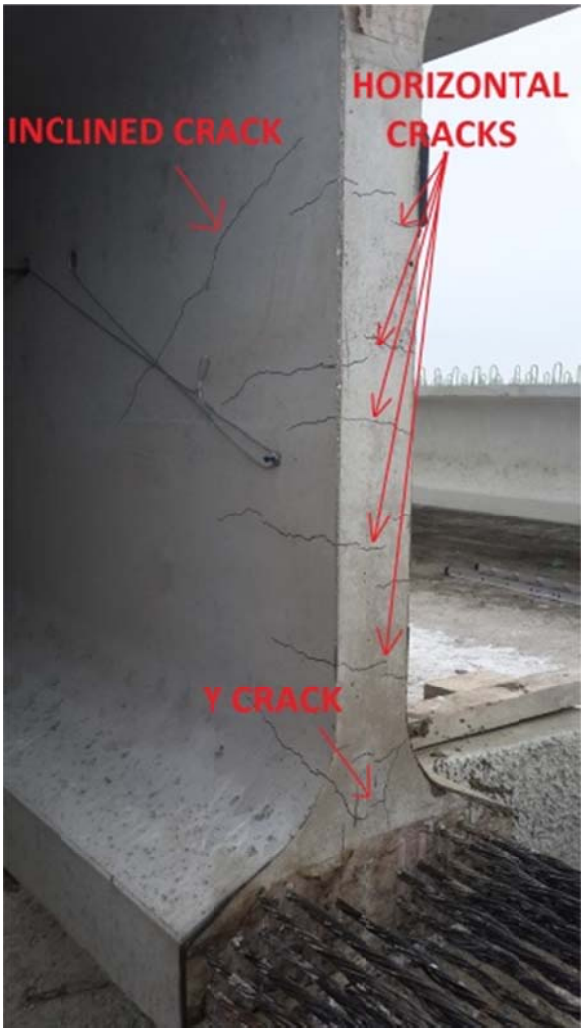

Figure 3-3**.** Inclined, Horizontal Web, and Y cracks shown on 72W girder.

Inclined Cracks: These cracks occur close to the path of draped strands. They are composed of either a combination of multiple small cracks or one long straight crack as in

Figure 3-3. Also, they are observed during inspections to be the longest cracks among the others occurring at the end of girders. One interesting observation of these cracks is that they sometimes do not continue to the girder end, meaning that their formation may not originate from the end but further inside the girder.

After prestressing, these girders are taken to a storage yard. Continued observation of cracks has been done during storage. Generally, the width of these cracks is between 0.004-0.010 inches. If these cracks are not closed by vertical loading on the girder or covered by the concrete end diaphragms, they may allow moisture penetration causing durability problems. However, these cracks are generally found to be closed by the principal compression stresses from shear force flow coming from added dead loads or service live loads. Therefore these cracks may not be of serious consequence.

Horizontal Web Cracks: Horizontal web cracks are horizontal cracks in the thin web with their location, length and distance between varying according to the girders' depth and the number of strands. Even though their widths range between 0.004-0.010 inches, these cracks propagate only a short distance from the end so the cracks may be buried inside of concrete diaphragms cast around the beam end on the bridge site. They are also likely to be closed as further loading is applied to the girder and the end reactions increase. Their effect on durability of the structure, though visually undesirable, may be tolerated.

Y Cracks: Y-cracks take shape at the junction of the bottom flange and web. These cracks often run vertically through the bottom flange where there is a high concentration of strands. The Y cracks are also the widest measured cracks, as wide as 0.02 inches. Rather

than experiencing closure with added girder loading, these cracks actually tend to open as more loading is applied. Therefore, these type of cracks are of serious concern because of a tendency to lead to aggressive salty water to penetrate in the concentrated location of tendons and cause corrosion of tendons. Corrosion spreading along the strands may put the structure in danger of shear failure so this type of cracks should be considered as a dangerous one

.

3.4 Splitting Resistance and Confinement Reinforcement at Anchorage Zone of Standard Girders

Reinforcement in the anchorage zone of Wisconsin W girders should comply with 5.10.10.1 and 5.10.10.2 Sections of the AASHTO LRFD Bridge Design Specification (3). While evaluating this reinforcing, the maximum strand numbers that each girder can accommodate from the WisDOT manual (14) was considered. As described in the AASHTO specification (3), the steel stress is limited to 20 ksi to control crack widths. This limit is very important, especially for I or W girders in their thin portions. Table 3-1 & Table 3-2 show sample calculations on amount of bursting steel reinforcing in the anchorage zone done for 72W and 54W girders. They seem to satisfy the splitting resistance condition.

72W Girder	
AASHTO 5.10.10.1 Splitting Resistance	
Pr=fs*As **Pr > 4% of the total prestressing force**	
Depth of prestressed girder (in), h=	72
Strand Number, n=	48
Area of a strand, A_{strand} (in^2)=	0.217
Tensile Strength of strands (ksi), f_{pu}=	270
Initial prestressing force at transfer (ksi), $0.75xf_{pu}$=	202.5
Total prestressing force at the transfer (kips), $nxA_{strand}x0.75xf_{pu}$=	2109
Stress in steel (ksi), f_s=	20
h/4 (in)=	18
Stirrup bars in h/4 in from the end	10#6+2#4
Total area of steels within h/4 in distance from end (in^2),A_s=	4.81
The splitting resistance (kips), Pr=	96.2
Pr/Total prestressing Force (%)=	4.56
Condition for Pr > 4%	Provided

Table 3-1. The calculations on amount of bursting steel reinforcing in the anchorage zone for 72W girder.

For the confinement or bursting reinforcement, the code suggests that they should be minimum #3 rebar with 6 inches apart from each other within 1.5*d from end of girders. This condition is provided in each WisDOT girder.

54W Girder	
AASHTO 5.10.10.1 Splitting Resistance	
Pr=fs*As **Pr > 4% of the total prestressing force**	
Depth of prestressed girder (in), h=	54
Strand Number, n=	42
Area of a strand, A_{strand} (in^2)=	0.217
Tensile Strength of strands (ksi), f_{pu}=	270
Initial prestressing force at transfer (ksi), $0.75xf_{pu}$=	202.5
Total prestressing force at the transfer (kips), $nxA_{strand}x0.75xf_{pu}$=	1845
Stress in steel (ksi), f_s=	20
h/4 (in)=	13.5
Stirrup bars in h/4 in from the end	10#6
Total area of steels within h/4 in distance from end (in^2),A_s=	4.42
The splitting resistance (kips), Pr=	88.357
Pr/Total prestressing Force (%)=	4.79
Condition for Pr > 4%	Provided

Table 3-2**.** The calculations on amount of bursting steel reinforcing in the anchorage zone for 54W girder.

3.5 Summary

Their efficiency, durability and economy make precast wide flange or bulb tee girders preferred in bridge projects. They can accommodate large numbers of strand resulting in high prestressing force, so some cracking has occurred in the anchorage zones at the girder ends..

Among all cracks described, “Y” cracks in the bottom flange are the most dangerous type of cracks because of the tendency to lead aggressive salt water to penetrate where concentrated tendons are located, possibly endangering the structures’ safety.

From a reinforcement point of view, WisDOT girders are satisfying the requirements of the AASHTO LRFD Design Specifications to control cracking at the ends. Since undesirably large cracks still frequently occur, the reinforcement is not satisfactorily controlling the cracking and additional measures may be necessary.

4 FINITE ELEMENT MODELLING

Because of cracking, in analytic modelling of the precast girders the stress-strain behavior should not be represented with linear analysis but with nonlinear analysis in the girder end regions. A software package, ABAQUS/CAE 6.12 (Dassault 2012) (14), capable of simulating non-linear concrete behavior, was used to investigate the girder ends using finite element analysis (FEA).

4.1 Geometry of the Girders

Models of standard 54W and 72W girders were developed according to the dimensions in standard WisDOT plans for cross-sections and the end reinforcement detailing.

The girder lengths and the number of strands were carefully chosen from the Wisconsin Highway Structures Information System (15). While choosing, it was desirable to have the maximum number of strands that each girder can accommodate and maximum length that each girder can span to observe conditions meeting the highest girder load capacity. With the high prestressing a larger amount of end cracking has been observed in practise. Table 4-1 shows the girders' length and number of strands modelled with Abaqus and maximum span length that each girder type is allowed in accordance with the WisDOT Bridge Manual (14).

Girder Type	Length (ft.)	Number of Strands	Real Life Project where these girders were used (15)	Maximum Span for single span-(ft.) (16)
54W	125	8 draped + 34 straight	B-05-0682	132
72W	154	8 draped + 40 straight	B-05-0381	160

Table 4-1. Types of girders modelled in Abaqus.

4.2 Review of Finite Element Models

Overall, the girder models are mainly constituted of three parts:

- Nonlinear end zone of concrete girder,
- Linear part of concrete girder, and
- Reinforcing steel.

Only end zone cracking is investigated in this study, so it is not necessary to model the full length of a girder with nonlinear material properties, as nonlinear computations can be demanding. Based on St. Venant's principle, the stresses and strains are anticipated to be in linear distribution over the depth after a distance at least equal to the beam depth away from the end zone disturbed region where the prestress force is applied (17). Therefore, the length of nonlinear modelling was restricted to 2 times the girder depth with the assumption that this will not cause significant error in overall results because there were no cracks observed in actual girders at a section 2 times depth of girder away from the end.

Moreover, the size of the models decreased by modelling only a quarter of the full girders. Girders are symmetric about the center of the girder's cross-section and about the

middle of the girder span. The pre-tensioned forces applied by strands are also symmetric about the center of a girders' cross-section. Assuming that girder dead load will be symmetric as well, the girders are modelled as in Figure 4-1. The shaded region is the end where non-linear modelling and small element size was used. The concrete voids where the ends of the prestressing strands would be located are also visible.

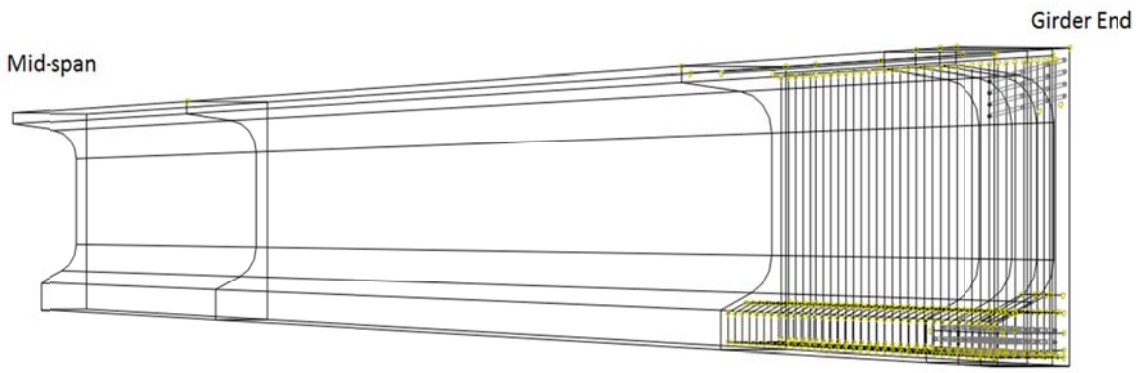

Figure 4-1. Model of Bonded 54W girder in Abaqus.

4.3 Properties of Materials

Up to the cracking strength, concrete theoretically behaves linearly and modelling finite elements with linear material property is easy and fast. However, once cracks occur in the body, reinforcing steels play a role and carries tensile stresses at the crack. Therefore, there will be some stiffness loss in the body. However, in between cracks there is still concrete around the reinforcements, which is enough to resist some amount of tensile stress in the concrete. This causes a decrease of the stress in the steel. The effect of concrete in tension in between cracks may be called tension stiffening (18) and is modelled in the analysis.

The cracks in the pretensioned girders were observed to occur during the de-tensioning process. Therefore, there is some stiffness loss in the body. Stiffness loss of concrete and the crack growth cannot be simulated with a linear elastic model.

4.3.1 Concrete Material Properties

There are three different constitutive models for concrete in Abaqus: “the Concrete Damaged Plasticity”, “the Smeared Cracking”, and “the Brittle Cracking” types. The “Concrete Damaged Plasticity” is used for the present model as it:

- enables modeling of concrete and other quasi-brittle materials in all types of structures,
- utilizes an isotropic damaged elasticity concept with isotropic tensile and compressive plasticity to describe the inelastic behavior of concrete under any arbitrary loading condition,
- is primarily designed for the analysis of reinforced concrete structures,
- can implement different degradation of the elastic stiffness in tension and compression (19)
- was successfully used in an initial phase of this research work (1).

Abaqus uses the work of Lubliner et al. (20) and Lee (21) in defining the concrete damaged plasticity constitutive model.

The equations for linear material properties, i.e. before cracking, are taken from the AASHTO LRFD Bridge Design Specifications (3) and the equations for nonlinear properties are obtained from the FIB 2010 Model Code (4).

The concrete damaged plasticity model requires input on the compressive behavior, tensile behavior of concrete, and concrete plasticity parameters. These are discussed below.

4.3.1.1 Compression Properties of Concrete

Initial Elastic Portion: The mechanical response of concrete under applied stresses may be assumed to stay within the linear regime up to approximately 40% of the design concrete strength. To represent this behavior, the modulus of elasticity, poisson's ratio, and density of concrete were used as input in Abaqus.

Because of data absence, the modulus of elasticity in the linear regime is calculated from section 5.4.2.4 of the AASHTO LRFD Bridge Design Specifications (3) and is based on the actual measured concrete cylinder strength just before de-tensioning.

$$E_C = 33000 K_1 w_C{}^{1.5} \sqrt{f'_C} \qquad \text{(ksi)} \qquad \text{Equation 4-1}$$

Where K_1= correction factor for aggregate (taken as 1),

w_C= unit weight of concrete (in ksf)

f'_C= compressive strength of concrete at de-tensioning (ksi)

In order to use this equation, the unit weight should be in between 0.09 – 0.155 kcf. It depends on the specified compressive strength of concrete according to Table 3.5.1-1 in

AASHTO LRFD BDS (3). In the precast plant, the strength value was observed to be always higher than 5 ksi so the equation is:

$$w_C = 0.140 + 0.001f'_C \qquad \text{for } 5.0 \text{ ksi} < f'_C < 15.0 \text{ ksi} \qquad \text{Equation 4-2}$$

The highest value was 7808 psi for a 72W girder so the w_C value is taken as 0.148 kcf which is in the range of specified values to use this equation.

The poisson's ratio was assumed to be 0.2 from section 5.4.2.5 of AASHTO (3) again because of a lack of physical tests.

<u>Inelastic Portion</u>: After the elastic limit, the concrete behavior is plastic. Therefore, the stiffness relation cannot be represented by the linear stress and strain relation. The compressive behavior can be defined by defining the values of yield stress and corresponding inelastic strain for the program.

The FIB model Code 2010 (4), section 5.1.8.1, estimates the compressive behavior of concrete by the following equation:

$$\frac{\sigma_c}{f_{cm}} = -\left(\frac{k*\eta-\eta^2}{1+(k-2)*\eta}\right) \qquad for \ \ |\varepsilon| < \ |\varepsilon_{clim}| \qquad \text{Equation 4-3}$$

Where:

$\eta=\frac{\varepsilon_c}{\varepsilon_{c1}}$ and $k=\frac{E_{ci}}{E_{c1}}$

ε_C: Concrete compressive strain

σ_C: Concrete compressive stress- psi

ε_{clim}: ultimate strain from Table 5.1.8 (FIB 2010 Model Code)

ε_{cl}: strain at maximum compressive stress from Table 5.1.8 (FIB 2010 Model Code)

E_{ci}: initial modulus of elasticity from Table 5.1.8 (FIB 2010 Model Code)

E_{cl}: secant modulus of elasticity= f_{cm}/ε_{cl} and also from Table 5.1.8 (FIB 2010 Model Code)

In the end, the compressive behavior is as shown in Figure 4-2:

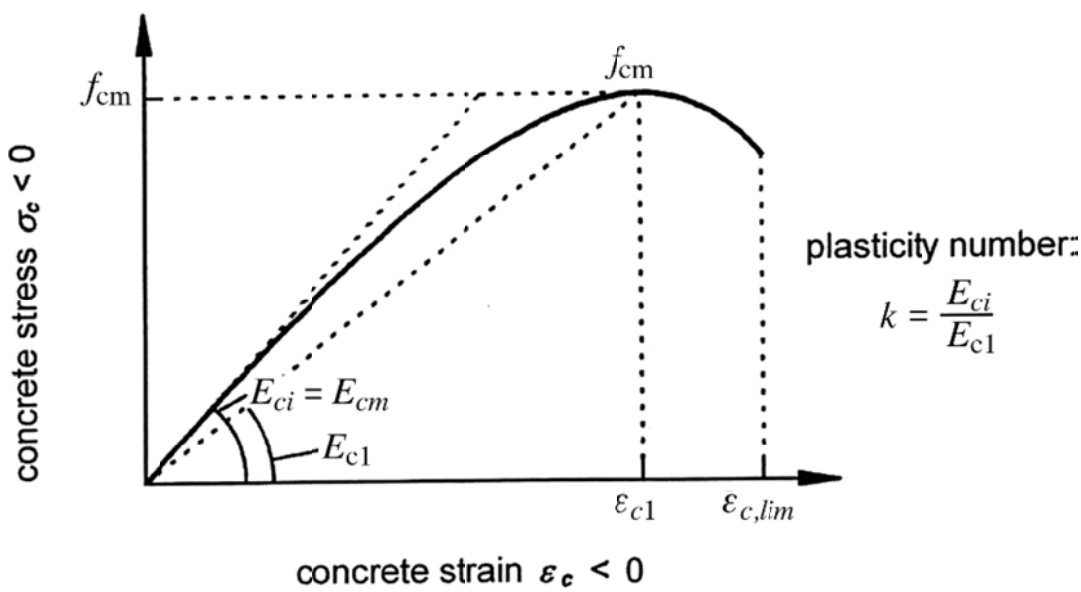

Figure 4-2. The graph of plastic constitutive behavior of concrete in compression.

According to the FIB code, the descending part should be thought of as the envelope of all possible stress-strain relations of concrete having tendency to be softened by micro-cracks. However, the correct shape does depend on load redistribution, member geometry or specimen, and boundary conditions. The code also states that if the modulus of elasticity is obtained from tests, an accurate stress-strain relation can be represented. It is unfortunate that all the tests on girder concrete were far from the laboratory where more complex cylinder

testing for specific characteristics could be conducted. If the concrete cylinders were tested later in the lab, they would not be the correct values because the concrete continues to gain strength and properties change.

After inputting the yield stresses and corresponding inelastic strain values to Abaqus, the constitutive model graph (Figure 4-3) of concrete compressive behavior for the 72W girder model having an initial 7800 psi concrete compressive strength is obtained. Please refer to the Appendix to see the details of the calculation.

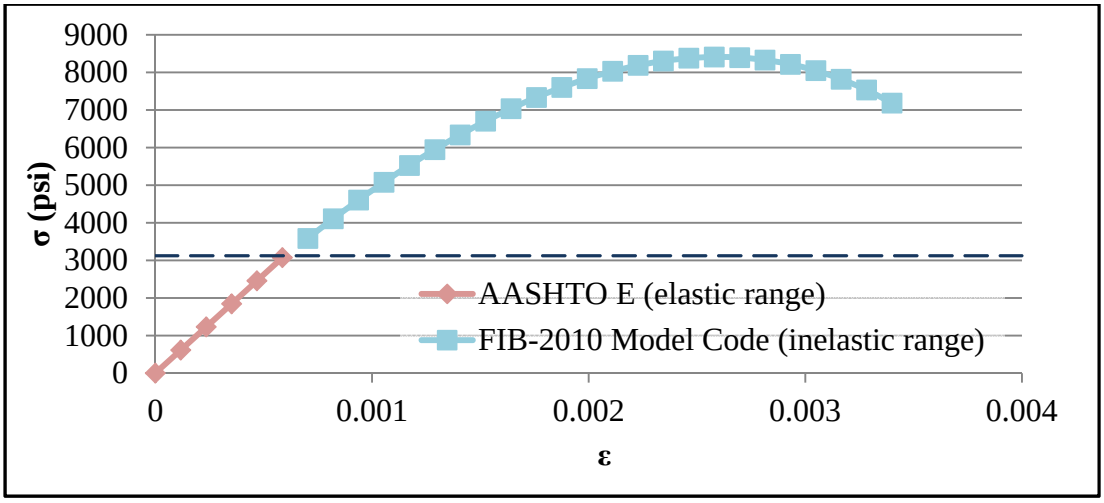

Figure 4-3. Compression constitutive graph with the model of a bonded 72W girder

4.3.1.2 Tension Behavior of Concrete

Like compressive behavior, the tensile behavior is defined in elastic and inelastic stages.

Elastic Portion: Up to cracking, concrete tension stresses can be assumed linearly proportional to strains. The modulus of elasticity, density and poisson's ratio are the same values used initially for compressive behavior.

The cracking strength, f_r, is taken as the limit for the elastic linear region. The cracking strength is assumed to be calculated from the AASHTO LRFD Bridge Design Specifications Section (3) C5.4.2.7:

$$f_r = 0.23\sqrt{f_C'} \qquad in\ ksi \qquad \text{Equation 4-4}$$

Where

f_C': Initial compressive strength of concrete at time of de-tensioning.

Inelastic Portion: After the concrete cracking stress is reached, cracks occur. Therefore, the model should be defined by non-linear tensile behavior. Abaqus allows users to represent the plastic tensile behavior based on strains, crack opening, or fracture energy. Crack opening was used here, and is explained by fracture energy concepts, because of mesh sensitivity concerns.

In the description of the concrete damaged plasticity model (14), if cracks occur in localized zones and the mesh does not provide additional cracks, the finite elements do not converge to a unique solution because the mesh refinement leads to narrower crack bands. This problem can be solved by two applications. Firstly, making use of reinforcing bars with the concrete element lessens the mesh sensitivity because the interaction between bars and concrete elements redistribute the cracks only if enough tension stiffening is provided.

Secondly, in case of little or no reinforcement in the model, Hillerborg's (22) fracture energy proposal is assumed to be enough to eliminate the concern. Hillerborg represents the energy required to open a unit area of crack, G_F, as a material parameter for brittle cracking. This approach explains the brittle behavior by a stress-displacement response rather than a stress-strain response. After concrete is in tension - so that the undamaged elastic strain is small, its length will be determined primarily by the opening at the crack. The opening does not depend on the specimen's length. Therefore, it is easy to apply this material property to any shape.

The fracture energy was taken from FIB 2010 Model Code (4) Section 5.1.5.2.

$$G_F = 73 * f_{cm}^{0.18} \qquad in \frac{N}{m} \qquad \text{Equation 4-5}$$

Where f_{cm} is mean compressive strength.

Section 5.1.8.2 of FIB 2010 Model Code (4) gives constitutive equations for concrete in tension by using crack opening and fracture energy. At the end, post cracking behavior will look as in the Figure 4-4.

$$\sigma_{ct} = f_{ctm} * \left(1.0 - 0.8 * \frac{w}{w_l}\right) \qquad for\ w \leq w_l \qquad \text{Equation 4-6}$$

$$\sigma_{ct} = f_{ctm} * \left(0.25 - 0.05 * \frac{w}{w_l}\right) \qquad for\ w_l < w \leq w_c \qquad \text{Equation 4-7}$$

Where

σ_{ct}: tensile stress in MPa

f_{ctm}: mean tensile strength of concrete (f_r, direct tensile strength of concrete) in MPa

w: crack opening

w_l: crack opening when σ_C is equal to $0.2*f_{ctm}=G_F/f_{ctm}$

w_C: crack opening σ_C is equal to $0 = 5*G_F/ f_{ctm}$

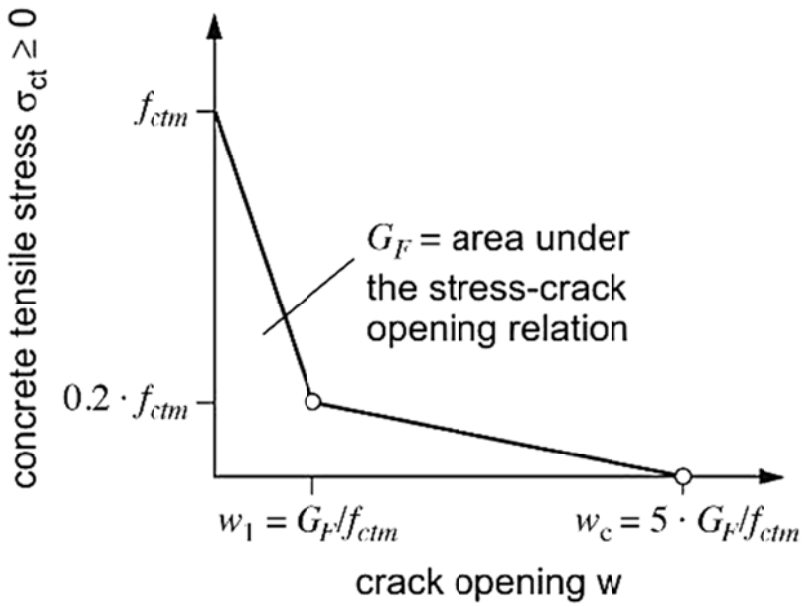

Figure 4-4. Post- Cracking Behavior Graph

Figure 4-5 shows the graphs of pre-cracking and post-cracking concrete behaviors of the 72W girder having an initial 7800psi compressive strength at de-tensioning. Please refer to the Appendix to see the details of the calculation.

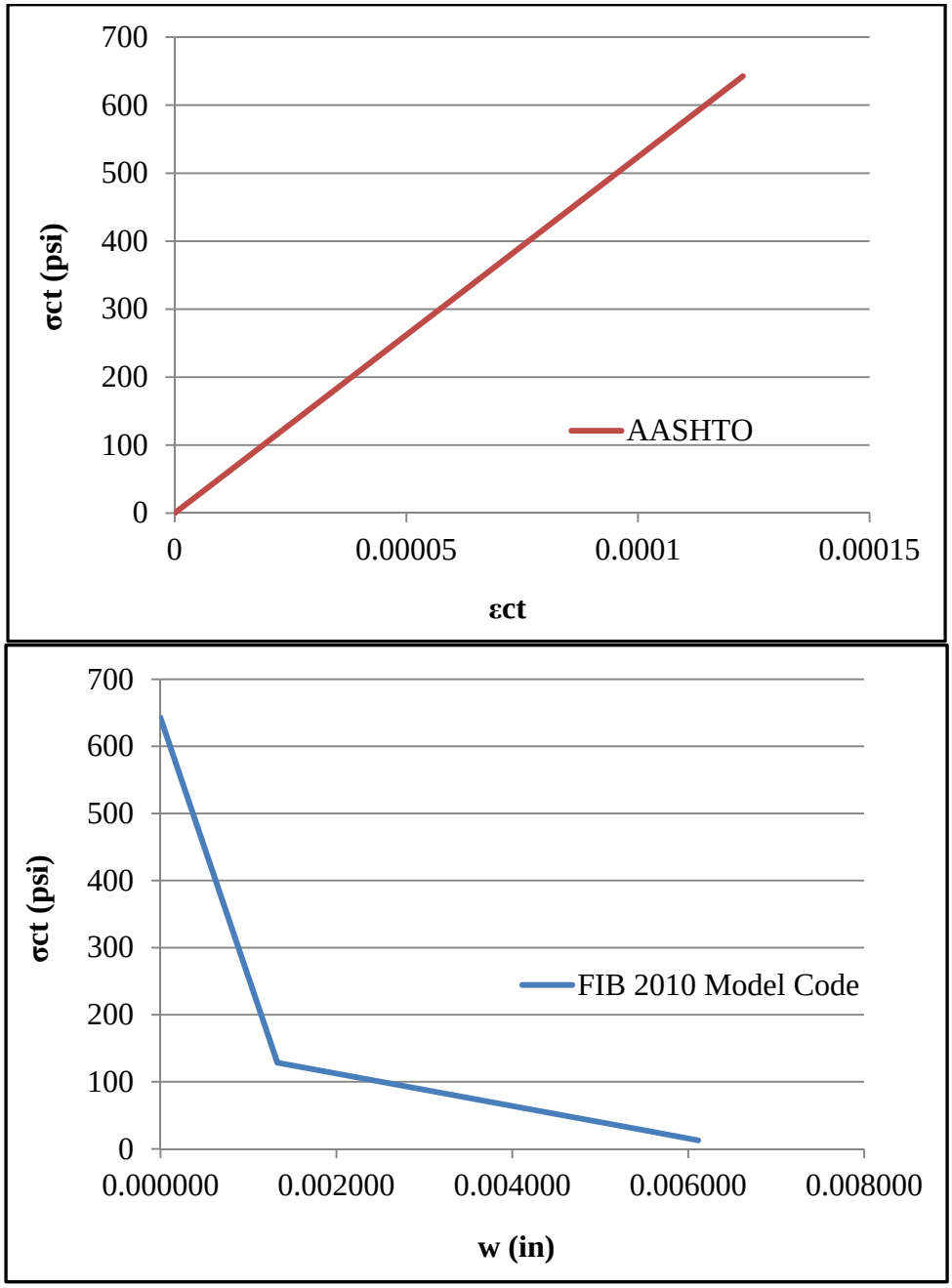

Figure 4-5. Tension Model Used in Abaqus: top = before cracking, bottom = post cracking. (initial behavior depends on strain, ε; post cracking depends on crack width, w)

4.3.1.3 Concrete Plasticity Parameters for Tension and Compression

There is another aspect in the definition of the concrete damaged plasticity model needed to define flow potential, yield surface, and viscosity parameters.

Dilation angle is the increasing change in volume of concrete under triaxial compression with low confining pressure or under uniaxial compression in the plastic range due to cracks growing parallel to the compressive stresses (23). The value of dilation angle for the girder concrete was picked as 31 degrees based on the previous work of Bae (24).

The eccentricity is the rate of function converging asymptotically (14). The default value is used for eccentricity which is 0.1. This value indicates that dilation angle is the same for a wide range of pressure stresses.

To define yield surface, f_{bo}/f_{co} and K values should be input to use the yield function proposed by Lubliner et. al. (20) but modified by Lee and Fenves (21) in order to include various strength in tension and in compression. f_{bo}/f_{co} is the ratio of initial equibiaxial compressive yield stress to initial uniaxial compressive yield stress, and again 1.16 is used - which is a suggested default value.

K is the ratio of the second stress invariant on the tensile meridian to that on the compression meridian. It should be in between 0.5 and 1.0, and a default value was used, which is 2/3 (Figure 4-6) (14).

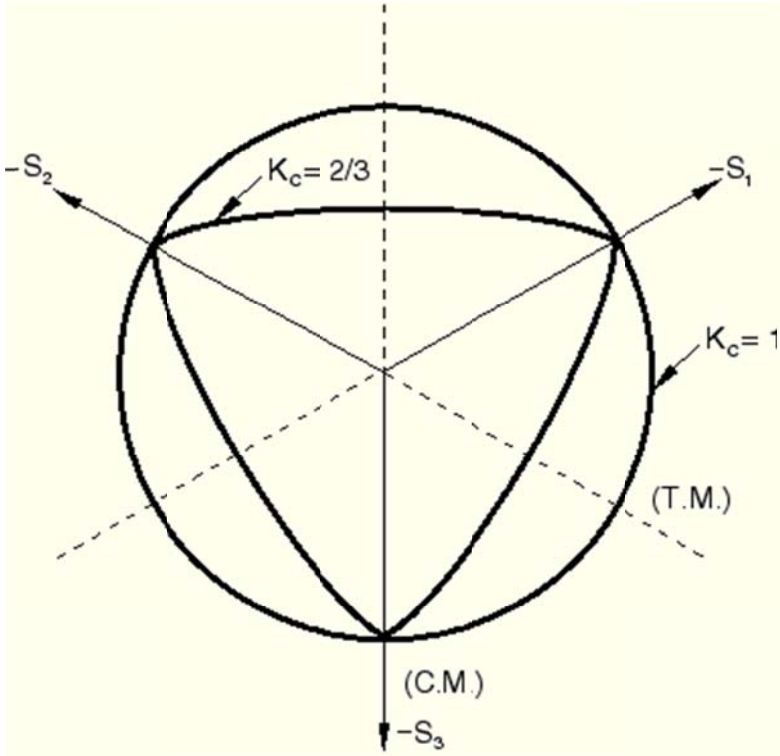

Figure 4-6. Yield surface in the deviatoric plane corresponding to different values of K

Lastly, concrete damaged plasticity uses viscoplasticity to overcome difficulties in implicit analysis caused by softening behavior and stiffness degradation. This property makes use of viscoplastic constitutive equations to permit stresses to be outside of the yield surface by applying consistent tangent stiffness for softening material for small time increments. However, no convergence problems occurred during analysis so this regularization was not used.

All the parameters and their input values are tabulated in Table 4-2 below.

Dilation Angle	Eccentricity	f_{bo}/f_{co}	K	Viscosity Parameter
31°	0.1	1.16	0.67	0

Table 4-2. Plasticity input parameters for models.

4.3.2 Reinforcement Bar Material Properties

As mentioned earlier, the web reinforcing bars, to h/4 in from girder ends, should not exceed 20 ksi stress for splitting resistance according to AASHTO LRFD Bridge Design Specification (3), Section 5.10.10.1. The analysis of girders in the Abaqus models showed that the reinforcing bars resisting stresses were well below the yield stress. Therefore, the yielding of reinforcing bars was not considered and they were modelled with linear elastic material. Modulus of elasticity of steel was taken as 29000 ksi based on AASHTO LRFD Bridge Design Specifications (3), Section 6.4.1, and poisson's ratio as 0.3.

4.3.3 Strand Properties

The bond interaction between concrete and strands is very complicated. Previous authors have achieved working models, but with a maximum of four strands. Hence, the strands are actually excluded from the girder models and the bond force from the strands was directly applied to the concrete elements along the interface where the strands would be located and over the transfer length of the strands. Further description of the strand-to-concrete bond forces will be provided in a following section on loads.

4.4 Interactions

4.4.1 Bond Between Reinforcing Bar and Concrete Bond

The rebar elements were modelled as embedded in concrete, meaning that concrete elements restrain the translational degree of freedom of steel elements. When concrete reaches its cracking capacity, the concrete deformations increase because of the strain

softening along with stress capacity drop. Then, the force that was in the concrete should pass to steel bars with a redistribution of strain. In this way tension stiffening is implicitly defined in Abaqus models by including in the concrete material property.

4.4.2 Interaction Between Girder and Formwork

For the interaction between the girder bottom and the bed or formwork, a “Surface-to- Surface contact” was preferred with small sliding formulation. In real life, the girders slide over the formwork, due to elastic shortening, while the formwork stays still. Therefore, the tangential behavior was set to be frictionless, on the other hand, the normal behavior was modelled as “Hard” contact but allowed separation after contact. Thus, the girder is initially supported on the formwork, but is allowed to lift off as camber develops during de-tensioning.

4.5 Boundary Conditions

The model is reduced by one fourth to decrease the computer running time because of symmetry, so the boundary conditions should be represented to account for the symmetry. For that purpose, symmetric boundary conditions were applied at mid-span about a vertical plane perpendicular to the length of the girder by setting all displacements in the longitudinal direction to zero. Further symmetry required that displacements in a transverse direction at mid-width be equal to zero as in the Figure 4-7. The x-axis in the Figure is a transverse axis perpendicular to the length, the y-axis is vertical, and the z-axis is along the length of the girder. Setting the displacement to zero will automatically set the rotations in the plane

direction to zero, which should be the case because the three dimensional concrete elements do not have rotational degree of freedoms.

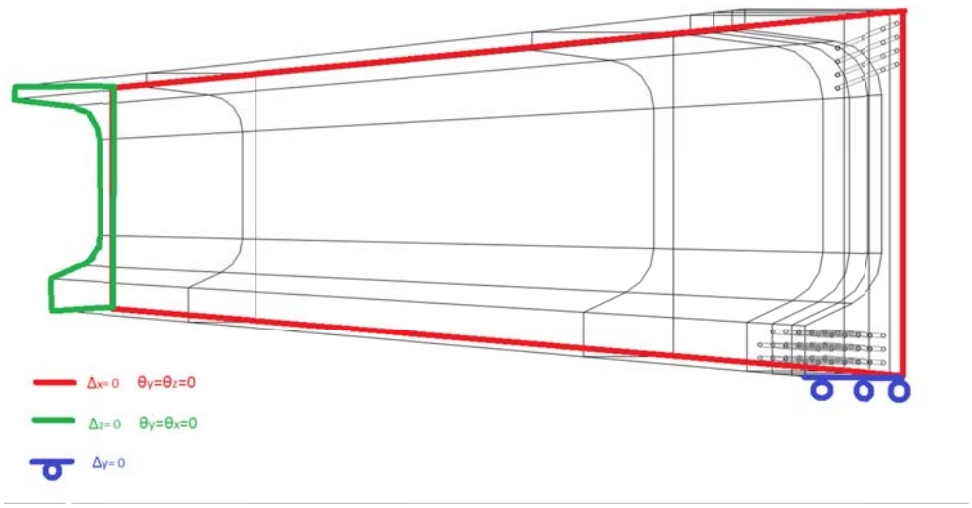

Figure 4-7. Boundary Conditions of models, mid-span section is at left, end at right.

The girder was assumed supported by the formwork vertically at the end, with displacements of the bottom flange equal to zero. The bottom at the girder end was restrained to zero displacement in the vertical or y direction so that the girder is free for rotations and for longitudinal deflection while cambering up. Also, for the rigid formwork, the reference point was restrained to displacement and rotation in all direction.

4.6 Loading

Right after the strands are cut, cracks were observed in the girder without service loads. Hence, only prestress force and the girder self-weight are considered in the finite element models.

Prestressing force is applied to the girder once the strands are cut. The actual transfer of the prestress is achieved by chemical bond, friction and mechanical interlock over a limited distance, namely the transfer length. However, this length is not clearly understood and may differ for each girder. To find this length, explicit modelling considering interaction between strand and concrete would be required. That modelling might include springs, friction and cohesion to represent the mechanical, friction and adhesion bond effects (1) as well as the Hoyer diameter expansion. However, there is considerable uncertainty regarding values of the needed input parameters and those input parameters might change along the length and the location of strands. This type of modelling has not been proven or calibrated by other researchers when more than a few strands are present and is generally too complex to incorporate along each of the strands in a full girder model. That is why during the girder tests 3 strain gauges were put along the strands to measure the actual transfer lengths. With that information, the prestressing force can be directly applied to concrete without explicitly modelling both strands and interaction between concrete and strands. This method does, however, neglect the effect of the increasing strand diameter when released.

The transfer length is selected here as 60 strand diameters from the end by considering both the test results and the AASHTO LRFD Bridge Design Specification (3),Section C5.11.4.2, where the diameter of strands is 0.6 in. Therefore, the transfer length was calculated as 36 inches from the girder end.

The change in measured strand stress during de-tensioning for the 72W girders is shown by the curve in Figure 4-8 (and its derivation will be described later). The graph was idealized as linear between the data points where the strand strain was measured. Therefore,

the graph was redrawn piecewise linear in Figure 4-9 and the bond stress between concrete and strand could be assumed to be constant (equal to the graph slope) between the data points as in Figure 4-10.

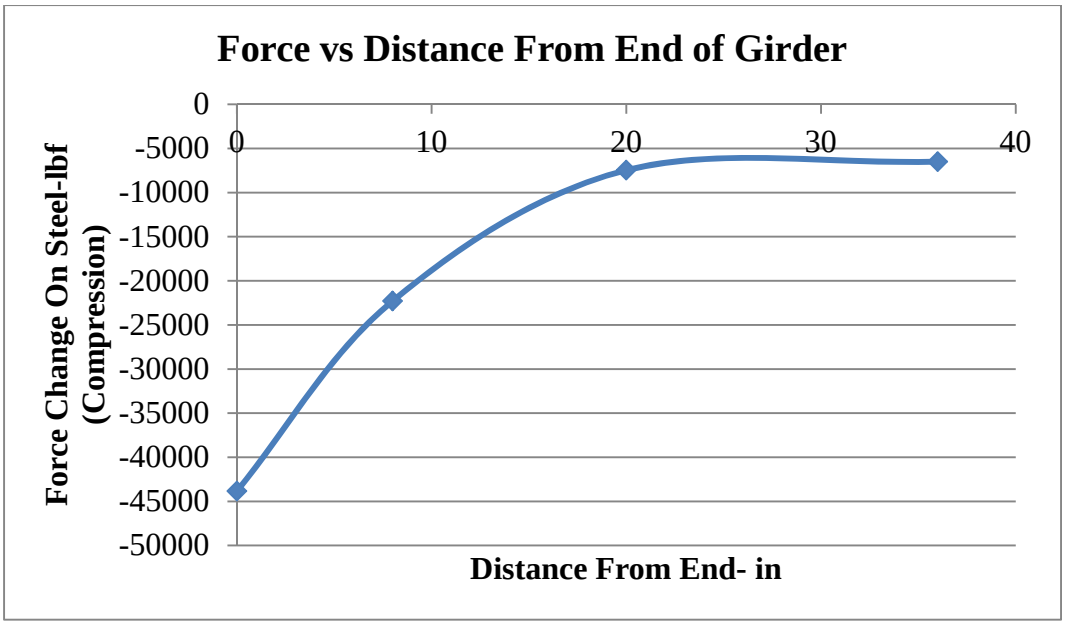

Figure 4-8. Measured prestressing force change in strand versus distance from end for 72W girder.

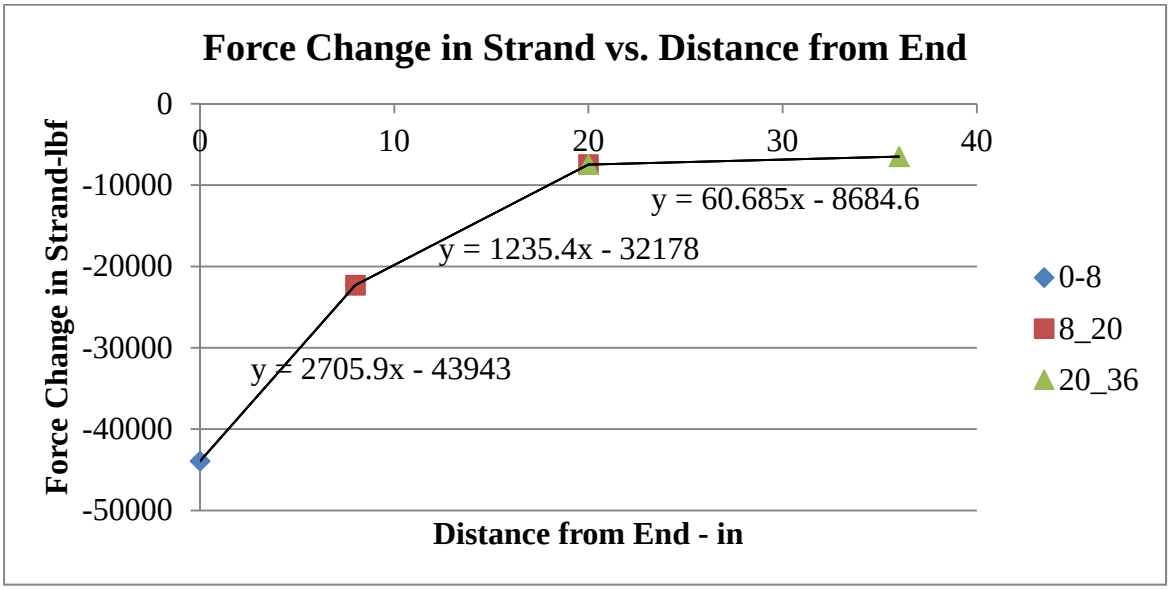

Figure 4-9. Prestressing force change in strand versus distance from end considering piecewise linear function for 72W girders.

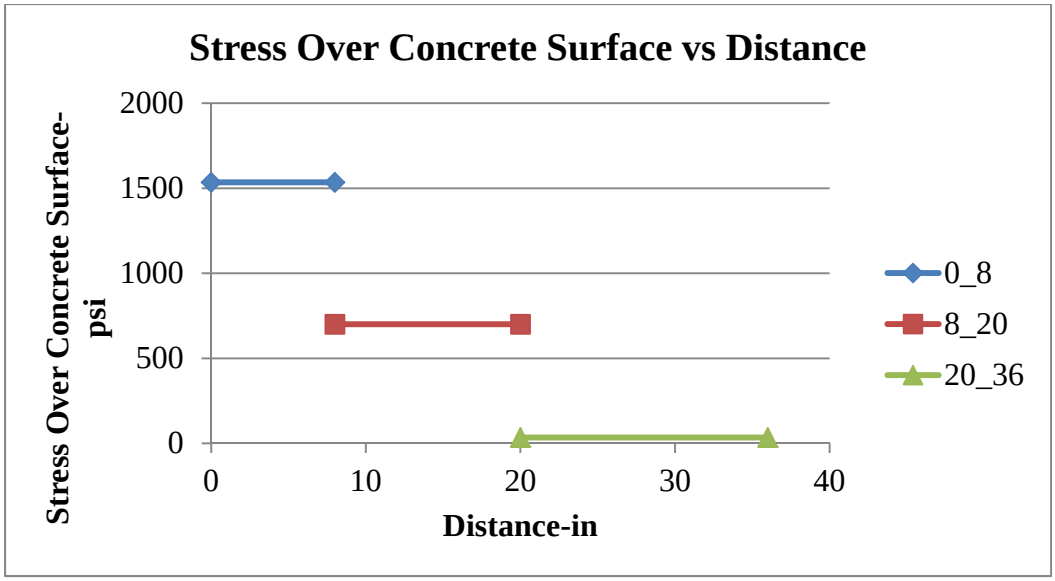

Figure 4-10. Surface traction force applied to concrete elements in models for 72W Girder.

Once the strands are cut, the girder will shorten due the compression stress in the concrete, which is called elastic shortening. The loss of the initial tension in the strands

causes a radial expansion because of Poisson's effect, which helps the locking of strands to concrete but causes outward pressure to concrete that might be excessive. This phenomenon is known as the Hoyer effect (25). To represent outward expansion Okumus (1) built a model in which both concrete and strands are shell elements and then applied positive thermal expansion for a corner strand where concrete cover is the least. From models she found out that the stress error in neglecting the Hoyer effect was small and will be ignored here.

The time dependent effects like creep, shrinkage, etc. were excluded because the cracks of interest form during de-tensioning which consumes less than an hour of time. The dynamic effects due sudden cutting of strands were also ignored. However, at the draped strand hold-down location a point load was applied to the girder as a vertical force since the actual hold down is released during the de-tensioning process.

Lastly, the effect of gravity load was included in the models. The models are resting on rigid formworks and the prestressing will camber the girders up but the gravity girder self-weight will bring the camber down. The self-weight reaction would create compression at the end edge of the girder. In the plants, a steel plate is often put to decrease this concentrated force effect and to lessen additional cracking due to the friction caused by the sliding of girders while elastic shortening and camber occurs. For this purpose, a bearing pad was placed at the bottom of girder to distribute vertical reactions and allow sliding.

4.7 Finite Elements

4.7.1 Concrete Elements

The shape of girders, the reinforcing steel, and the holes for strands increase the irregularity of the girder so hexahedral elements that are more computationally effective could not be used with the automated meshing properties of Abaqus. Instead, tetrahedral elements that are effective for filling irregular shapes were used for the nonlinear region. Those are 4 node, first order interpolation elements and defined as C3D4 in the Abaqus Library. For the linear region, 6 node triangular prism elements (C3D6) were utilized as shown in Figure 4-11.

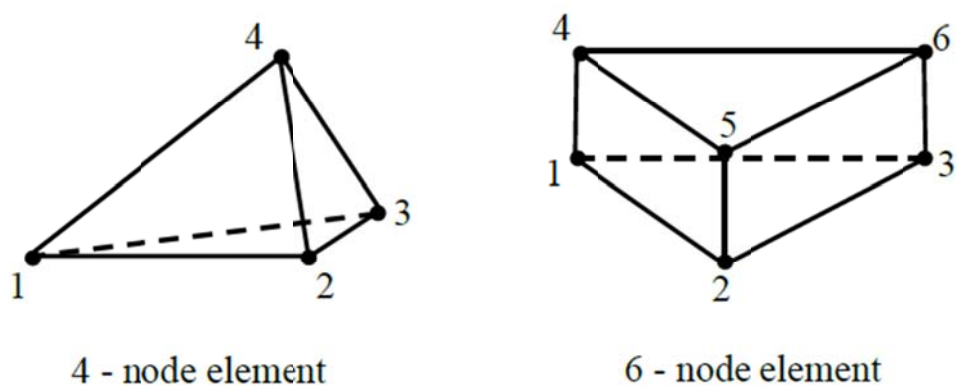

Figure 4-11. 4 node tetrahedral and 6 node triangular prism elements

According to the Abaqus Theory Manual (14), second order elements are generally better than first order elements for elasticity problems but small refinement is needed. However, for plasticity problems first order elements are generally preferred. Besides, the

computation takes a lot of time and results are almost similar. Hence, first order elements were used.

4.7.2 Steel Reinforcement Bar Elements

For simplicity, the reinforcing steel bars were modelled as 2 node linear trusses (T3D2) in Figure 4-12.

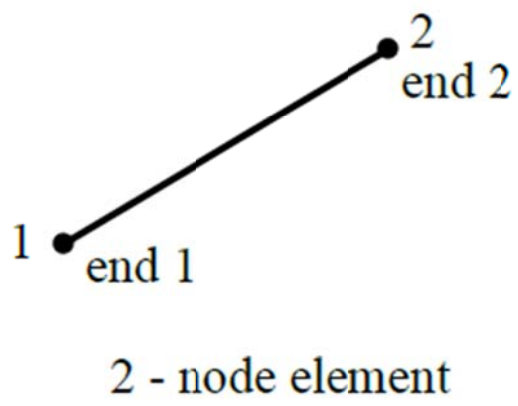

Figure 4-12. 2 Node linear Truss elements

4.8 Meshing

Using nonlinear material properties considerably increases the computational time. Even though a finer mesh will give more accurate results, it is not reasonable due to the large time requirements associated with computation. Therefore, a finer mesh was utilized only for the area of interest, i.e. the nonlinear girder end zone, in order to get reasonable results. However, in the linear zone the element sizes were gradually increased up to mid-span as visible in Figure 4-13.

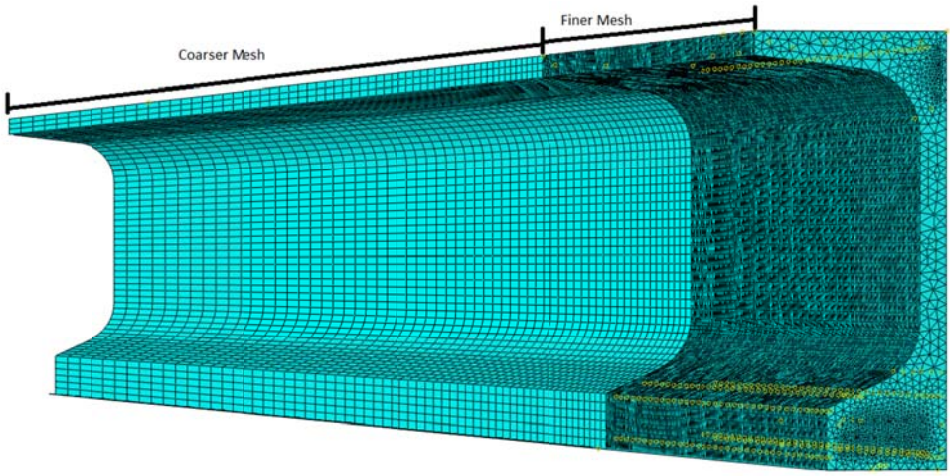

Figure 4-13. Mesh example of 54W girder.

There is an error indicator in Abaqus to judge the accuracy of a model with different mesh sizes. However, these errors are not errors in strains or stress. Okumus (1) found out that if the models are built with 1.2- 1.5 inch mesh size, the error and CPU time are reasonable. Therefore, maximum 1.2 inch tetrahedral elements were used for the inelastic region, as are the re-bar elements for compatibility.

4.9 Solution Method

In each step, the equations were set to be solved with a direct method rather than an iterative method, because the iterative method applies approximate solutions for system equations. Once convergence is likely, the iterative method is faster than the direct method but otherwise, it takes lots of time and the origin of any problems cannot be easily found (14). Moreover, a Full Newton solution method was utilized for the analysis.

Abaqus allows users to change the initial increment for load steps to avoid unnecessary iterations. For that purpose, the initial increments of steps which are observed to have cracks or nonlinear behavior were decreased to accelerate the analysis.

4.10 Assumptions, Simplifications and Limitations

To save time and disk space, some behavior of the girder ends is either ignored or simplified. As mentioned before, one of the aims of this study is to create a correct FEA model but the main goal is to locate the cracks and to find a method to prevent them.

Finite element modelling is by nature an approximate representation of real behavior and some errors are inevitable, particularly while simplifying the boundary conditions, material properties, etc. The accuracy of the models can be checked with data taken from measurements in girders at precast plants as described in the next chapter.

<u>Some assumptions, simplifications and limitations are as follow:</u>

- The transfer length of all strands was kept the same regardless of their location. Even though the length may change according to the location and confinement, AASHTO LRFD Bridge Design Specification allows use of an assumed single length.
- Bottom flange stirrups are epoxy coated but they are assumed to have the same perfect bond behavior as bars without an epoxy coat. Also, bar slip was not simulated.
- Strains induced by creep and shrinkage, and thermal change were ignored during the short interval for de-tensioning. These strains would be negligible, especially when compared to strains introduced by the prestressing.

- The bond loss between strand and concrete was ignored.
- Any dynamic loading effect due to sudden cutting of strands was ignored as it depends on multiple factors that are not well known.
- The restraint on the girder provided by uncut strands while releasing others was neglected. This restraint has been found in some circumstances to cause vertical cracks across the bottom flange width at the end (26). Vertical cracks were not observed in any girders at the precast plants.
- The values of compression strength used in the analysis were taken from the cylinder tests at the time of prestressing. Therefore, those values are not 28 days strength. However, all constitutive equations taken from AASHTO LRFD Bridge Specification or FIB Model Code 2010 and used to normally predict material properties are intended for 28 day concrete strength.
- Radial expansion of strands was not considered because the contact properties between strand and concrete are very complex and may change according to location of strands.

5 TEST AND FEM MODELS FOR 72W GIRDER

The ends of prestressed concrete bulb tee girders fracture because of the transfer of prestress to slender concrete sections and those cracks are a concern for the sustainability of the structures. There are several methods to control cracking such as increasing the area of the first five web bars, changing strand cutting order, lowering or spreading harped strands, debonding some of the strands at the ends of girders, etc. However, most of them are only effective in reducing or eliminating one type of crack except for debonding of strands (Table 5-1). Debonding seems to be the best methods to restrain all types of cracks according to previous research of Okumus (1) based on finite element analysis.

With that understanding, the effectiveness of debonding was tested on an actual 72W girder. An AASHTO rule is that only 25% of total strands can be debonded. The columns of strands close to the mid-section were left bonded at the ends. To evaluate just the effect of debonding, all other properties of a normal bonded girder and an unbonded 72W girder were kept the same except the number of strands bonded at the ends.

Control Method			Inclined Cracks	Web Cracks	Y Cracks
1	Increase in Reinforcement Area of	The closest two bars	MILD	MODERATE	NONE
2		Bars further away	NONE	NONE	NONE
3		Bottom flange stirrups	NONE	NONE	NONE
4	Debonding Some Strands at the End		HIGH	MODERATE	HIGH
5	Debonding All Strands for 12in from the End		MILD	HIGH	HIGH
6	Change in Strand Cutting Order		NONE	NONE	MODERATE
7	Draped Strands	Removed	HIGH	NONE	NONE
8		Lowered	NONE	MODERATE	NONE
9		Lowered & Spread	HIGH	MODERATE	NONE
	Combination of 1 and 4		HIGH	HIGH	HIGH
	Combination of 5 and 9		HIGH	HIGH	HIGH

HIGH = can eliminate cracking MILD = can reduce strains

MODERATE = can reduce strains significantly NONE = has negligible impact

Table 5-1. Crack control effectiveness of the methods that Okumus (1) examined for 54W girders.

5.1 Girder Properties:

The two girders were chosen from girders of span 6 (largest span) on a WisDOT project, a fourteen span bridge on Wisconsin Highway 96, in Wrightstown, Wisconsin (Structure number:B-5-381, and project number: 4075-28-71 (15)). Each span has seven identical 72W girders. The two test girders are 72W pretensioned girders manufactured at Spancrete, Inc. in January, 2015. The reinforcement for these girders is as shown in Figure 5-1.

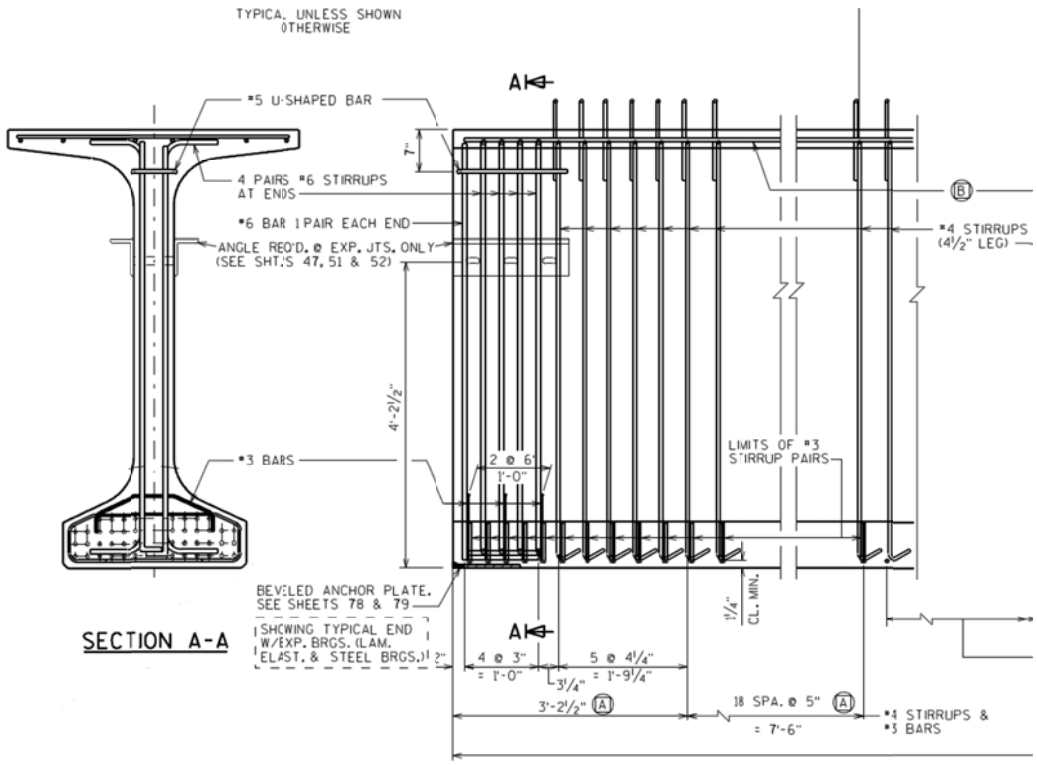

Figure 5-1. 72W cross section and reinforcement details of end zone.

WisDOT uses three different types of reinforcement bars in these girders. #6 reinforcement bars make up the first five vertical web bars with 4.25 in spacing; after the first five web bars #4 U-shaped welded wire meshes with 4 inch spacing are used in the web; and finally, #3 epoxy coated re-bars for bottom flange bursting stirrups.

Both test girders were 154.75 ft. long, and had 2109 kips total initial prestressing force. The normal bonded girder had 8 draped and 40 straight, 0.6in diameter, 270 ksi low relaxation strands (Figure 5-2), on the other hand, the debonded girder was redesigned in compliance with the AASHTO LRFD Bridge Design Specifications (3) 5.11.4.3. The Specification limited the number of debonded strands to 25% of the total number of strands. The debonding was designed with lengths of $90d_b$ between three sets of srands that were

bonded at staggered distances from the girder end (where d_b is the diameter of strands) as detailed in Figure 5-2. The de-bonded girder had 12 de-bonded strands with debond lengths of 4.5 ft., 9.0 ft. and 13.5 ft. from the girder end for sets of four strands each. Also, two less draped strands were used in the debonded girder so the final configuration is 6 draped 42 straight strands, 12 of which were de-bonded as in the Figure 5-2.

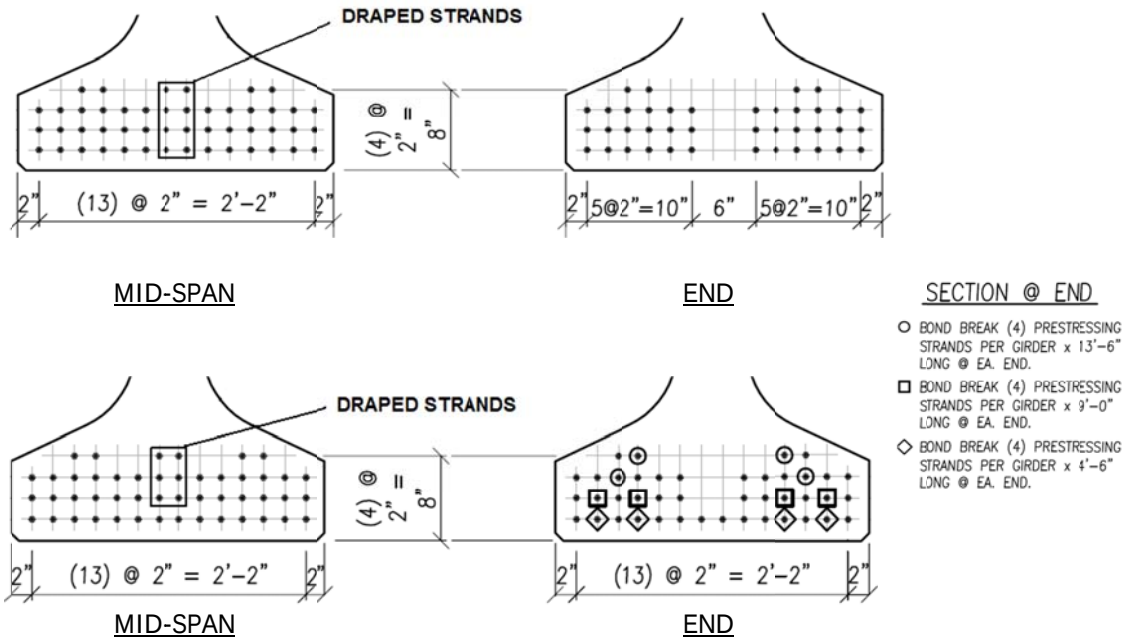

Figure 5-2. Bonded girder strand pattern (top) and de-bonded girder strand pattern (bottom).

The bonded prestressed girder is designed according to working stress design, i.e., concrete stresses should not exceed the allowable stress limits of concrete in compression and tension according to AASHTO. The concrete stresses in the 25% de-bonded girder were also checked to see that they remained within allowable limits. The initial measured concrete strength of the standard design (bonded) girder was 7808 psi prior to de-tensioning, and the initial measured concrete strength of the debonded girder was measured as 7015 psi.

Table 5-2 shows the expected concrete stresses at bottom and top fibers for various distances from the ends of the girders. Those results were compared with allowable stress limits of concrete in compression and tension which were calculated as $0.6*f_{Ci}$ for compression and $-0.24*(f_{Ci})$^0.5 for tension according to AASHTO. In calculations, elastic losses were included because they occur right after de-tensioning. Also, the stresses are a combination of stresses due to pre-tensioning and due to self-weight of girders assuming that the girders immediately camber upward at mid-span. Figure 5-3 and Figure 5-4 show these values plotted. All the concrete stresses at various locations satisfy the allowed AASHTO limits.

The effect of de-bonding on reducing concrete stresses close to the anchorage zone can be seen by looking at the maximum compression stresses in Table 5-2. Maximum concrete stress occurred 3ft. from the ends in the bonded girder. On the other hand, the maximum concrete stress was located at mid-span in the de-bonded girder because a staggered de-bonding pattern distributed pre-stressing force over a larger transfer length compared to applying all the pre-stressing over a short transfer length as in the case in of the bonded girder.

Type:	distance -ft.:	0	3	6	9	12	15	30	60	77.38	All. Stress Limit
Bonded	Bottom Stress	0	4.066	3.993	3.925	3.862	3.805	3.602	3.605	3.857	4.685
	Top Stress	0	0.006	0.085	0.157	0.224	0.284	0.501	0.497	0.229	-0.265
25% debond	Bottom Stress	0	3.024	2.935	3.307	3.667	3.595	3.730	3.585	3.751	4.209
	Top Stress	0	0.033	0.127	0.092	0.070	0.146	0.365	0.519	0.342	-0.251

Table 5-2. Concrete stresses (ksi) in both bonded and de-bonded girders.

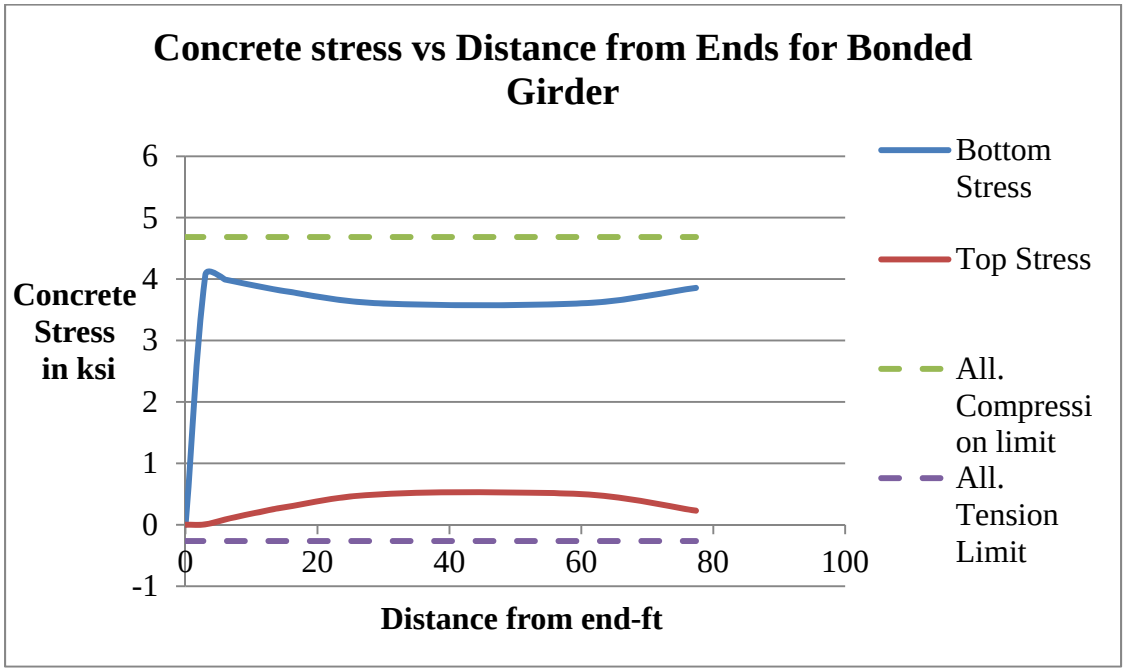

Figure 5-3. Concrete stress vs Distance from Ends for Bonded Girder.

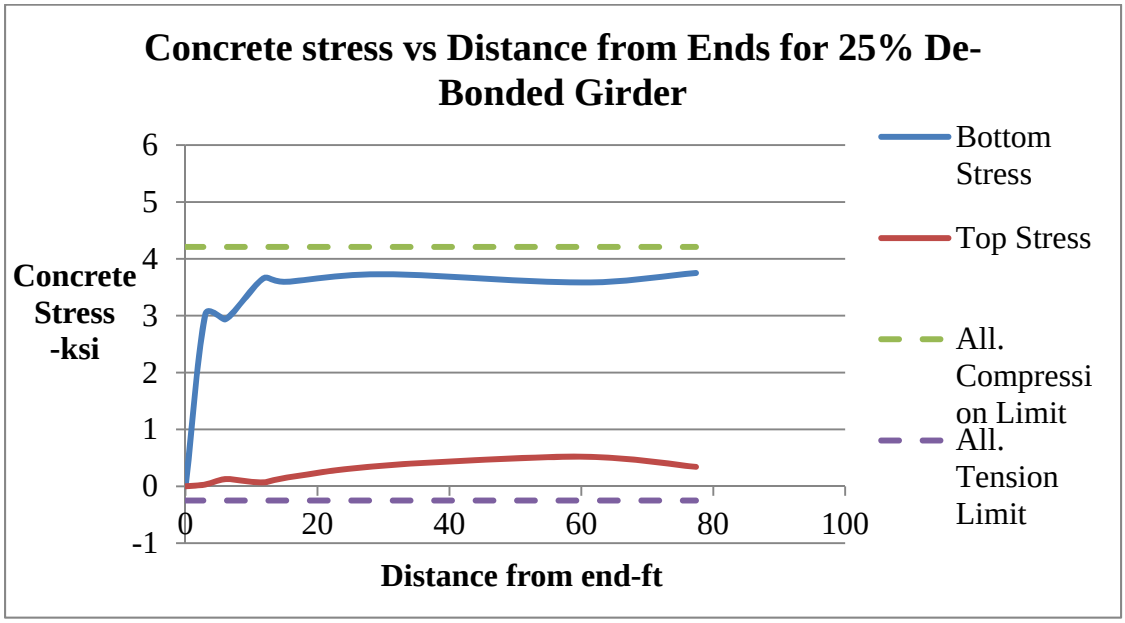

Figure 5-4. Concrete stress vs Distance from Ends for De-bonded Girder.

The debonding is achieved by just placing plastic sheathing around strands as in Figure 5-5. Even though this type of debonding is assumed to debond the strand from the concrete, there may be some transfer due friction but it is small compared to the force transferred by bonding, therefore, this was ignored.

Figure 5-5. Plastic shield around strand for de-bonding.

There were two large hydraulic jacks to tension and de-tension the strands in the Spancrete Plant, one for stressing the draped strands and the other one is for straight strands. When the girder is ready to detension, the force in the hydraulics is gradually released. However, this procedure is not done continuously. The pressure from the jacks is released in an amount equal to the tension in two strands. Then two strands are flame cut at the girder ends. This process is repeated. Strands are cut according to a specific sequence as in Figure 5-6. In this figure the strand locations are represented as a number, and those numbers denote the cutting sequences for each strand set. Note that, the strands are cut by pairs of two to preserve symmetry about a vertical (y-) axis. Also, the numbers represent the step number in which prestress force will be applied to concrete finite elements in a subsequent associated analysis procedure. One difference, however, is that in the analysis the prestress force of all

draped strands was applied in one step as if all were cut at once. Note that in the bottom flange the strands were cut proceding from the outside of each row and moving inward.

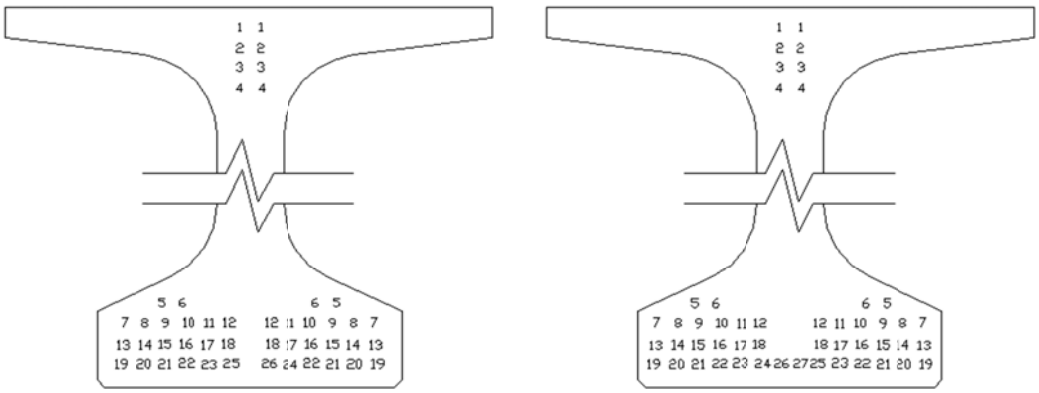

Figure 5-6. Strand cutting order for bonded girder (left) and debonded girder (right).

5.2 Instrumentation:

To obtain information about the strains in both the concrete and steel in the cracking zone, two different gauge types were placed inside of both girders: foil strain gauges and vibrating wire gauges. All the locations for the gauges were selected according to results from an initial analytic model of the girders. Therefore, all gauges were placed where highest tensile strains were expected (crack locations). To compare the effectiveness of debonding, all the gauges were put in the same positions in the normal and debonded girders.

On steel bars and tendons, 3 mm and 1 mm, 350Ω or 120Ω foil strain gauges (15) were used respectively to obtain strain data. These gauges were glued on to the steel re-bar surfaces oriented parallel to the length of the re-bars. To protect the gauges from aggregate

damage during casting, moisture proof and cushioning protection was applied around them (Figure 5-7).

Figure 5-7. Strain Gauge on re-bar (left), and after water-proof (right).

Before strand detensioning began, these gauges were attached to a data acquisition system set to scan the gauges every two and half seconds to collect data. Three of the gauges were put on one strand at different distances from the girders' end to measure the prestress transfer length. Thirteen other strain gauges were mounted on reinforcing bars. Detailed locations can be seen in Figure 5-8 and Figure 5-9.

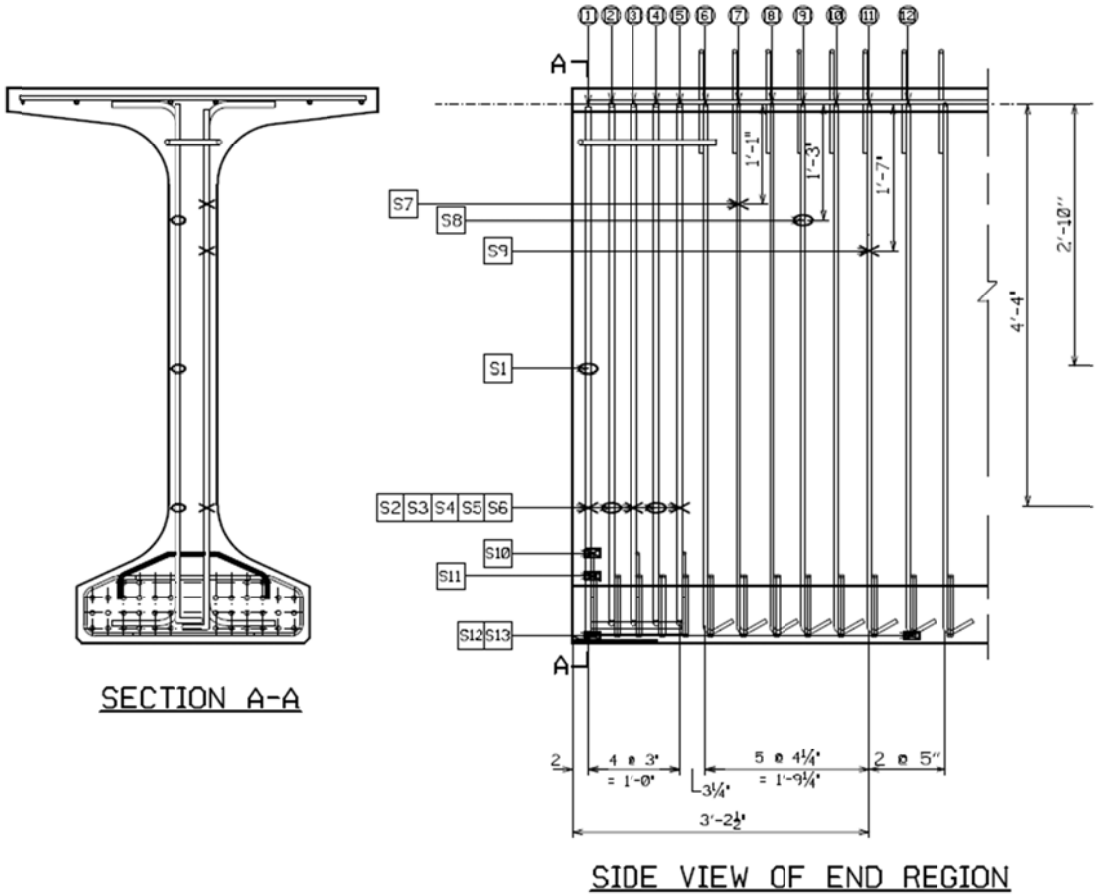

Figure 5-8. Locations of strain gauges at re-bars.

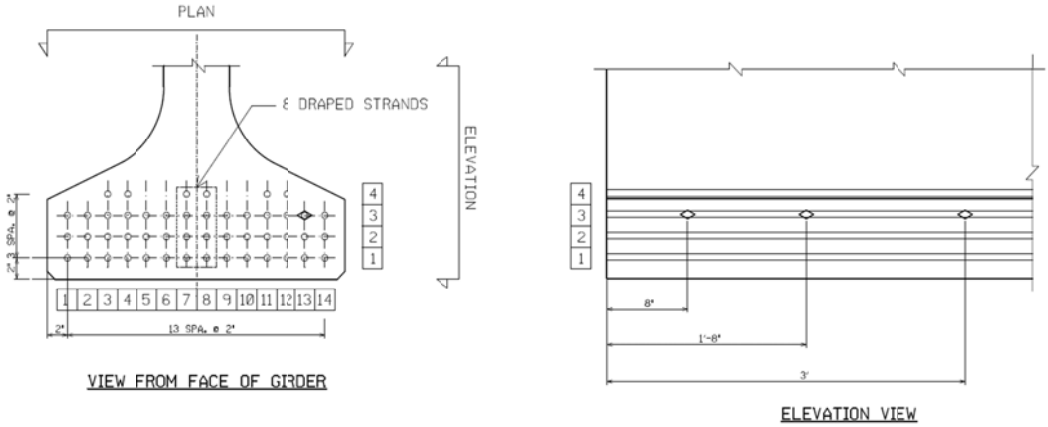

Figure 5-9. Location of strain gauges at strand.

The other gauge type used was 2” and 6” length Geokon Model 4202 vibrating wire gauges (27). These type of gauges were placed across the expected location of cracks (from analyses) so that strains in concrete during cracking could be observed. Locations and orientation can be seen in Figure 5-10.

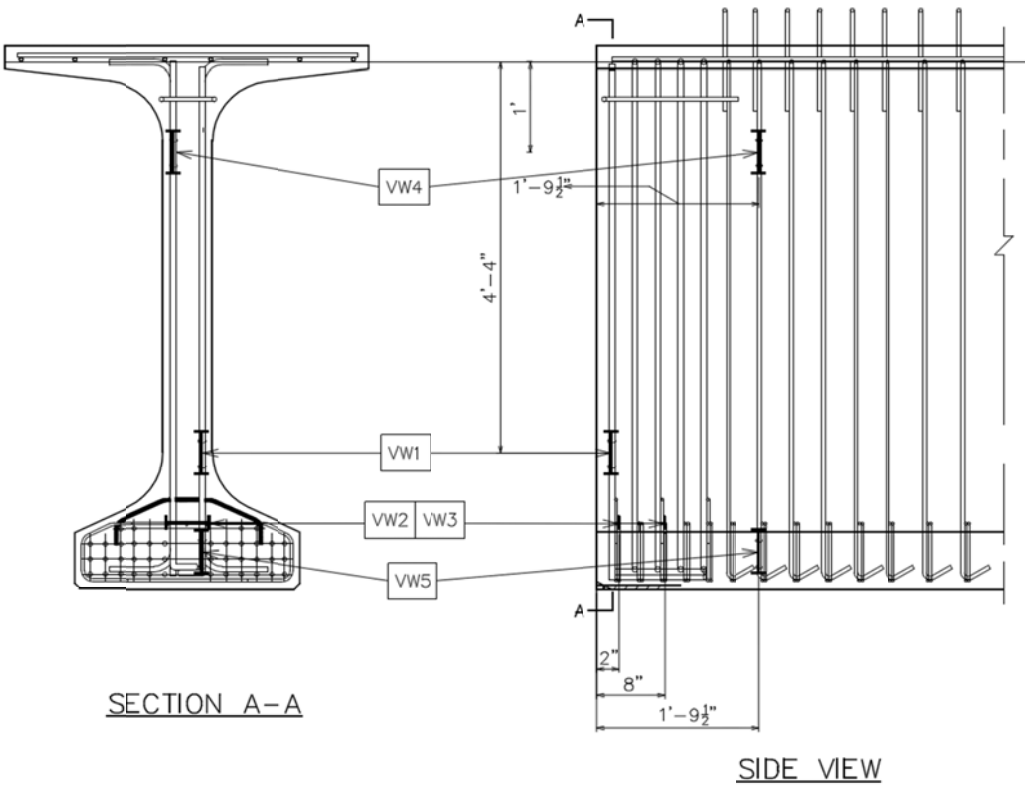

Figure 5-10. Vibrating Wire Gauge Locations.

Readings from these gauges were taken after each row of strands was cut, except for draped strands. Only one data reading was taken after all the draped strands were cut.

5.3 Test Data & Discussion

Data that will be represented below for all gauges was collected during stress release of the tendons. Just after erection on the bridge, one more reading from the vibrating wire gauges was taken. Unfortunately, the wires of the strain gauges were burned during cutting of the strand stubs so a final erection reading of strains in reinforcing bars could not be observed.

5.3.1 Gauges on Strands

The foil gauges were 1 mm (0.04 in) in length FLA-1-11-5LT type, glue on gauges (27). They were put exactly at the same location in both girders (please refer to Figure 5-9 for the locations of gauges). The purpose of these gauges is to estimate the transfer length of strands having no shielding at the end zone, and to use this information in modelling of girders in the Abaqus software program. No gauges were placed on one of the debonded strands because the plastic used for shielding was extending well into the girder (a minimum of 54 in from end). The final strand strain results, after all strands were cut, are shown below in Figure 5-11 and Figure 5-12 for both bonded and 25% de-bonded girders and are also listed in Table 5-3.

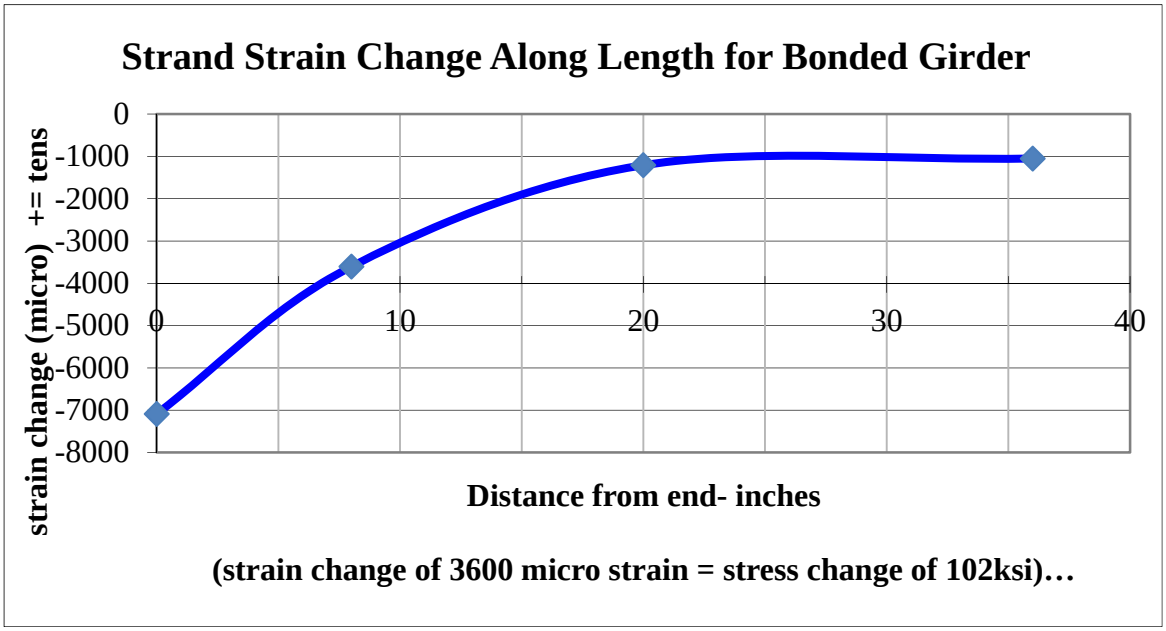

Figure 5-11. Strand test data for bonded girders.

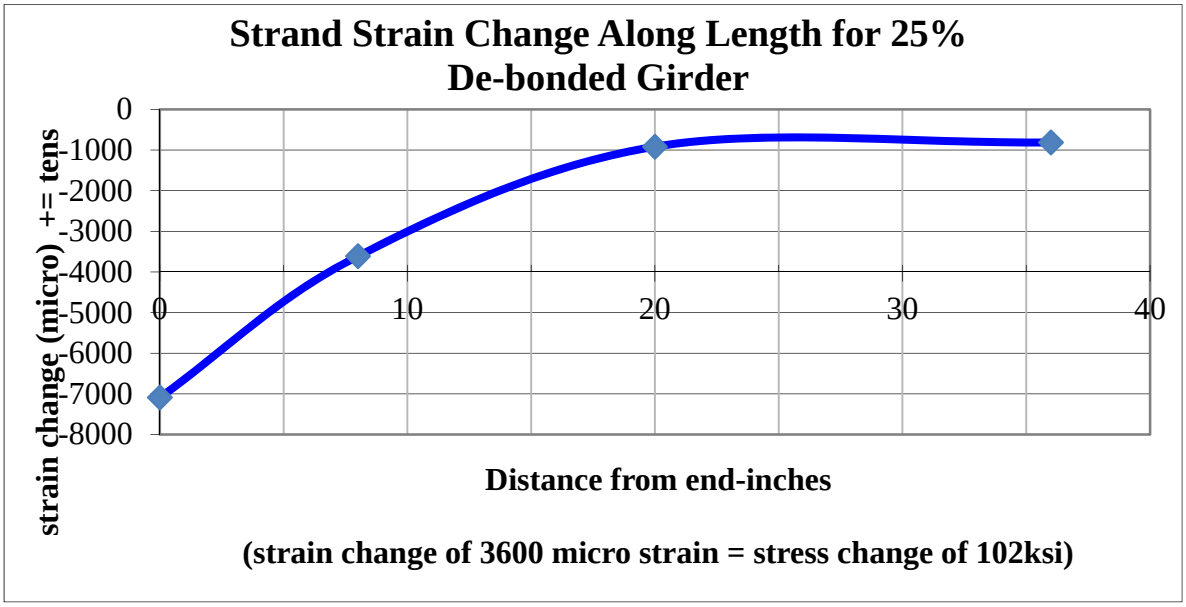

Figure 5-12. Strand test data for de-bonded girders.

Strain Change in Strand on Release (Micro inches, - = comp.)			
	at 8 inches	at 20 inches	at 36 inches
Bonded Girder	-3605	-1208	-1051
25% Debonded	-3611	-916	-811

Table 5-3. Strain Changes at Designated Strain Gauge Locations

The strain-distance diagrams in Figure 5-11 and Figure 5-12 are not linear but curve so the uniform bond stress assumption of the AASHTO LRFD Bridge Specification along the transfer length does not actually occur in this case. The strain change appears to reach a constant value after approximately 20 to 25 inches – which may be an effective transfer length. This length, however, should be shortened by 4in. to account for the lack of bond where protective coatings were placed over the gauges. To model the bond stress in the finite element analysis model, the strain diagrams were predicted to have a piece wise linear shape with a constant (but different) bond stress in between the gauge location with segments as shown in Figure 5-13 and Figure 5-14.

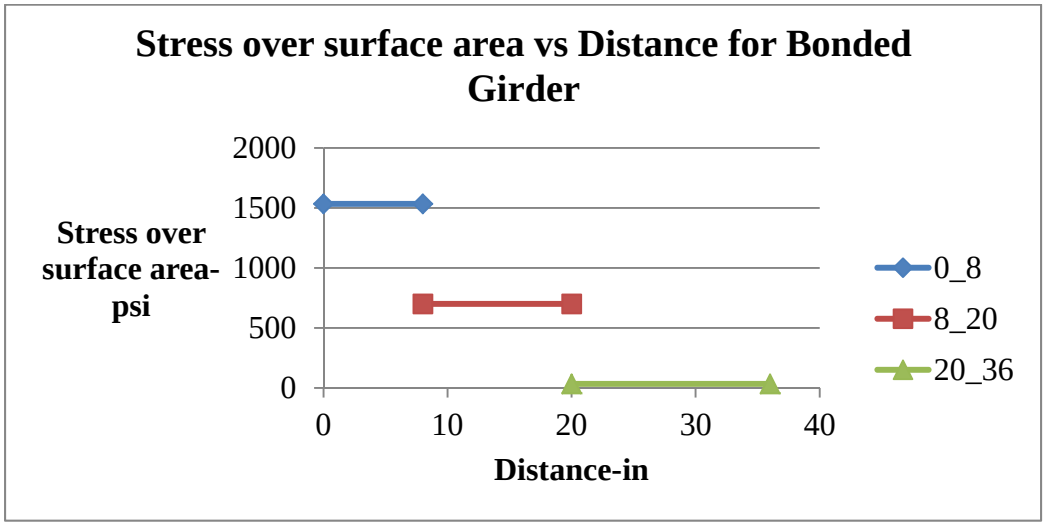

Figure 5-13. Bond Stress vs distance from ends of bonded girders.

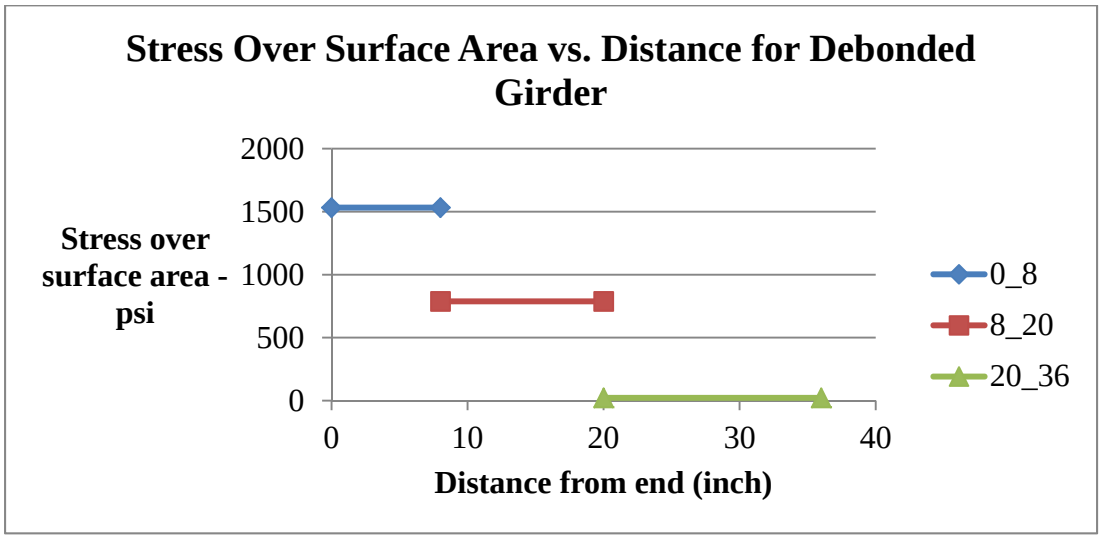

Figure 5-14. Bond Stress vs distance from ends of debonded girders.

The stress change between 20in. and 36in. from the end is small (23 psi for bonded and 32 psi for de-bonded girder), meaning that the transfer length could be assumed to be 20in. whereas the 36in. transfer length proposed by AASHTO was used in the analytical girder models.

5.3.2 Strains in Reinforcing Bars

Strains were continuously measured during de-tensioning. To interpret the results between girders, the strain data is divided into three categories, and labelled as “strain change of reinforcing bars in horizontal crack region, 20” up from bottom (gauges S1,S2,S3,S4, S5 and S6)”; “strain change of reinforcing bars in inclined crack region, near top (gauges S7, S8 and S9)”; and “strain change of reinforcing bars in Y crack region: bottom flange stirrup bars (gauges S10, S11, S12 and S13)” (Please refer to Figure 5-8 to see the details of locations).

This strain data was partially collected to confirm the accuracy of an analytical model in Abaqus software. After the model is complete, this data and data from the model will be compared. Also in all of the rebar plots, a strain of 690 με corresponding to the 20 ksi limit on splitting zone reinforcement of AASHTO LRFD BDS 5.10.10.1 for crack control, is also shown.

5.3.2.1 Strain Change of Reinforcing Bars in Horizontal Crack Region

The data plots are below in Figure 5-15 and Figure 5-16. The aim of these gauges is to capture high strains that would indicate formation of the horizontal crack right at the junction between the web and bottom flange (S2, S3, S4, S5 and S6), and along the web (S1). Therefore, the gauges showing large tensile micro strains probably are in the location of cracks. Strains in reinforcing bars exceeded the AASHTO limit, even though the splitting reinforcement was designed to meet AASHTO.

In the plots, the effect of de-bonding can be seen. In bonded girders, all the tension strain values are approximately 200 micro strain larger than in the de-bonded girder because

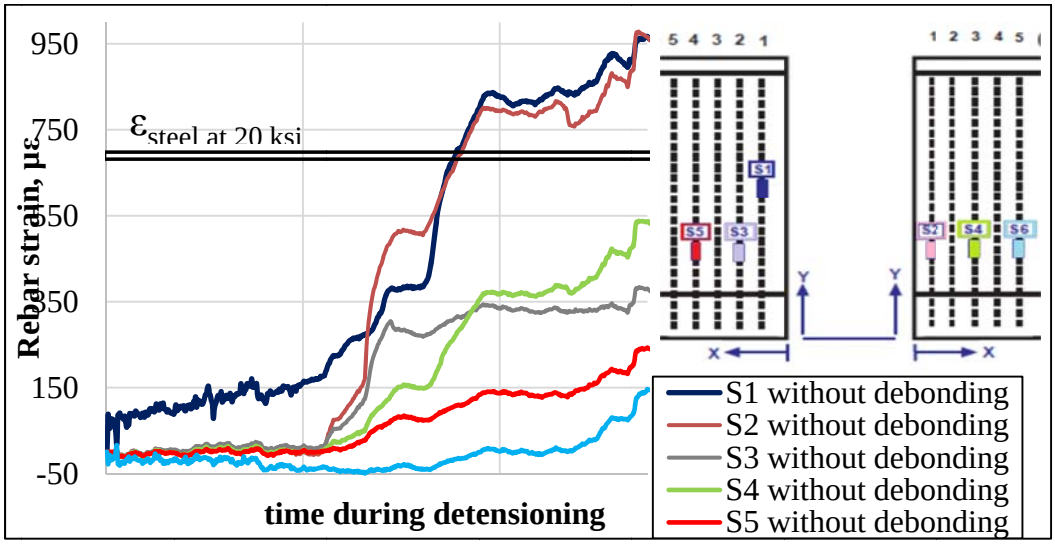

Figure 5-15. Bonded girder: Strain change of reinforcing bars in horizontal web crack region, most are 20" up from bottom (gauges, S2, S3, S4, S5 and S6).
(Tension positive, compression negative)

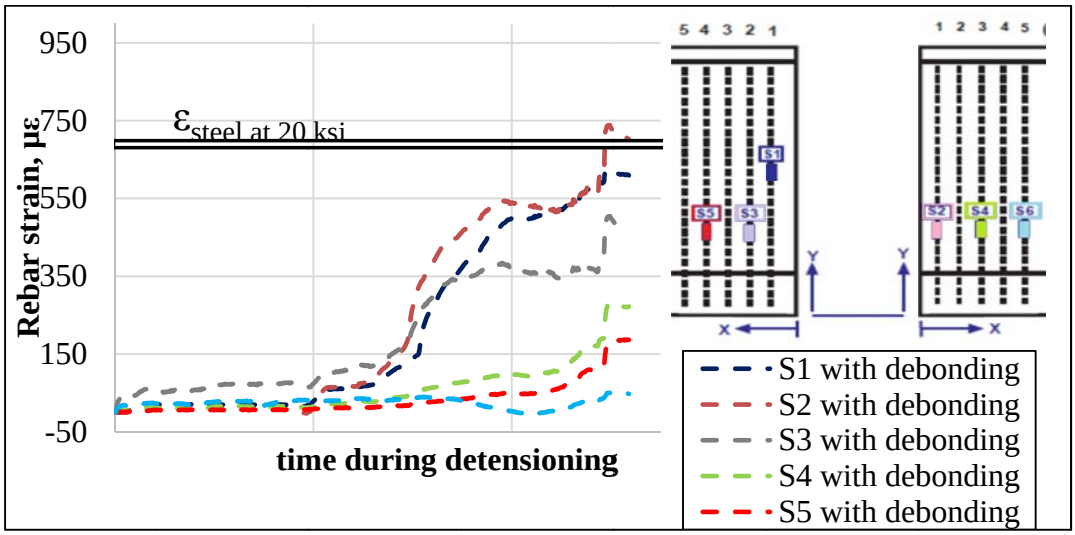

Figure 5-16. Debonded girder: Strain change of reinforcing bars in horizontal web crack region, most are 20" up from bottom (gauges S2, S3, S4, S5 and S6).
(Tension positive, compression negative)

de-bonding increases the transfer length, reducing the compressive and tensile strains in the concrete. Only the strain in S3, the one around the web cracking region, increased with de-bonding but it is not in a critical region.

The strains in the vertical web splitting reinforcement are maximum for the bar closest to the girder end, and rapidly decrease for bars away from the girder end. It is questionable whether more than the first two to four bars are providing any advantage. Moreover the outer bar, with gages S1 and S2, in the bonded girder seems to just exceed the 20ksi limit even though it was designed to meet the AASHTO splitting reinforcement limit. On the other hand, the limit was satisfied in the de-bonded girder.

5.3.2.2 Strain Change of Reinforcing Bars in Inclined Crack Region

These gauges were placed very close to the draped strands hoping to cross the inclined cracks. All the values in Figures 5-17&18, however, are less than 60 με. Therefore, it seems that the locations of the cracks were mis-predicted. In the de-bonded girders, the data showed that all gauges are primarily in compression so de-bonding prevented this region from cracking. On the other hand, data from the bonded girder shows that both tension and compression strains were present. Tensile strains may have caused cracks around that region. Note that the strain gauge S9 in the bonded girder must have been damaged during casting of concrete with subsequent poor operation and the data is omitted in Figure 5-17.

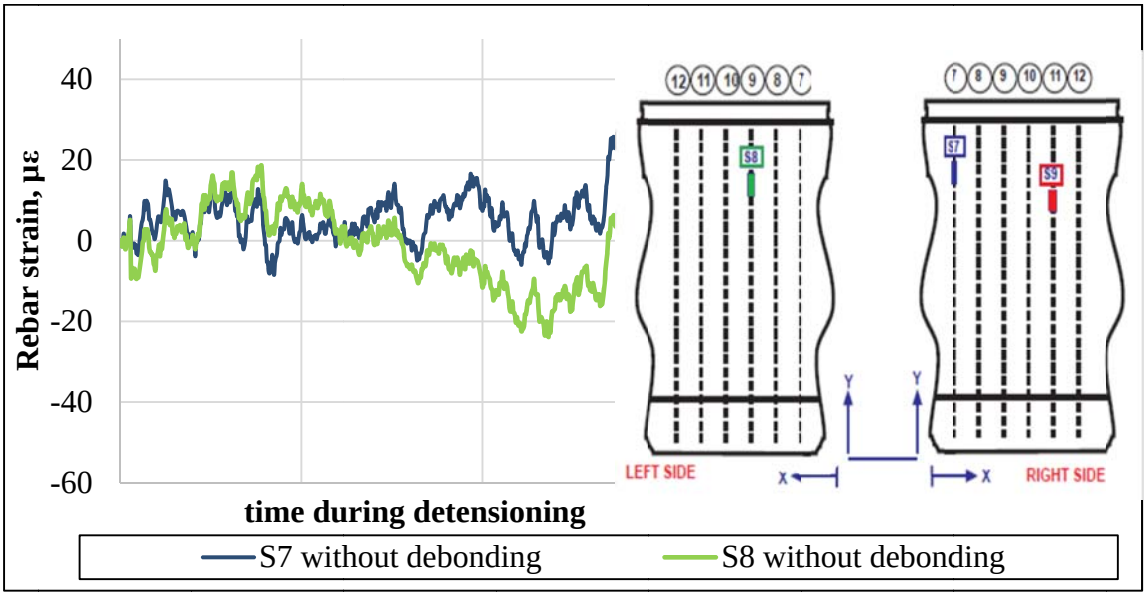

Figure 5-17. Bonded girder: Strain change of reinforcing bars in inclined crack region, close to top of girder (gauges S7, and S8). *(Tension positive, compression negative)*

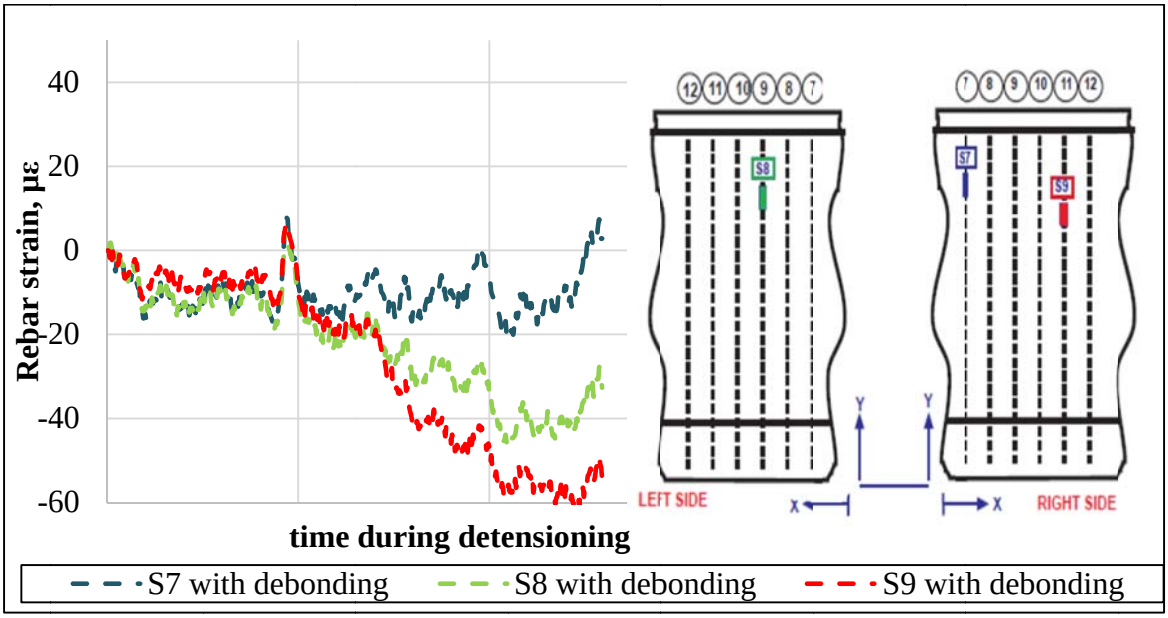

Figure 5-18. Debonded girder: Strain change of reinforcing bars in inclined crack region, close to top of girder (gauges S7, S8, and S9). *(Tension positive, compression negative)*

5.3.2.3 Strain Change of Reinforcing Bars in Y Crack Region

Other gauges were placed to capture reinforcing steel strains created by Y cracks in the bottom flange (S10 to S13). The effect of de-bonding can be seen from Figure 5-19 and Figure 5-20. In the de-bonded girder, gauge S12 reached 450 micro strain in tension. However, in the bonded girder, a crack apparently occurred across the bar of gauge S10, and it experienced up to 1500 micro strain in tension, which is 3.3 times higher than maximum tensile strain in the de-bonded girder. This is evidence that de-bonding can have a significant impact on controlling the Y-cracks. The S13 gauge tension strain actually increased with de-bonding, but it is negligible in amplitude and it occurs in the 12th bar layer from the beam end where stresses are added by shielded strands that are just becoming bonded, while transfer had already occurred in the bonded beam.

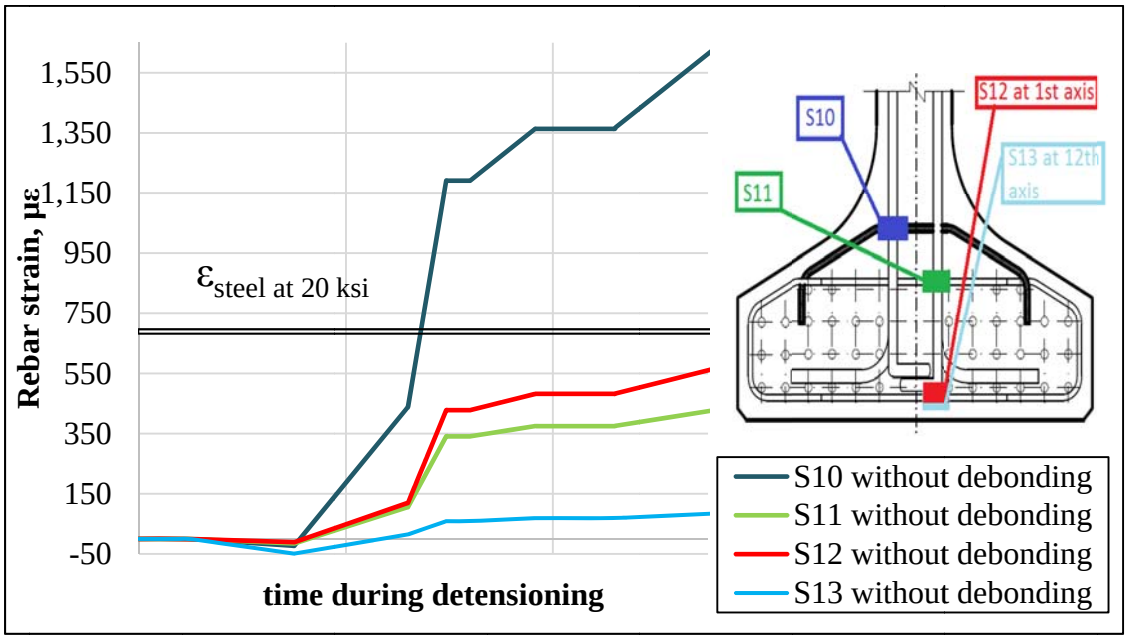

Figure 5-19. Bonded girder: Strain change of reinforcing bars in bottom flange (gauges S10 – S13). *(Tension positive, compression negative)*

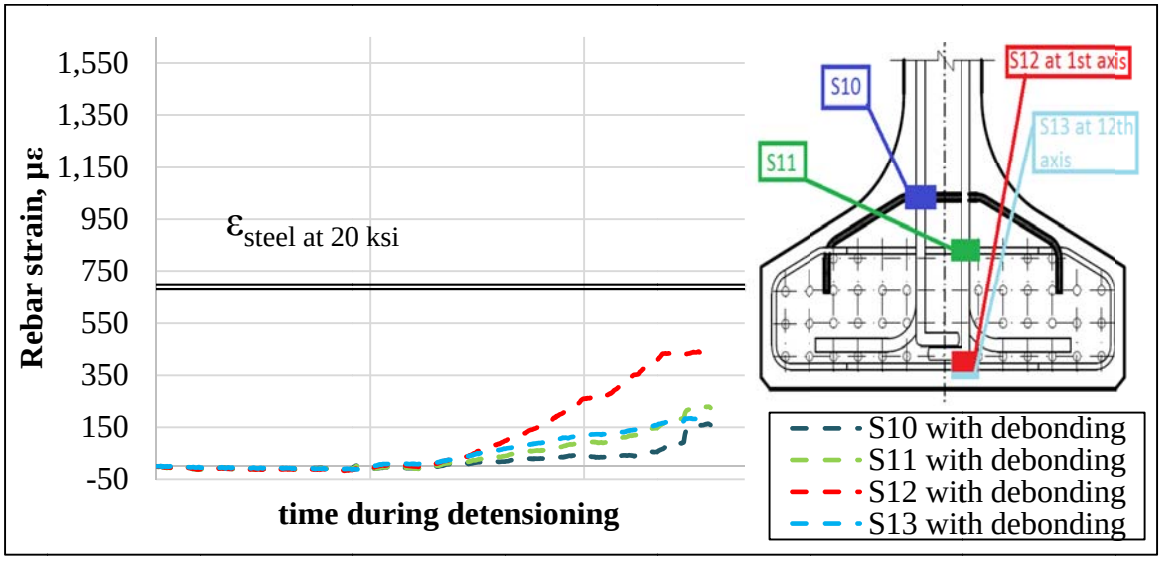

Figure 5-20. Debonded girder: Strain change of reinforcing bars in bottom flange (gauges S10-13). *(Tension positive, compression negative)*

5.3.3 Strains in Concrete:

The vibrating wire gauges were intended to capture concrete strains near expected crack locations. The locations were shown in Figure 5-10. Hence, VW1 and VW4 were vertical near the web and inclined cracking regions, respectively, and other gauges were embedded in the bottom flange near the Y crack region.

Figure 5-21 and Figure 5-22 show the strains observed from vibrating wire gauges in de-bonded or bonded girders during strand release.

Figure 5-21 shows the comparison of vibrating wire gauges in the web and inclined crack region. Figure 5-22 shows the results of gauges embedded in the Y crack region. There is also one line representing the strain at which concrete is expected to crack, which is calculated as 132 με based on the AASHTO cracking stress. In the figures there are ranges

along the horizontal axis for times when draped strands, top row strands, middle row strands, and bottom row strands were flame cut. The intention is to show the trends in strain change as de-tensioning occurs. Unfortunately, the exact times that the various strands were flame cut could not be measured because observers were not allowed to get close to the formwork during strand release.

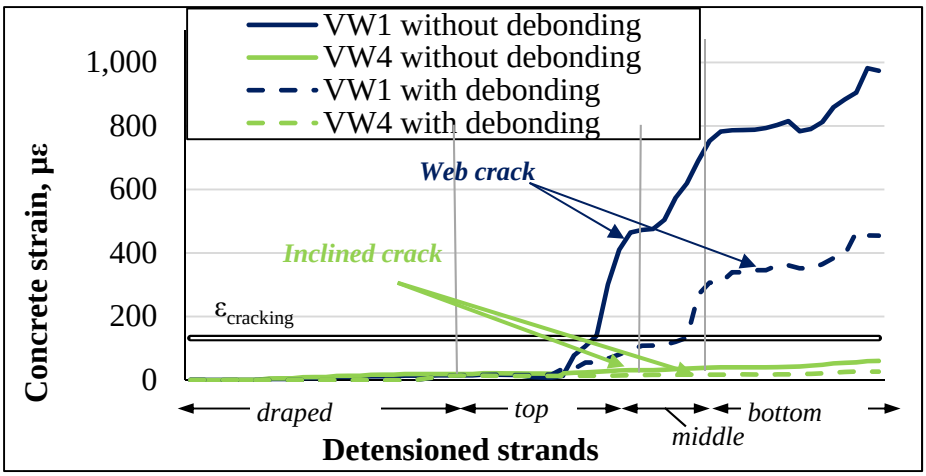

Figure 5-21. Strain change of vibrating wire gauges near the web and inclined cracking region. *(Tension positive, compression negative)*

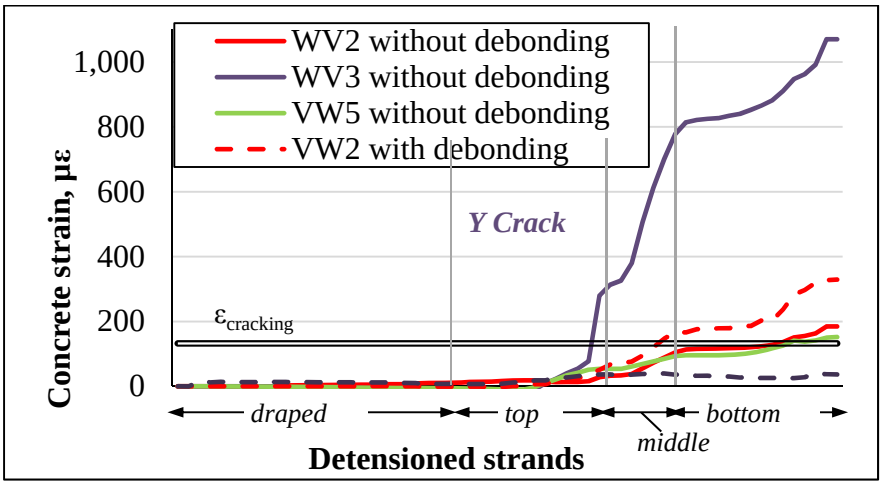

Figure 5-22. Strain change of vibrating wire gauges near the Y cracking region. *(Tension positive, compression negative, V5 is vertical)*

The web cracking region strains in the concrete (VW1) were decreased by 54% with de-bonding but strains in bonded and de-bonded girders are both still above the cracking limit of the concrete. The strains in the inclined cracking region (VW4) are small because of an error in prediction of the gage location, i.e., not aligning with the inclined crack location.

The vertical VW5 in the de-bonded girder bottom flange did not work so its value was omitted in Figure 5-22. VW2 and VW3 were horizontal and parallel to the flange width. The strains of VW2, were low and similar in both girders. On the other hand, the bonded beam had strains nearly 21 times as high as the de-bonded beam in the transverse horizontal VW3 (third stirrup) location. This high strain must be associated with the more concentrated transfer of strand stress to the concrete over a short length in the bonded beam and likely cracking. Having high concrete strains further inside of the girder (VW3) than strains near the end (VW2) might indicate that any Y cracks are initiated internally and then possibly grow toward the beam end.

After the girders were transported to the construction site and put into the planned bridge span location, another measurement of the VW gauges was taken.

Table 5-4 shows strains observed from the vibrating wire gauges in the de-bonded or bonded girders after all strands were released and after erection. Web cracking strain in the bonded girder (VW1) stayed the same between the de-tensioning and erection. Web strains strain in the de-bonded girder increased by approximately 300με or 66% between those times.

The bonded girder, however, gave higher concrete strains than the de-bonded girder at locations other than VW2 (Y crack region). The strains in the horizontal VW2 gauge increased by 300με in both girders between de-tensioning and erection but the strain of that gauge in the de-bonded girder is 33% higher than in the bonded girder. The reason may be that the VW2 gauge in the de-bonded girder crossed a Y crack but the crack did not pass through the gauge in the bonded girder as illustrated in the end view of Figure 5-23. Though VW2 results were small in the bonded girder, the Y crack was actually larger but the gauge missed the Y crack location as is clear in the figure.

Figure 5-23. Location of vibrating wire gauges VW1 and VW2 in both bonded (left) and de-bonded (right) girders.

Overall the largest measured concrete strain in the de-bonded girder was 750 micro strain (VW1 – web). The tensile strain nearly reached 1600 micro strains (VW3- Y crack) in the

bonded girder. Therefore, it can be said that compared to the bonded girder, the de-bonded girder concrete experienced less tensile strain, resulting in smaller crack widths at the end.

	DEBONDED			
	Micro Strains in Vibrating Wire Gauges			
	VW1	VW2	VW3	VW4
After all strands released	454	329	37	26
At Erection	755	618	n.a.	58

	BONDED				
	Micro Strains in Vibrating Wire Gaugesx10^-6				
	VW 1	VW 2	VW 3	VW 4	VW 5
After all strands released	974	185	1070	60	152
At Erection	952	464	1582	407	201

Table 5-4. Data from vibrating wire gauges in debonded and bonded girders.

Figure 5-24 shows a side view of the general location of vibrating wire gauges in each girder. This indicates how close the gauges were placed to crack regions. Figure 5-24 shows that the VW1, VW2, and VW3 gauges in the bonded girder either crossed or were near to cracks; and VW1 and VW2 in the de-bonded girder were close to cracks. The results in Table 5-4 also seem to agree in some cases with these observations.

Figure 5-24. Location of vibrating wire gauges in bonded (left) and de-bonded (right) girders.

5.4 Girder End Cracks

After de-tensioning of the girder was finished, the girders were taken to the precast yard until needed for erection. When moved to the yard the cracks were inspected at the ends and numbers, widths and the lengths were recorded. It was also observed that crack lengths and sizes increased as girders were lifted to carry them from the bed to the yard.

A comparison of girder ends is shown in Figure 5-25. Even though the concrete strains decreased with 25% de-bonding, the number of cracks had not changed. However, the lengths and widths did get smaller.

Without de-bonding With de-bonding Without de-bonding With de-bonding

Figure 5-25. Cracks at the ends of bonded and de-bonded girders.

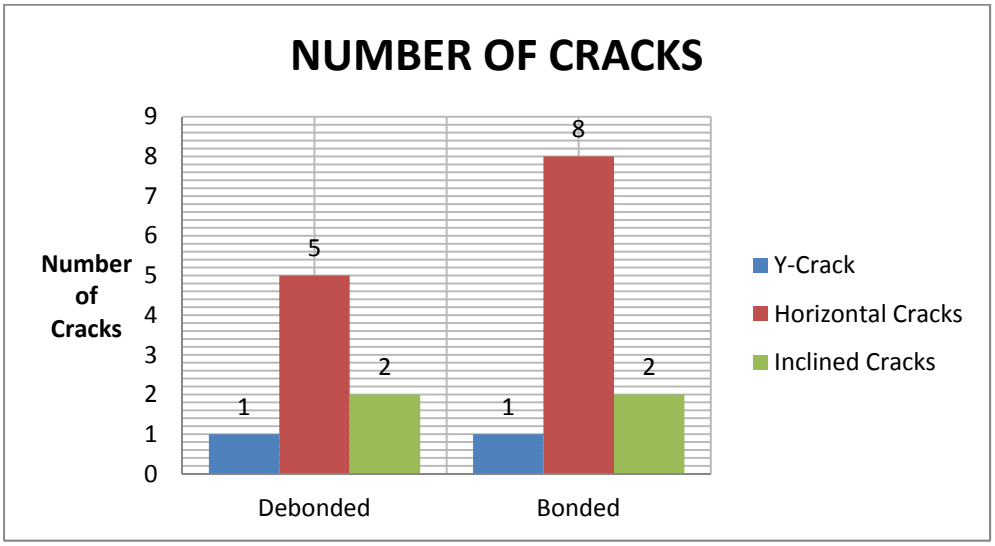

Figure 5-26. Number of visible cracks found in each girder.

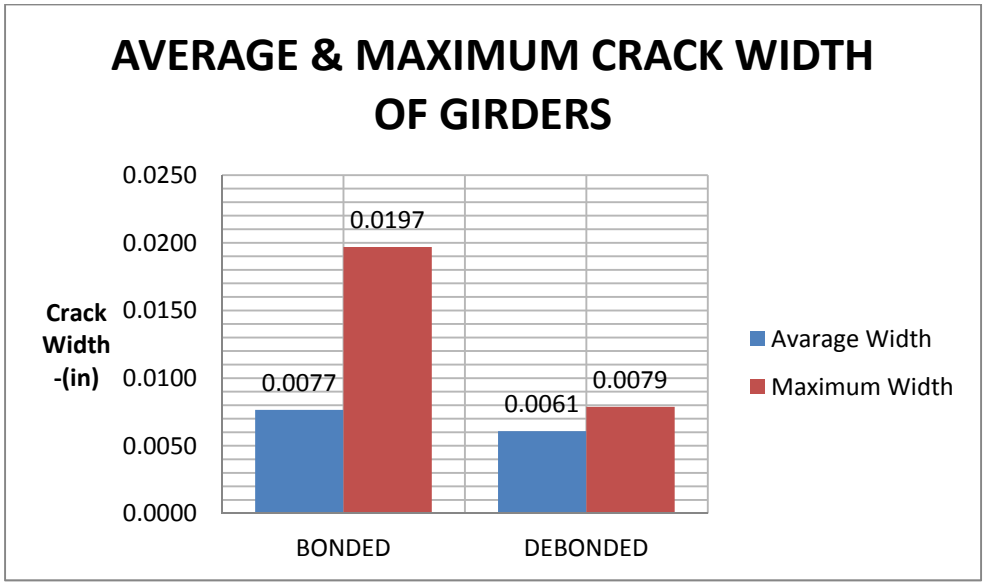

Figure 5-27. Average & maximum crack widths.

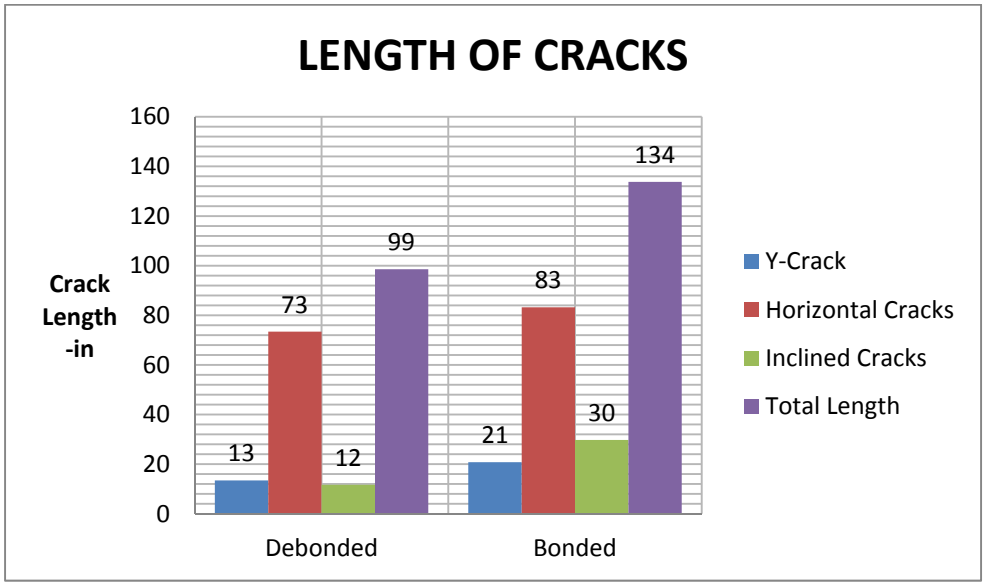

Figure 5-28. Total length of cracks at girder ends.

The number of inclined and Y-cracks seems to be same for the girders according to Figure 5-26, but more horizontal cracks did develop in the bonded girder.

In the bonded girder, Figure 5-27 shows that both average and maximum widths are larger than in the de-bonded girder. Of most importance, the maximum crack width in the bonded girder is large (0.0197 in) and may allow moisture or corrosives to enter the concrete. De-bonding 25% of the strands reduced the maximum crack width of the Y cracks by more than half. The wide Y crack was observed in the bonded girder in the region where bottom strands are concentrated so it may easily lead the aggressive salt water to strands and induce corrosion. These cracks were measured right after the girders were carried to the yard. Analytic predictions show that the Y cracks are expected to grow as additional vertical loads are applied.

Another visual indicator observed just after testing is the length of cracks. These lengths were measured at one end of the girders. It is clear in Figure 5-28 that the bonded girder may have a higher potential to expose strands to corrosion by cracking than the de-bonded girder. The total length of cracking was reduced 25% by de-bonding 25% of the total number of strands. However, it should be noted that length of each type of cracks decreased significantly in the de-bonded girder, especially in inclined and Y- cracks in regions where most of the strands are located, so the risk of strands getting corroded decreased.

5.5 Comparison with Finite Element Model Results

The Abaqus software program was used to analytically model the girders that had been monitored during de-tensioning. The properties of the models were definmed following the same procedure as described in Chapter 0 but some changes were made according to each girder's uniques condition - such as concrete strength, to better simulate the test girder conditions. The transfer length of the strands in all girders was assumed as the AASHTO suggested value of 36in. which varied some from strain gauge data from strands.

Observers were not allowed to get close to the girder during de-tensioning. Therefore, the exact time at which all draped strands, the top strand layer, second layer and third layer were flame cut, could not be recorded. The final strains when all the strands were cut was well known. Hence, only the strains after the last detensioning step will be compared with finite element model results.

5.5.1 Bonded Girder

The initial concrete strength of the bonded girder was observed to be 7800 psi from cylinder tests before de-tensioning of strands. This value was used to calculate a cracking and strain using the AASHTO tension stress equation based on compressive strength, which suggested a limit of 126με. This limit is used to judge likely cracking in both test girders and models. Reinforcing bar strains were compared with 690με corresponding to the 20 ksi limit on splitting zone reinforcement of AASHTO LRFD BDS (3) Section 5.10.10.1.

Figure 5-29 shows the comparison of regions where girder end cracks are likely, predicted by the Abaqus model, with the actual cracks at the bonded girder end. To spotlight expected crack locations in the model results, the maximum strain would be greater than the cracking strain value of the concrete or $-1.26*10^{-4}$(light blue to gray shaded regions). The model envisaged the location of cracks quite well except for the location of an inclined crack. A gray color indicates locations where wide cracks are expected. The light blue to red would be regions with narrower cracks.

5.5.1.1 Comparison of Vibrating Wire Gauge Results with Finite Element Models

Vibrating wire gauges measure the average concrete strain over the full gage length. Therefore, to compare vibrating wire gauge results with the finite element model strains - an averaging of the finite element strains near the caps of the gages was used. Figure 5-30 is a comparison between test data strains and predictions from the finite element model. The strains are in micro strain and graphs were plotted with the strain vertically, and VW gauge number horizontally. A detailed location of each vibrating wire gauge is in Figure 5-10.

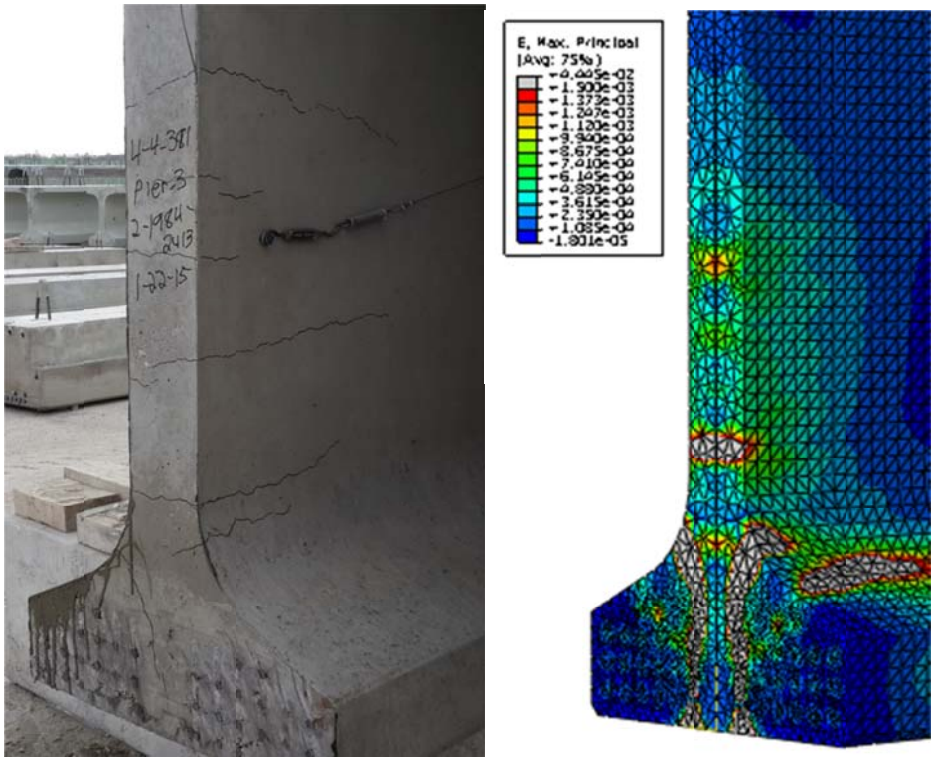

Figure 5-29. The comparison of actual girder end cracking with Abaqus model strains for bonded girder. *(tension is negative)*

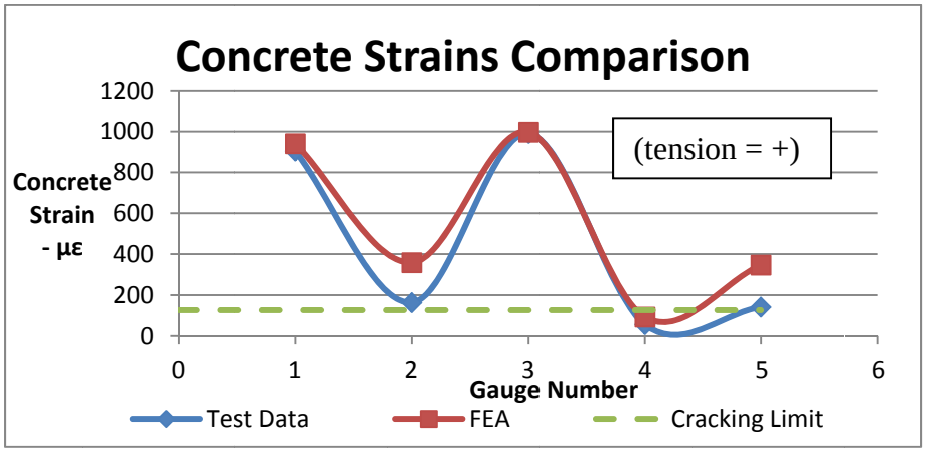

Figure 5-30. Concrete strain comparison for bonded girder.

Concrete is a heterogeneous material, nonetheless, the concrete of the FEM models is taken as a uniform homogenous material. In other words, there are many factors affecting the comparison. Basic factors include: a distribution of aggregates throughout the body that is unknown but its effect is inevitable as there will be discontinuities in material properties, the concrete strength likely vaies over the 72in. depth of the girder, the assumed relationship between cracking stress and compression strength is approximate. Discontinuities can result in discrete cracks – which are not exactly simulated in the model. If a local discrete crack occurs across a gage, but it is not simulated at that location by analysis the indicated strains could differ significantly. Therefore, the accuracy of a correlation, as in Figure 5-30, might be considered quite good, especially with the small strains that are present.

Even though matching measured concrete strain with finite element model results is challenging, the comparison for the VW1, VW3 and VW4 gauges in Figure 5-30 is quite good. The comparison of the other gauges (VW2 and VW5) is not as good, but is acceptable. The reason for the disagreement in the VW2 comparison is that the VW2 gauge in the bonded girder did not physically cross a Y crack, i.e., the crack did not pass through VW2 in bonded girder as in Figure 5-23. In the model, however, there should be a Y crack in the location where the gauge was embedded. Because the VW 5 gauge was actually attached to a reinforcing bar, it may have been restrained from accurately measuring concrete strain during the test.

Another observation is that as in Figure 5-24; VW1, VW2, and VW3 were either near to or crossed cracks. In the comparison, strains from both the model and test data results are over the assumed cracking limit for the concrete holding those gauges. As such, the

prediction was quite accurate. The model also predicted that at the location of VW5 cracking should have just started. Test data showed that the average strain there was at the cracking limit of concrete and an actual crack may not yet have occurred.

Table 5-4 lists the last strain measurements taken after erection. According to those values the strains around the VW5 gauge had nearly reached the FEA predicted result. Perhaps crack formation in the concrete develops slowly time wise, but is immediate in the FEM analysis, and it can be said that the model would fit better if actual data were taken a couple of days after de-tensioning to allow that crack growth to occur.

5.5.1.2 Comparison of Strain Gauge Results with Finite Element Model

Reinforcing bars are more homogeneous than concrete. Hence, the correlation between measured and predicted strains should be closer than in concrete.

Figure 5-31 compares predicted and measured reinforcing bar strains in the bonded girder. The vertical axis is for strain and the horizontal axis is the gauge number where strain was measured. The gauge placements were shown in Figure 5-8. Even though the girder was designed with rebar not to exceed the 20 ksi AASHTO limit, the gauges on certain re-bars (S1, S2, and S10) showed strains over this limit.

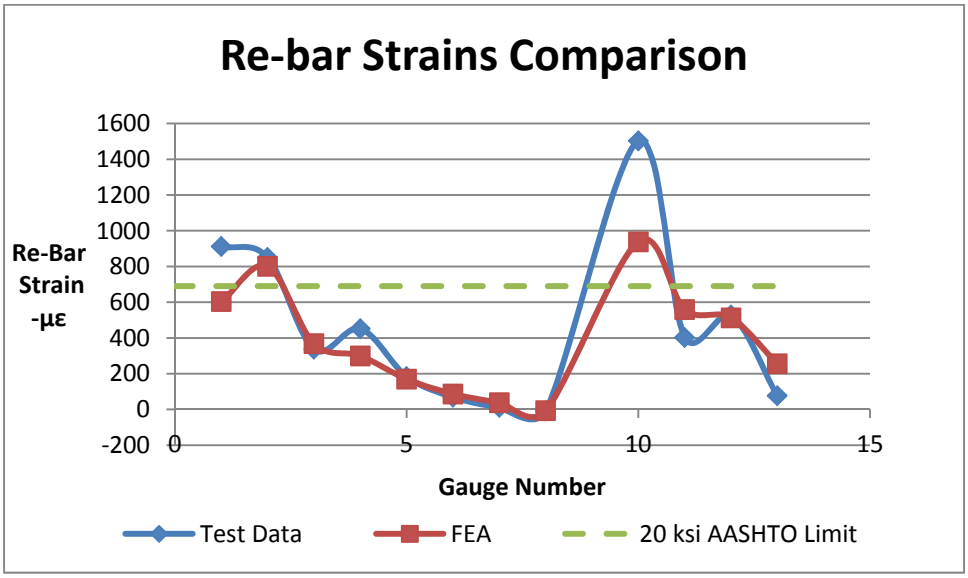

Figure 5-31. Reinforcing bar strain comparison for bonded girder.
(positive is tension)

The strain difference at S1 and S10 is large, but for the other gauges the correlation is quite good. The reason for this mismatch with the two bars is likely due to a crack occurring near the location of the strain gauge and creating a high local strain in the bar. In the FEM model the bars were discretely connected to the concrete elements, rather than with continuous bond, and the strain associated with a crack is averaged over the element length.

5.5.2 25% De-bonded Girder With Strands Bonded in Staggered Lengths

The initial concrete strength for this girder with 25% debonding was 7015 psi from cylinder tests before de-tensioning of strands. The cracking strain of the concrete is calculated as 128με. The concrete strains from both test and model were compared with this cracking limit. Again, reinforcing bar strains were compared with 690με corresponding to the 20 ksi limit on splitting zone reinforcement of AASHTO LRFD BDS (3) Section 5.10.10.1.

Comparison of predicted strains and cracking regions at the girder ends showed good correlation as visible in Figure 5-32 with the model accurately predicting crack locations. Again any contour color above light blue in the reference block is beyond the cracking limit of the concrete. The model showed the region where cracks will occur in Figure 5-32 as gray-red in color for bursting or Y cracks and light blue or green in contour color for the location of other smaller cracks.

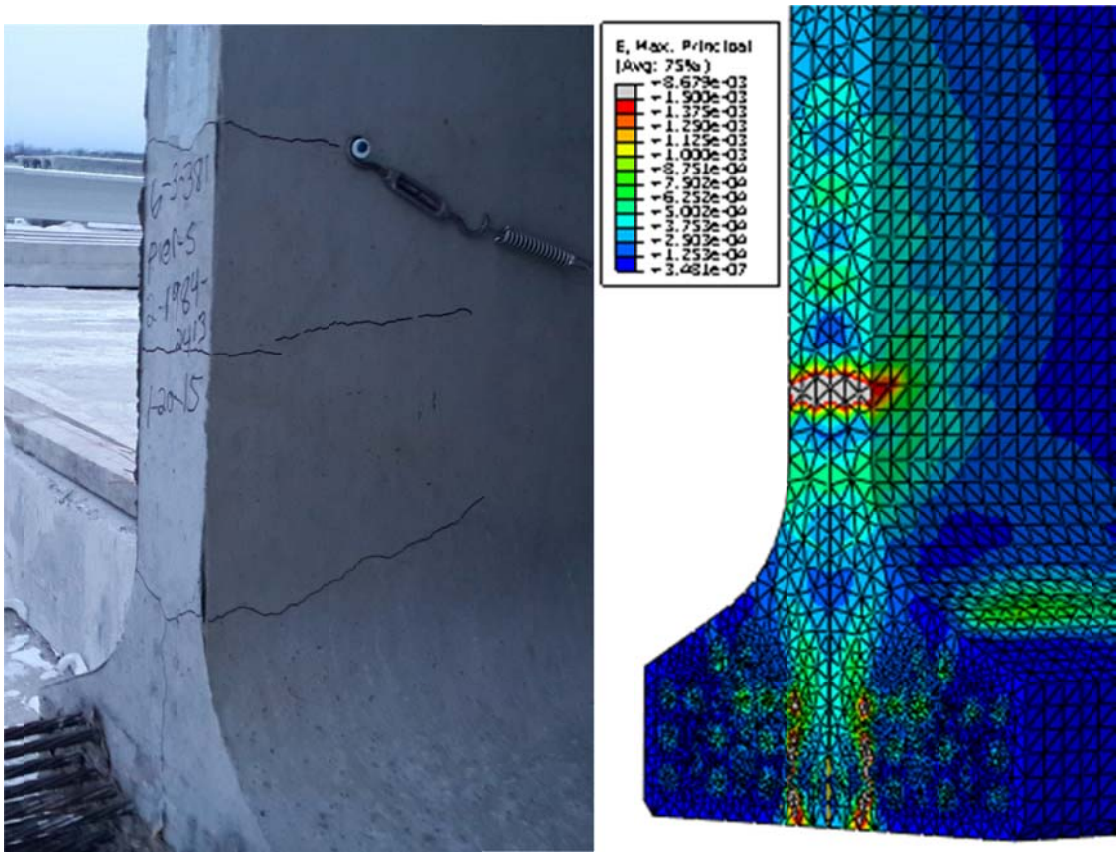

Figure 5-32. The comparison of actual girder end cracking with Abaqus model strains for the de-bonded girder.

5.5.2.1 Comparison of Vibrating Wire Gauge Results with Finite Element Models

Figure 5-33 shows the comparisons between measured and predicted concrete strains. The strains are in micro strain and the graph was plotted with concrete strains vertically and VW gauge number horizontally. The results from VW3 and VW5 were omitted because their results were questionable due to intermittent operation during the test.

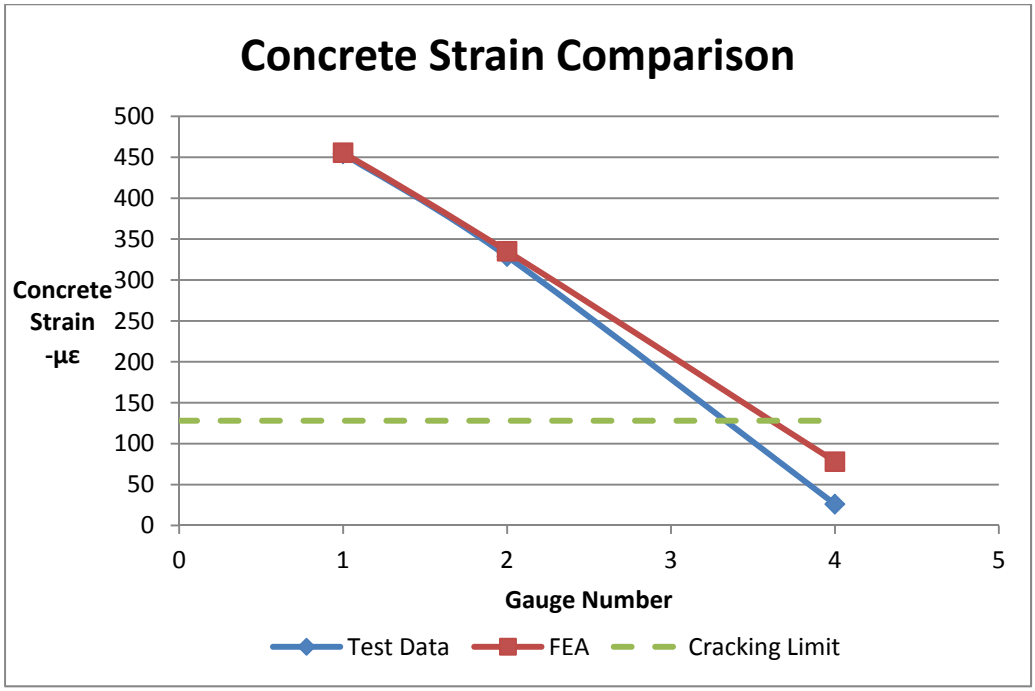

Figure 5-33. Concrete strain comparison for de-bonded girder.

FEA results and test data results almost matched and there is a good correlation. These are strain change results after all the strands were cut. The analytic model can be judged to be working well.

In Figure 5-24, VW1, and VW2 passed through cracks. Therefore, strains from both predicted and measured results are over the cracking limit. The prediction of crack locations was quite accurate.

5.5.2.2 Comparison of Strain Gauge Results with Finite Element Models

Figure 5-34 compares reinforcing bar strains in the 25% de-bonded girder. The vertical axis is for strain change and the horizontal axis is for strain gauge number (as shown in Figure 5-8). All the strain values, both from the predicted model and measured data, were below the 20 ksi AASHTO limit.

In the comparison, the measured strains near the gauges matched with finite element results except for the one gauge on the first vertical web bar: S1. There is a large difference between the strains shown. The reason is again attributed to the formation of a crack within 1in. of the S1 gauge location causing a high local strain, while the FEM model provides what is more like an average strain due to discrete bonding of the steel and concrete. Overall the FEM model is judged to be quite accurate in strain predictions.

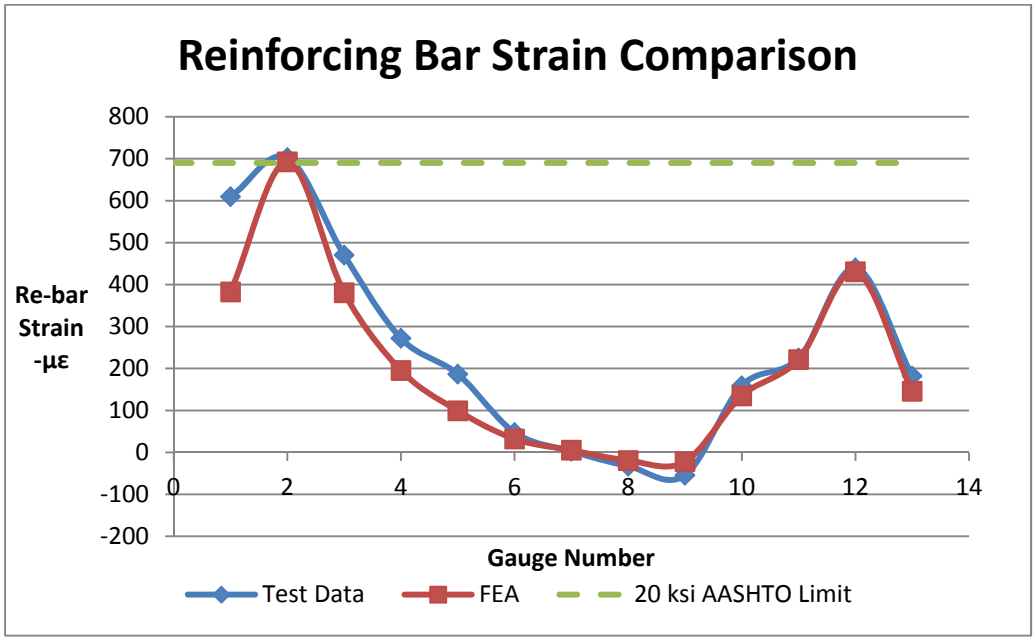

Figure 5-34. Reinforcing bar strain comparison for de-bonded girder.

5.6 Observations and Summary

Reinforcement bar strains were compared with the strain limit according to the AASHTO LRFD BDS 5.10.10.1 requirement intended to control cracking. Although the reinforcements of the girders were designed not to exceed a 20 ksi stress limit (or 690με strain) per AASHTO, the gauge stresses (or strains) of the first vertical web reinforcing bars in the girder without de-bonding (S1, S2, and S10) exceeded this limit. The stresses turned out to be as high as 28 ksi in web reinforcement and 45 ksi for confinement reinforcement in the girder without de-bonding. On the other hand, 25% strand de-bonding brought reinforcing bar stresses below the AASHTO limit for crack control.

In the inclined crack zone, strains both in reinforcing bars and in concrete were very small because the gauges missed the actual inclined crack position.

Concrete strains in the vibrating wire (VW1) gauge in the horizontal web cracking region showed that 25% de-bonding decreased tensile strains in concrete by 54%, but it did not prevent cracking as strains were still not below the cracking limit. Full elimination of cracking would likely require more debonding than 25%.

Gauges on bottom flange confinement reinforcing bars in the Y cracking region showed the beneficial effect of de-bonding. The single bar at the very end of the girder crossing the Y crack (S10) had very high strains in the girder without de-bonding, and therefore it is partly effective for restraining the Y cracks. It is expected that it would be more effective if it was not epoxy coated because better bond would reduce crack widths further. The strains in this rebar were reduced to 10% of the bonded amount with de-bonding, but a narrower Y crack still occurred in the girder with de-bonding. The strain at the bottom flange first stirrup (VW2) location showed little difference between the two girders. At the third stirrup (VW3) location, however, the bonded beam had strains nearly 21 times as high as the de-bonded beam had. This difference suggests that the Y crack crossed the gauge in the bonded beam or that cracking might initiate 8in. into the girder and then grow towards the girder end.

The maximum crack width of the Y cracks was reduced with de-bonding 25% of the strands by more than 50% compared to the bonded beam, and decreased the total length of cracks by 25%. Therefore, de-bonding has the potential to eliminate cracks, particularly if more than 25% of the strands can be de-bonded.

In a comparison of strain results from vibrating wire gauges, three out of five gauges agreed quite well with test results in the bonded girder. VW2 and VW5 did not match with

measured strains. The reasons may be due to effects of local cracking and attachment of gauges to rebar – effectively restraining the deformation of the gauge. In the 25% de-bonded girder, however, there is a good correlation between measured and predicted results for working gauges. Also, the models predicted the location of cracks accurately.

As the strain gauges were put on uniform material (re-bars), the results of a measured and predicted comparison are better than in concrete. The comparison of the strain gauge on the first web bar (S1) both in the bonded and in de-bonded girder did not match the predicted value because of cracks that occurred approximately 1in. below the location of the gauges. The gauges missed the crack, but the analytic model caught it.

5.7 Conclusion

25% de-bonding of the strands with staggered debond lengths decreased strains in reinforcing bars and concrete considerably by increasing the transfer length of pre-stressing force at the girder end and by decreasing the number of draped strands needed. A higher amount of de-bonding, however, is needed to prevent Y cracking completely. The change in the number of draped strands does not impact Y cracking strains as Y cracks are caused by the eccentric distribution of bottom flange strands in the direction of the width of the girder and the vertical reaction force of the girder self-weight.

The number of cracks stayed the same with 25% de-bonding but widths and length of the cracks decreased compared to the bonded girder. De-bonding decreased the tension strains in

concrete and in reinforcing bars. A higher percentage of debonded strands, however, is required to completely eliminate Y cracking.

6 TEST AND FEM MODELS FOR 54W GIRDERS

Previously, strains in two 72W girders manufactured by Spancrete, Inc. were measured during and after detensioning. One of these girders had 25% of the prestress strands debonded following the rules statedint Section 5.11.4.3 of the AASHTO LRFD Bridge Specification.

From the tests and analyses of 72W girders, it was apparent that 25% strand debonding did not eliminate the horizontal and Y cracks at the girder end. Therefore, two different debonding patterns were tried on 54W girders at County Materials Corporation in October 2015. Strains were again measured during detensioning and compared with analytically predicted strains.

6.1 54W Girders Fabricated by County Materials Corporation

6.1.1 Properties of 54W Girders

Three 54W girders were built and monitored to evaluate end crack control as a portion of the 18 girders used in building bridge B-05-0682. Plans for the girders #4, 5 and 6, part of the second bridge span, are in the Highway Structures Information System (14). The girders were 54in. in depth with 48in. wide top flanges. All the standard WisDOT end details, except the strands of the girders, are shown in the Figure 6-1.

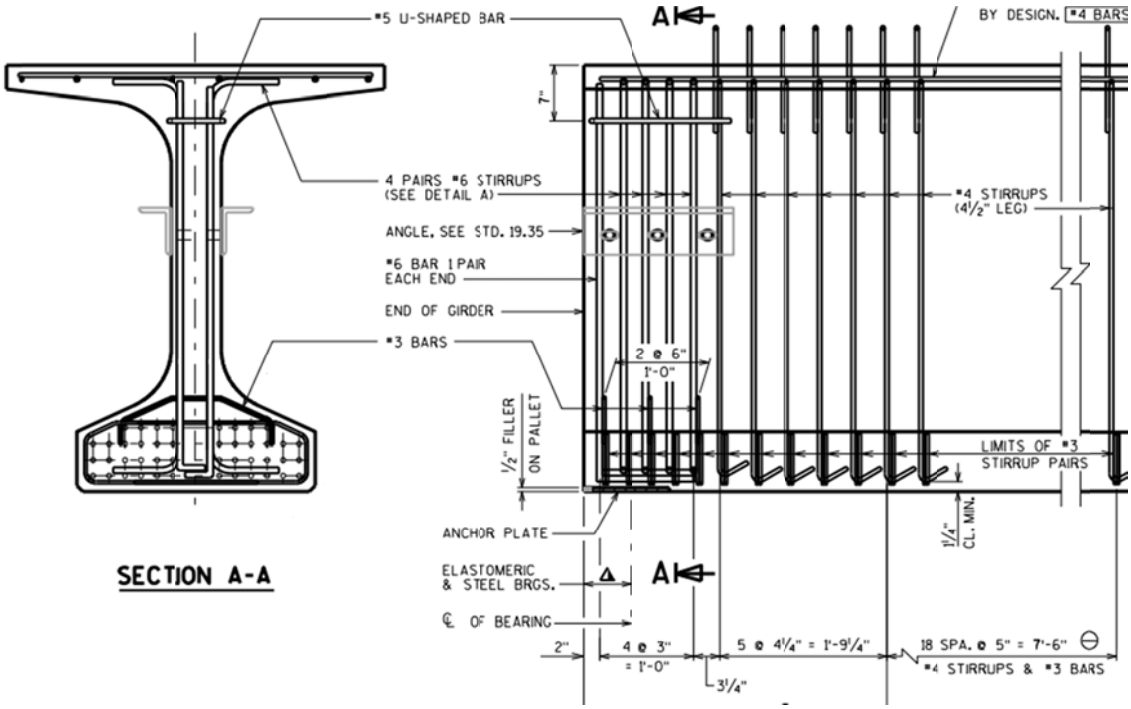

Figure 6-1. End details of 54W girder.

The girders were 125 ft. long and originally were designed with 42 strands, 8 of which were draped strands. Strands were 0.6 inches in diameter and of 270 ksi low relaxation type. Moreover, the strands were originally placed with 2 in spacing as shown in the overall diagram of strand locations in Figure 6-2. One girder used the original strand pattern (normal girder), a second had 38% of the strand debonded with staggered debond lengths; and the third had 62% of total strands debonded over 8 inches in the bottom flange but 8 strands in the bottom strand row were left bonded to prevent vertical crack formation as the girders shortened and slid along the casting bed during de-tensioning.

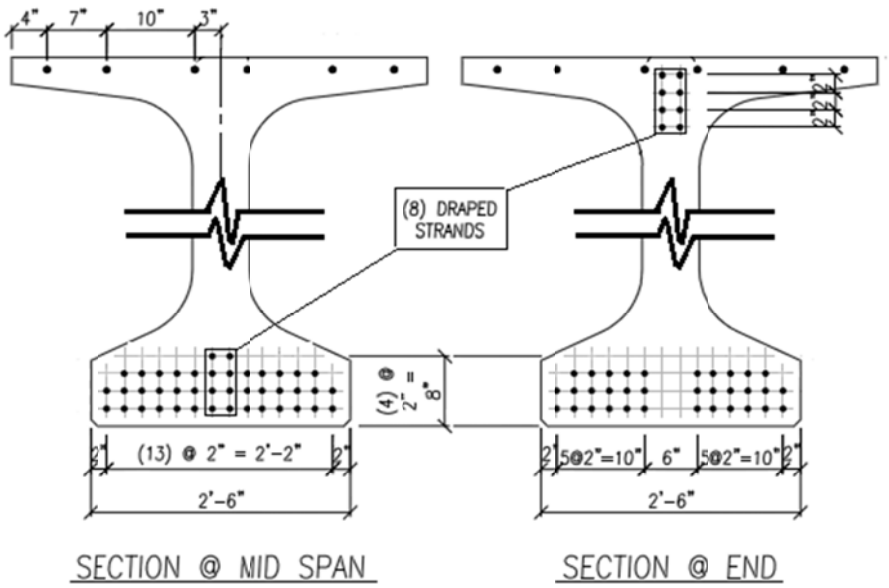

Figure 6-2. Original strand pattern at the ends of girders.

The initial measured average concrete cylinder strength of the standard design (bonded) girder was 7820 psi at de-tensioning. The initial measured concrete strengths of the debonded girders were measured as 8140 psi for the 38% debonded girder and 7975 psi for the girder that is debonded by 8in. Table 6-1 shows the calculated resulting concrete stress at bottom and top fibers at various distances from ends of corresponding girders expected after de-tensioning. Those results were compared with allowable stress limits of concrete in compression and tension which were calculated by $0.6*f_{Ci}$ for compression and $-0.24*(f_{Ci})$^0.5 for tension according to AASHTO LRFD BS. In calculations, elastic losses were included because they occur right after de-tensioning. Also, the stresses are a combination of stresses due to pre-tensioning and due to self-weight of girders. Figure 6-3 through Figure

6-5 show the plots of these values. All the concrete stresses at various locations are below the allowed AASHTO limits.

Girder Type	Distance-ft.:	0	3	6	9	12	15	62.5	All. Stress Limits
Bonded	Bottom Stress	0	1.900	3.770	3.708	3.654	3.607	3.845	4.692
	Top Stress	0	0.612	0.252	0.317	0.374	0.423	0.172	-0.265
38% debond	Bottom Stress	0	1.900	2.592	3.252	3.654	3.607	3.845	4.884
	Top Stress	0	0.612	0.487	0.395	0.374	0.423	0.172	-0.271
8in. debond	Bottom Stress	0	0.748	3.770	3.708	3.654	3.607	3.845	4.785
	Top Stress	0	0.821	0.252	0.317	0.374	0.423	0.172	-0.268

Table 6-1. Concrete stresses (ksi) at bottom and top fibers of the corresponding girders.

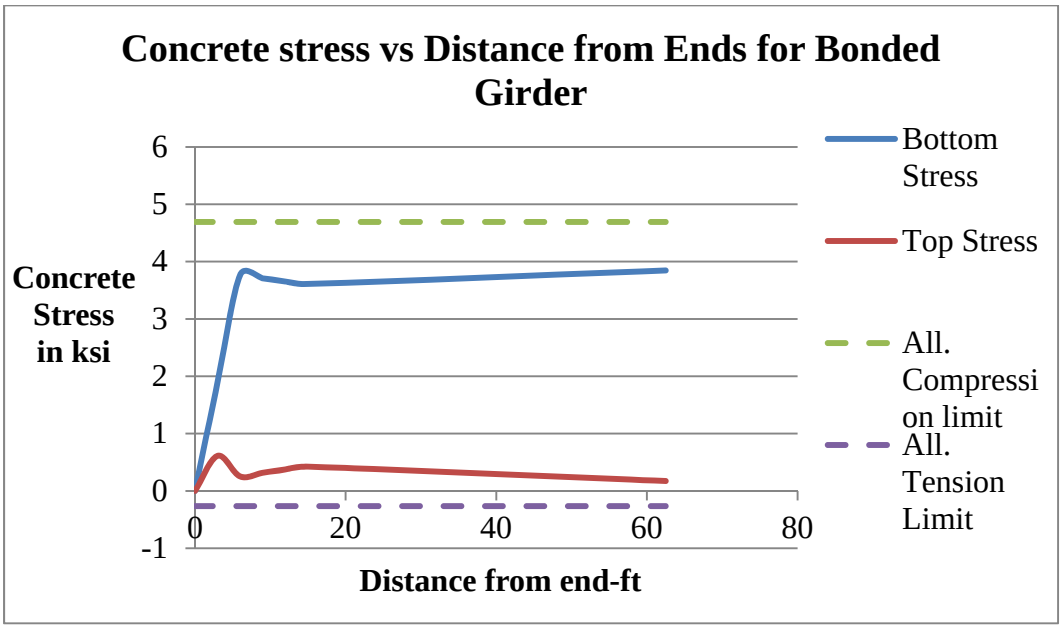

Figure 6-3. Bottom and top concrete stresses in bonded girder.

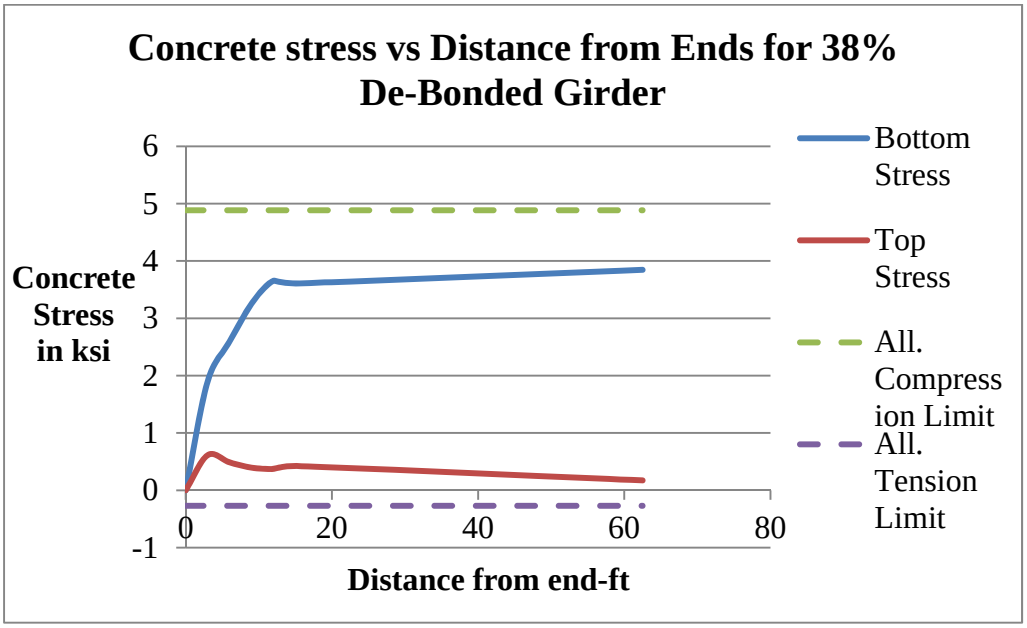

Figure 6-4. Bottom and top concrete stresses in 38% de-bonded girder.

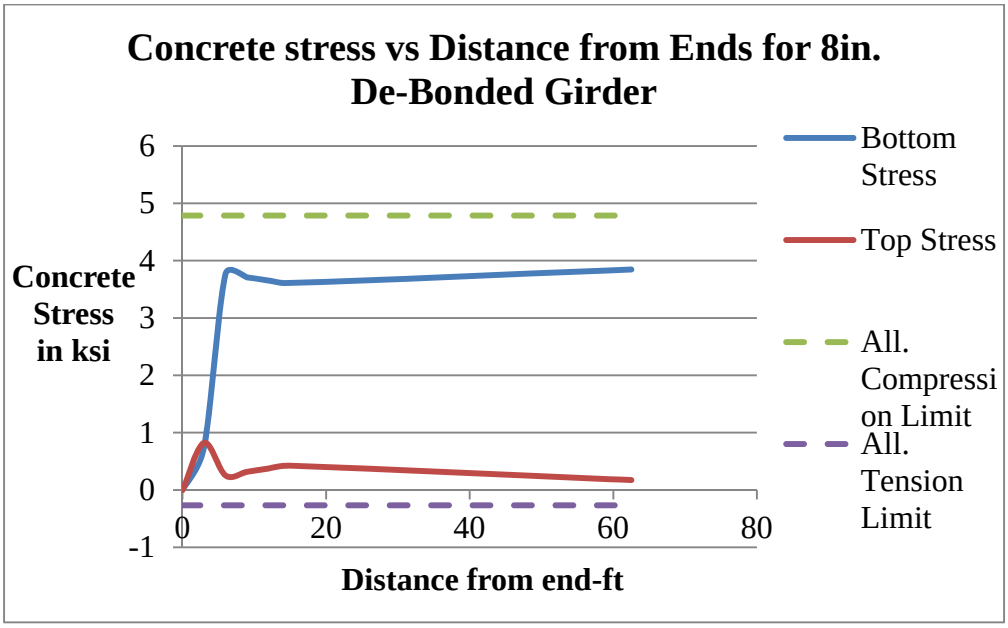

Figure 6-5. Bottom and top concrete stresses in 8in. de-bonded girder.

County Materials uses a single jack to stress the strands one by one. When detensioning, two symmetric strands in each row were cut by flame at each end of a girder. From a previous study of Okumus (1) it was suggested that it is better to cut the strands starting from the inside of a layer and working to the outside, so this cutting order was followed. In the County test girders a cutting sequence as in Figure 6-6 was applied. The number on the strands indicates the sequence in which each set of symmetric strands was cut. In Figure 6-6, the numbers also represent the step number in which prestress force is applied to finite elements in the associated analysis procedure. One difference, however, is that in the analysis the prestress force of all draped strands was applied in one step as if all were cut at once.

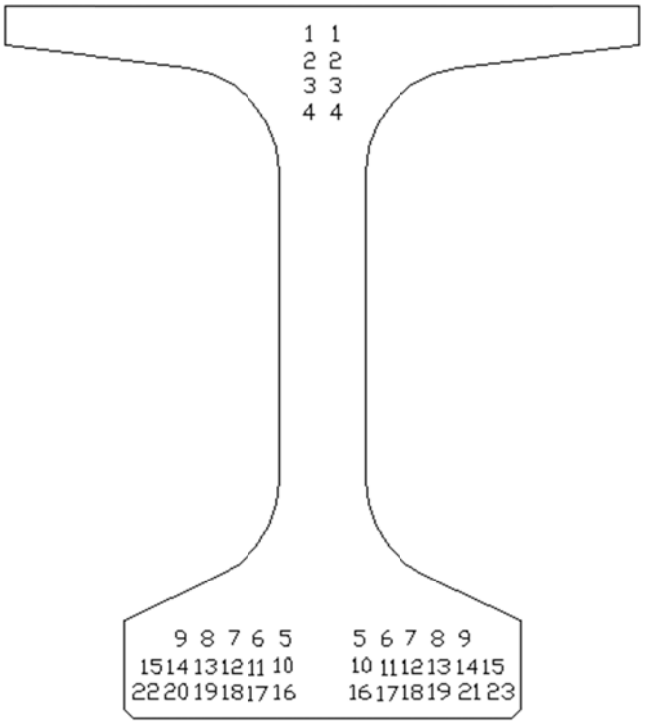

Figure 6-6. Strand Cutting Sequence.

6.1.2 Debonding of W54 Girders

Y and horizontal web cracks are consistently observed in the standard design W54 girders. To eliminate these cracks two alternate girder designs were employed. In the first alternate design 38% percent of all strands were debonded with staggered debonded lengths. In the second girder 62% of all strands were debonded at the girder end, all with debonded length of 8 inches. In both of these debonded girders, 8 draped strands were still used. Also, 8 strands in the bottom strand row were left bonded for the 8in. debonded girder. This small set of bottom strands in this girder was left bonded to insure that some reinforcing was present at the girder end. The strand layouts for these two designs are shown in Figure 6-7. They were expected to be the most effective methods to control web and Y cracking according to the previous study of Okumus (1).

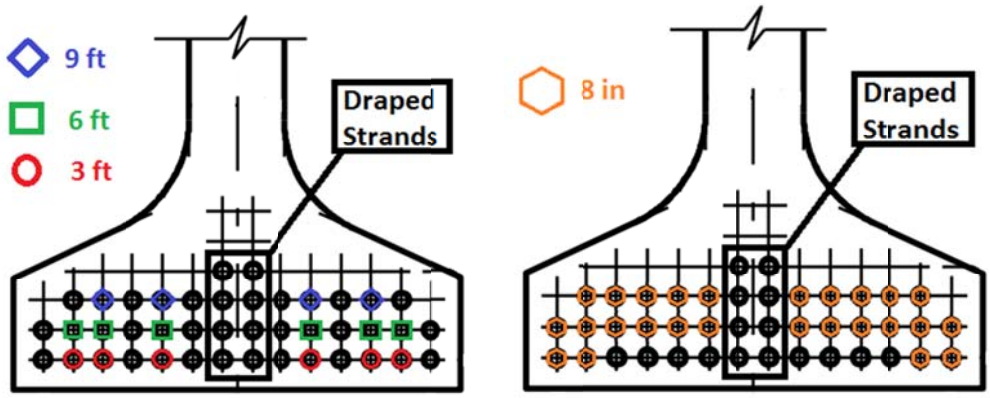

Figure 6-7. 38% debonded girder with staggered pattern (left with debonded lengths shown by symbols) and 62% debonded girder with 8in debond length (right).

6.1.3 Gauge Instrumentation

Vibrating wire and foil strain gauges were used inside the girders to obtain strain measurement. The vibrating wire gauges were embedded inside the concrete to collect concrete strains and temperature of the concrete whereas foil strain gauges were placed on the surface of steel bars and strands. The target gage locations were kept constant in all three measured girders.

Foil Strain Gauges on Strands: Three gauges were put on the surface of one strand per girder. The purpose of these gauges is to estimate the prestress transfer length of strands. They are manufactured by Tokyo Sokki Kenkyujo (27).These gauges were 1mm (0.04in) in length and were longitudinally glued on one of the seven strand wires as in Figure 6-8. After gluing, a protection coating was applied. They were first covered with microcrystalline wax, then Butyl rubber, and finally duct tape was used to provide some mechanical protection. The coating covered 2 inches of the strand length.

Figure 6-8. At the left, strain gauge on strand and at the right, the gauge after protection.

The prestress transfer length was assumed to be nearly the same for all strands regardless of their location. That is why only one of the strands was instrumented, and the longitudinal locations of the three gauges are shown in the Figure 6-9. The farthest gauge was placed at 36in ($0.6*d_b$) from the end of the girder, near the end of the transfer length according to

AASHTO LRFD Bridge Specification Chapter 5, Section C5.11.4.2 in the normal girder and the 38% debonded girder. In the third girder with 8in. debonding the gauges were placed on a debonded strand. The gauges on that strand, however, were shifted by 8in. inward. In other words, instead of 8in., 20in. and 36in. from the end, the gauges were placed at 16in., 28in., and 44in. from the end to have similar bond lengths.

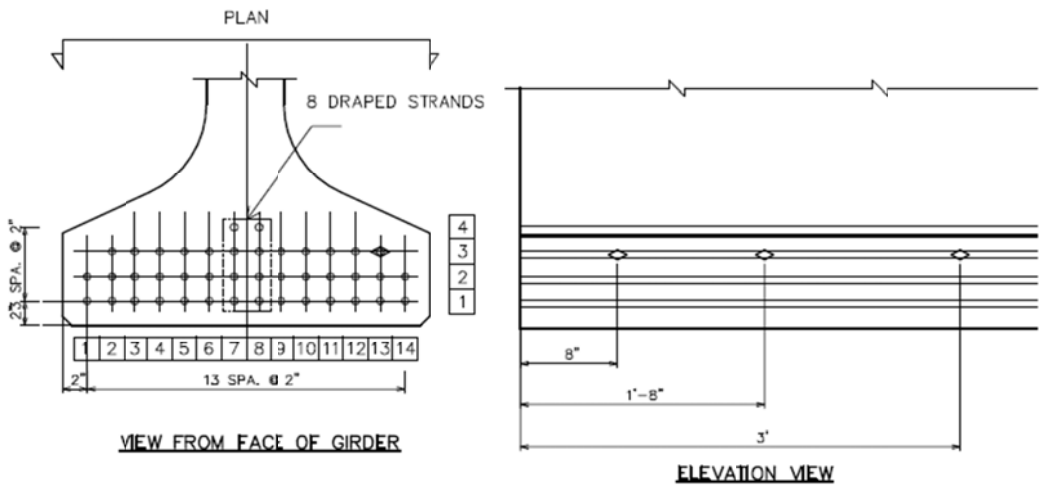

Figure 6-9. The location of Strain Gauges at Strand. Elevation view (right), and cross section view (left).

Foil Strain Gauges on Reinforcing Bars: Five strain gauges were used per girder, three of which were mounted on web bars and two of which were put on bottom flange stirrups. The same protective coating was utilized for these strain gauges. There were two types of gauges that were used in these girders. They are both 3 mm (0.12in) in length but one is 120 ohm and the other one is 350 ohm. Moreover, these gauges were glued parallel to the steel bar length.

A preliminary analysis model was used to predict locations of probable high strain and the gages were then placed in those locations as detailed in Figure 6-10. Gages labelled S1, S2 and S3 were placed on the first, third and fifth vertical web reinforcing bars respectively as in the side view of Figure 6-10. The gages labelled S4 and S5 were placed on the end stirrup and 8th stirrup in, respectively, as marked in the end view of Figure 6-10.

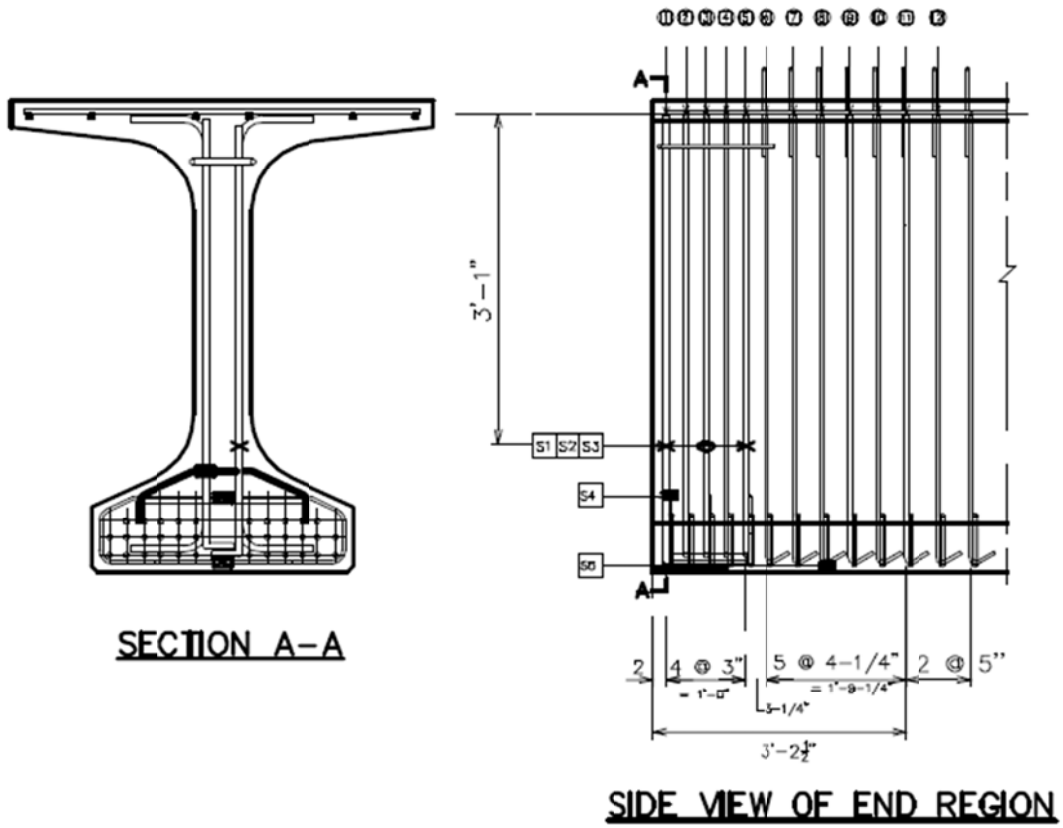

Figure 6-10. Location of Foil Strain Gauges.

Vibrating Wire Gauges Embedded Inside of Concrete: Vibrating wire gauges were embedded inside the concrete, helping to collect concrete strain data. Four were used per girder. Two Rocktest 6 in. long model 4200 and two Rocktest 2 in. long model EM-2 (29)

vibrating gauges (Figure 6-11) were used in this case. They measure the average strain occurring over the gage length. They can also measure temperature of the concrete. These gauges did not need any protection and they were held in place by attaching to re-bars either by soft plastic straps or wires as shown in Figure 6-11.

Figure 6-11. The 2in. (left) and 6in. (right) vibrating wire gauges.

The locations of these gauges were at expected high strain points, also decided by the simple analytic models that were built prior to casting. The critical locations that gauges were placed are shown in Figure 6-12. The VW1 gauge at the right in Figure 6-11 was placed vertically. The VW2 gauge was put horizontal on the 3rd stirrup near the top of the bottom flange. The VW3 and VW 4 gauges were placed in an inclined manner (Figure 6-11 left) on the 5th and 8th stirrups because in the analytical model the maximum principal strain directions were observed to be inclined. With the gauges placed in the same direction as the

expected maximum principal strain direction, the largest strain measurements were expected - increasing the signal level compared to noise and improving the accuracy of the data.

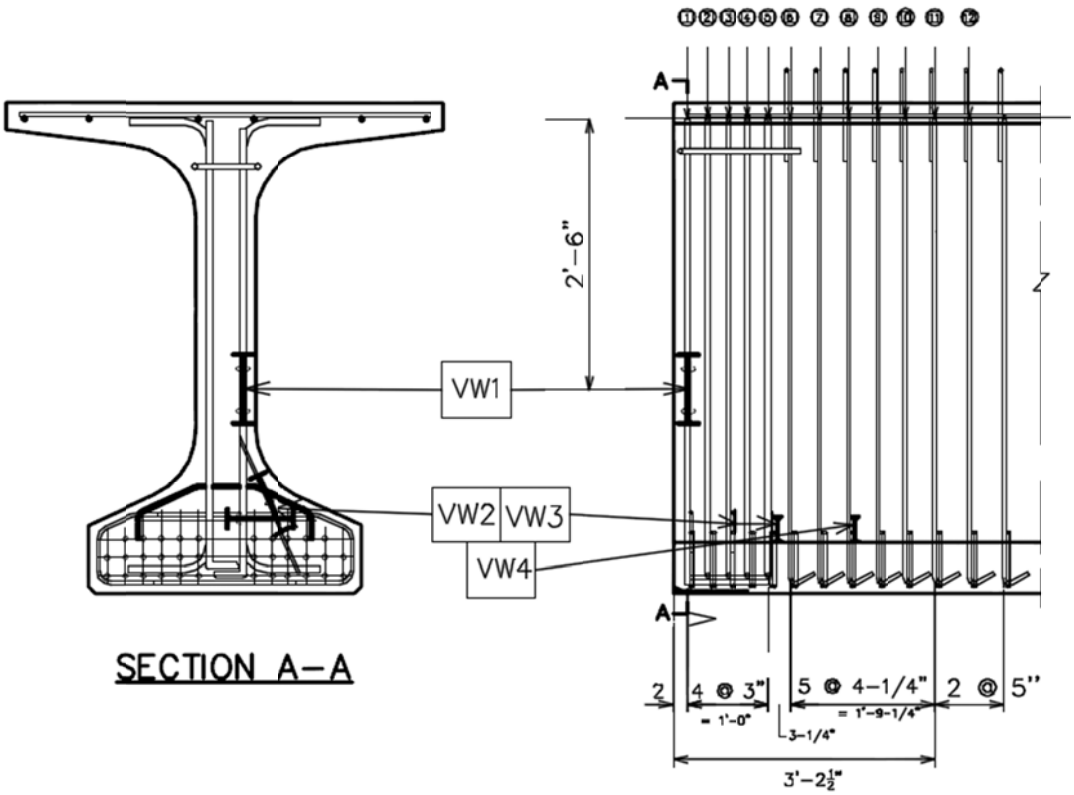

Figure 6-12. Location of Vibrating Wire Gauges.

6.1.3.1 Test Results

During de-tensioning, the strains were measured in the following manner for all girders: right after all draped strands were cut, after the top strand layer was flame cut, after the second layer was cut, and finally after all strands were cut.

Strain Gauge Results On Strands: The small 1mm strain gauges are very fragile. During the test, the gauge at 8in. from the end was broken in two of the girders. This most likely

occurred due to relative slip between the strand and the concrete that effectively scraped the gauge off or ripped the lead wire off the gauge. Therefore, the transfer length could only be estimated from the unbroken strain gauge data. The last strain results, after all strands were cut, are shown in Figure 6-13 for the girder with 38% debonding. Data from all three girders is listed in Table 6-2. Note that the location of the gauges were shifted by 8in. because the strand was debonded. from the end for the 8in. debonded girder design. Therefore, the results for this girder in Table 6-2 were given after the strand started to bond.

Strain Change in Strand on Release (Microstrain -με, negative = comp.)			
	at 8 inches	at 20 inches	at 36 inches
Bonded Girder	n.a.	-2469	-770
38% Debonded	-4057	-2288	-419
8 inch Debonded	n.a.	-2188	-758

Table 6-2. Strain changes at locations along strand upon release.

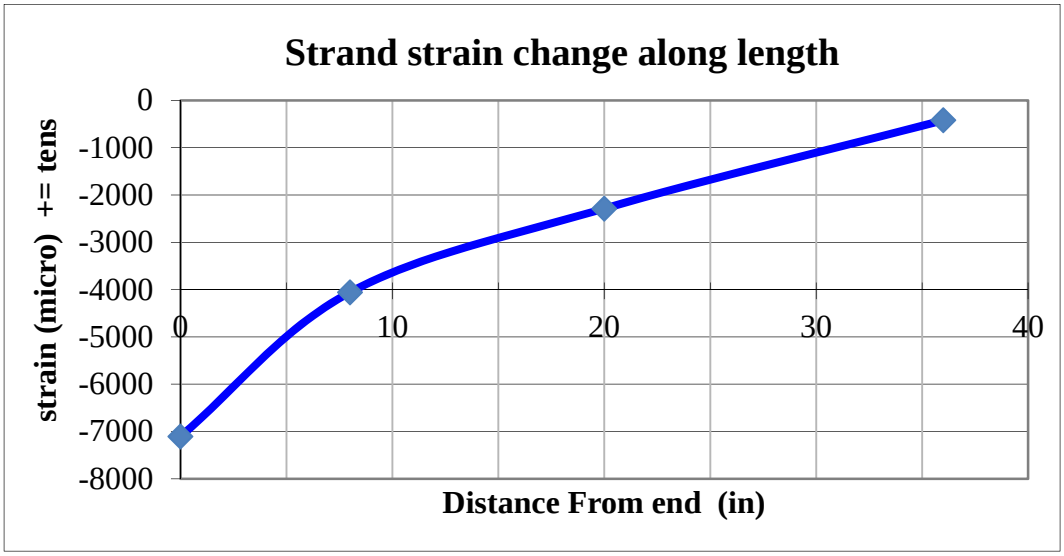

Figure 6-13. The Change in strain at locations along strand of 38% debonded beam.

The change in strain of the gauges at 36in. from end is small (419 to 770 $\mu\varepsilon$) meaning that the transfer length probably ended near to 36in. from the girder end. Some change in strain will occur even at the end of the transfer length due to the elastic shortening of the beam. With just under 12% prestress loss due elastic shortening the shortening strain would be near 800 micro strain, very close to the remaining strain at 36in. shown in Table 6-2. Based on the strain measurements it appears that the transfer length was 36in., minus the two regions were gages were placed and no bonding occurred, or 36-4=32 inches. A length of 36 inches, as suggested by AASHTO, was used in the analytical girder models.

The strain curve of Figure 6-13 is not linear so the uniform bond stress assumption of the AASHTO LRFD Bridge Specification along the transfer length did not actually occur here. Though nonlinear, the variation is not as great as reported by Arab et. al. (9) where the bond stress was assumed to vary in a parabolic fashion and a transfer length of 34 inches was apparent. To model the actual bond stress accurately in an analytical model the strain diagram along the length, of Figure 6-13, was assumed to have a piece wise linear shape with a constant (but different) bond stress in each of the segments. The slope in Figure 6-13 is highest near the end of the strand, implying a high bond stress, and becomes lower further in. For the analytical model, the bond stresses between strand and concrete were assumed to be constant with different values along the length as shown in Figure 6-14.

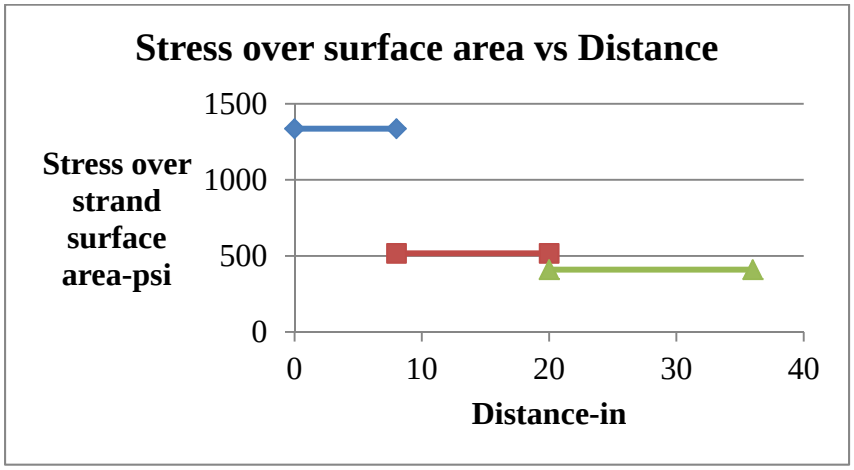

Figure 6-14. Bond Stress Variation Used in the Analytical Models.

Strain Gauge Results On Reinforcing Bars: As mentioned before, three strain gauges were mounted on web bars and two strain gauges were put on bottom stirrups.

The result of strain gauges on web bars: Two of the web bar strain gauges in the 38% debonded girder, namely S1 and S3, were damaged during casting. This likely occurred with the lead wire being ripped off the gauge as the concrete fell into the form or as the vibrator passed by the gauge during consolidation. Therefore, the results of those gauges are omitted. Figure 6-15 through Figure 6-17 show strain gauge data obtained from the tests. The gauge locations can be seen from Figure 6-10.

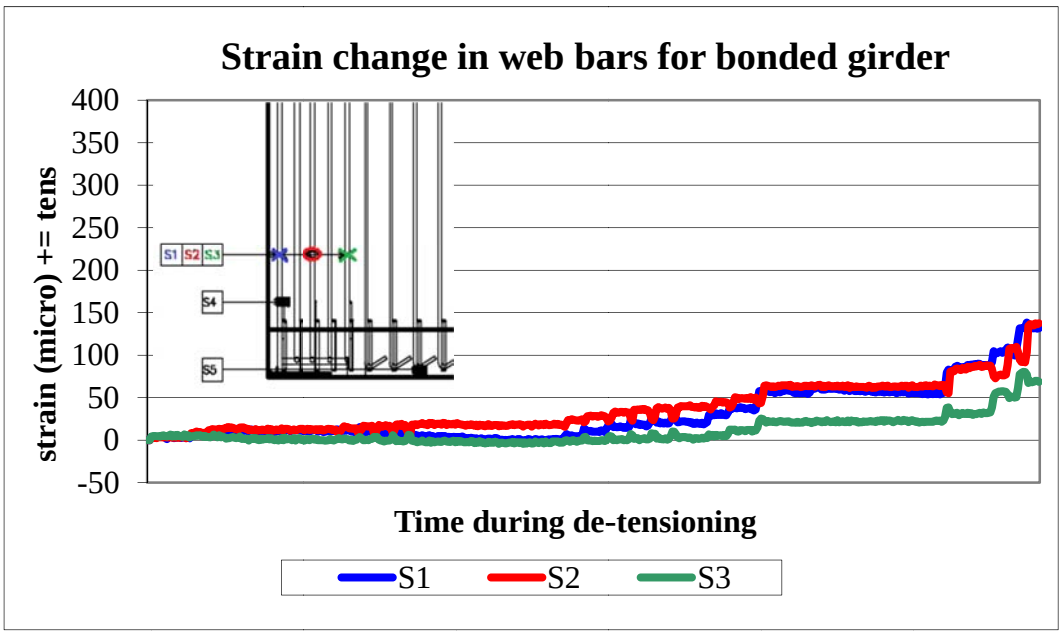

Figure 6-15. The test results of web bar strain gauges S1, S2, and S3 for bonded girder *(positive is tension).*

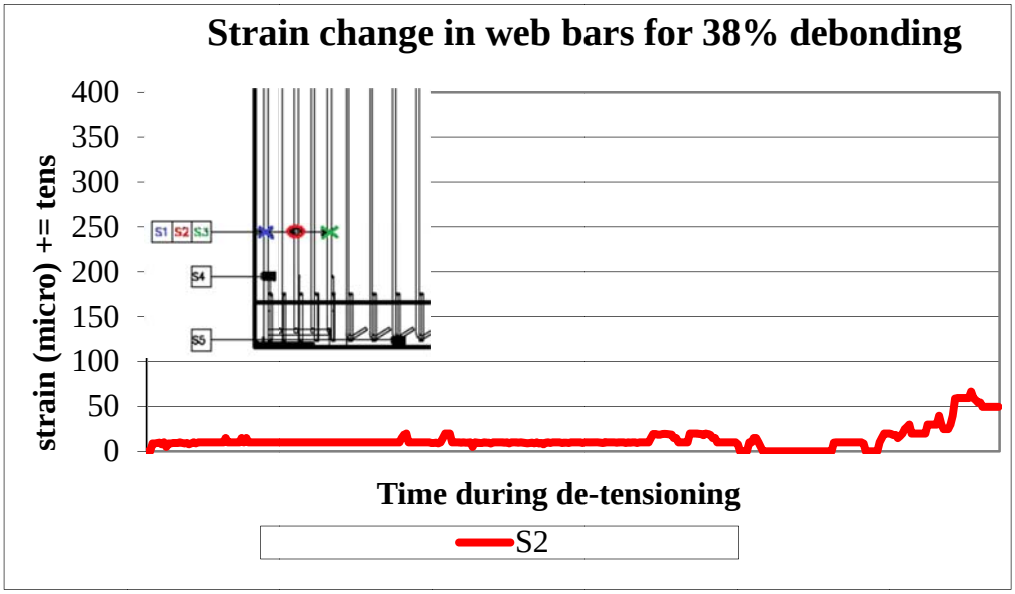

Figure 6-16. The test results of web bar strain gauge S2 for 38% debonded girder. *(positive is tension)*

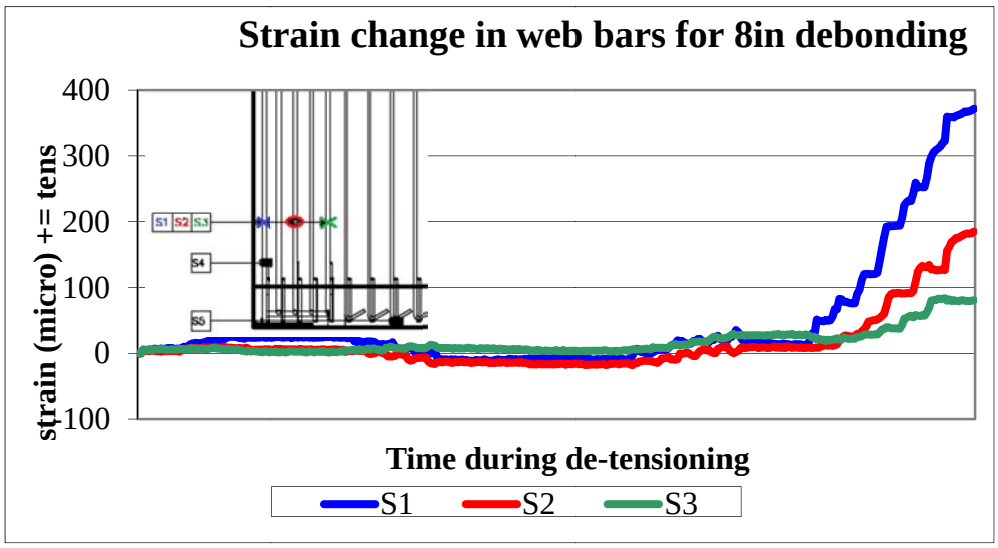

Figure 6-17. The test results of web bar gauges S1, S2, and S3 for debonded 8in. girder. *(positive is tension)*

Figures 6-15 and 6-16 show that debonding 38% of the strand reduced the web bar strain by nearly 50%. It appears, however, that the 8in. debonding method may not have worked in reducing web tension strains that could lead to horizontal web cracking, but may increase web strains. All three of the web bars showed higher strains with 8in. debonding than in the normal girder. The S1 bar of the 8in. girder developed 372 micro strain while the bonded girder only showed 132 micro strain. The expected cracking strain was 122 micro strain. Since the S1 gauge did not work in the 38% debonded girder, only the bonded and 8in. debonded girder results were compared.

The S2 gauge was mounted at the 3rd web bar. Luckily, all these gauges worked during testing. The bonded beam S2 gauge had a peak of 137 micro strain, with 38% debonding the peak was 66 micro strain, and with 8in. debonding the peak was 185 micro strain. The measured S2 bar web strains, when compared with the normal bonded girder, decreased by

52% with 38% debonding and increased by 35% with debonding only 8in. from the girder end.

At the fifth web bar, 14in.inside the girder, the S3 gauge showed that there was no meaningful difference in tension strain between the normal bonded girder and the 8in. debonded girder. The gauge in the 38% debonded girder was not working. The low strains can be taken as an indication that this bar is not effectively working to resist cracking and a redesign of the beam (shown in Figure 6-1) could reduce the number of sets of #6 bars at the end of the beam from 5 down to 3.

The result of strain gauges on bottom flange stirrups: The S4 gauge was at the top of the first "banana bar" (small horizontal top stirrup), and the S5 was at the bottom of the eighth "chicken leg" stirrup. Figure 6-18 through Figure 6-20 show the strain results with the detailed gauge locations from Figure 6-10.

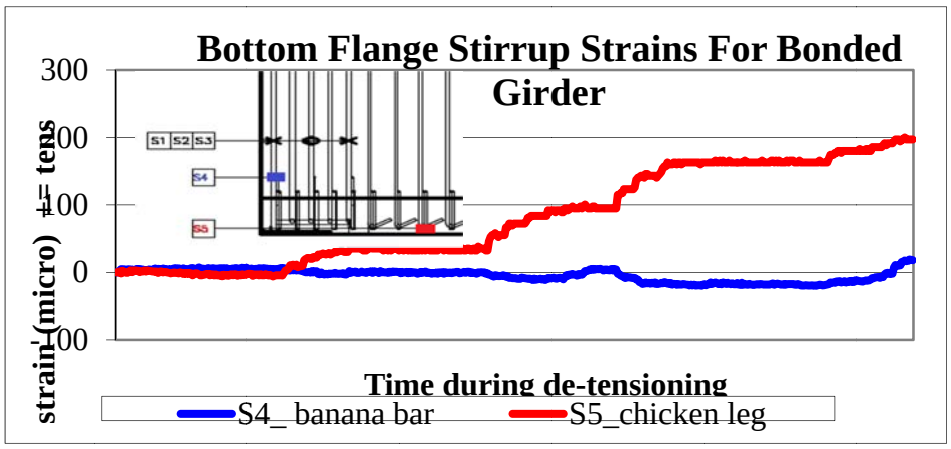

Figure 6-18. The test strain results for S4 (on banana bar) and S5 (on chicken leg bar) stirrups for bonded girder. *(positive is tension)*

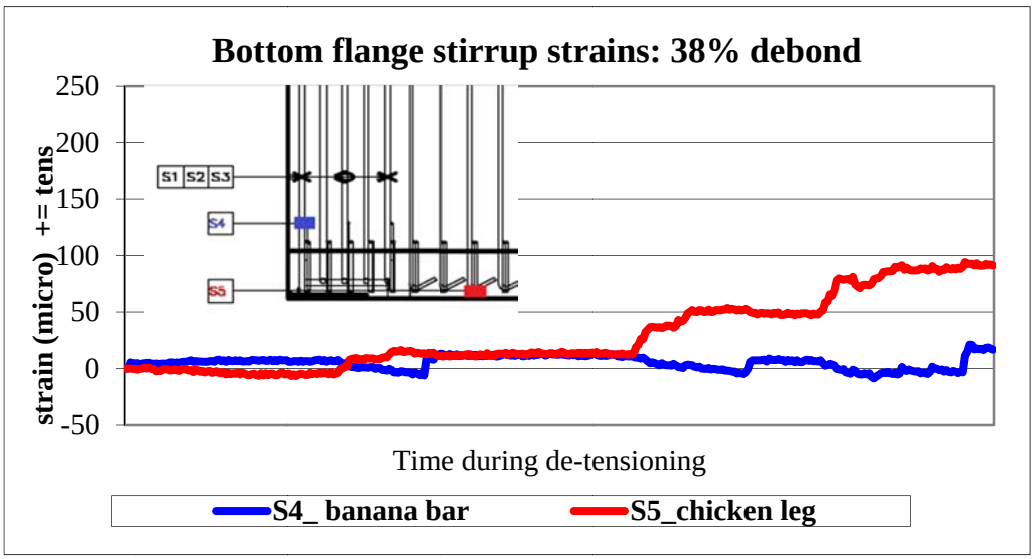

Figure 6-19. The test strain results for S4 (on banana bar) and S5 (on chicken leg bar) stirrups for 38% de-bonded girder. *(positive is tension)*

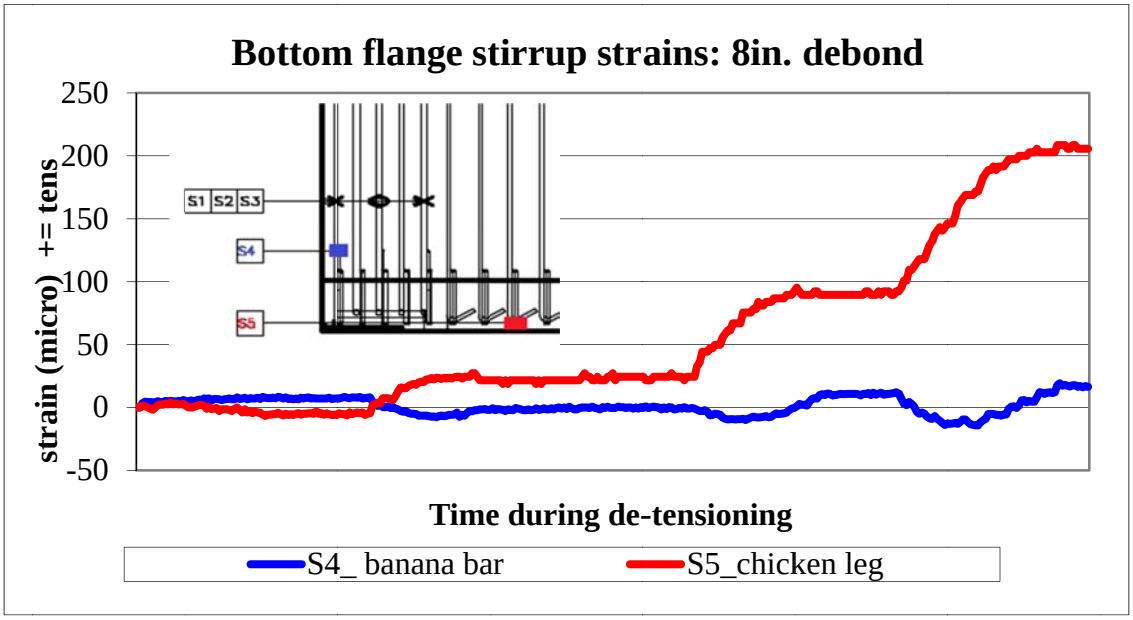

Figure 6-20. The test strain results for S4 (on banana bar) and S5 (on chicken leg bar) stirrups for 8in. de-bonded girder. *(positive is tension)*

The S4 gauge was intended to signal development of a Y crack but the strain results are very small. The bonded girder had a peak S4 tension of 19 micro strain, the 38%

debonded had 21 micro strain and the 8in. debonded showed 19 micro strain. These bars are very short and epoxy coated. The small strains indicate that they are ineffective, particularly since they are in a region where the Y crack is expected to occur. Visual observations showed that there were Y cracks in this vicinity. The lack of strain in the bars, likely due to poor bonding with the epoxy coating, suggests that these bars should either be eliminated in the design or used without epoxy coating to improve their bond.

The S5 gauges were on the bottom of the flange stirrup leg, at approximately 26in. from the end of the girder. The strains in these bars would indicate that they are effective and represent the degree of bursting strain developing in the girders. The bursting stress is caused by the transfer of force from the strands to the concrete. It would be expected that the girder with 38% debonding, staggered at locations 3ft, 6ft, and 9ft into the beam, would show little bursting strains because few strands are transferring force at any particular location. The transfer occurs gradually over the first 12ft of the girder. The measured strain results agree with the expected behavior. The S5 gauge in the bonded girder reached 200 micro strain in tension, only 94 micro strain occurred in the 38% girder, but 208 micro strain developed in the 8in. debonded girder. There was virtually no strain difference between the bonded girder and the 8in. debonded girder because all strands were transferring force to the concrete in the same region.

Strain Results from Vibrating Wire Gauges: Average strain changes in the concrete were measured at 4 different locations in the girders during detensioning. As described earlier, the gauges were placed across regions where high tension strains were predicted by a preliminary analytical model, and thus locations where cracks might occur. It was

anticipated that any development of concrete cracks across one of the gauges would be signaled by an abrupt large increase in strain measured by the gauge.

The cracking limit of the concrete was estimated using rupture equations from the AASHTO LRFD Bridge Design Specifications. AASHTO uses 1820*(sqrt fc') as the elastic modulus and 0.23*(sqrt fc') as the rupture strength. The cracking strain is obtained by dividing cracking strength by elastic modulus, and is approximately 126 micro strain by averaging all girders tested.

The debonded girders and bonded girder were detensioned on different days and at slightly different rates. Therefore, there is a difference in the data point numbers versus the strands being cut shown along the time axis (x-axis) in Figure 6-21 through Figure 6-24. The main information, however, to be gleaned from the data is the peak strains measured. The figures show the results of all the vibrating wire gauges and the details of the gauge locations were given in Figure 6-12. Note that results for all gauge locations are not always visible because some of the gauges became damaged during the concrete placement and did not subsequently work.

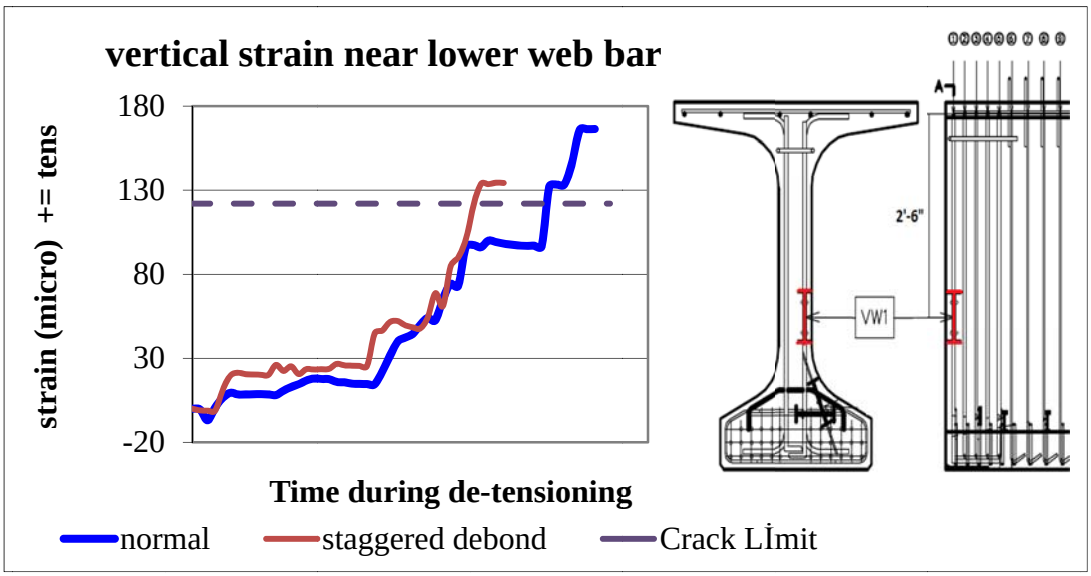

Figure 6-21. Strain results for vibrating wire gauge VW1. *(positive = tension)*

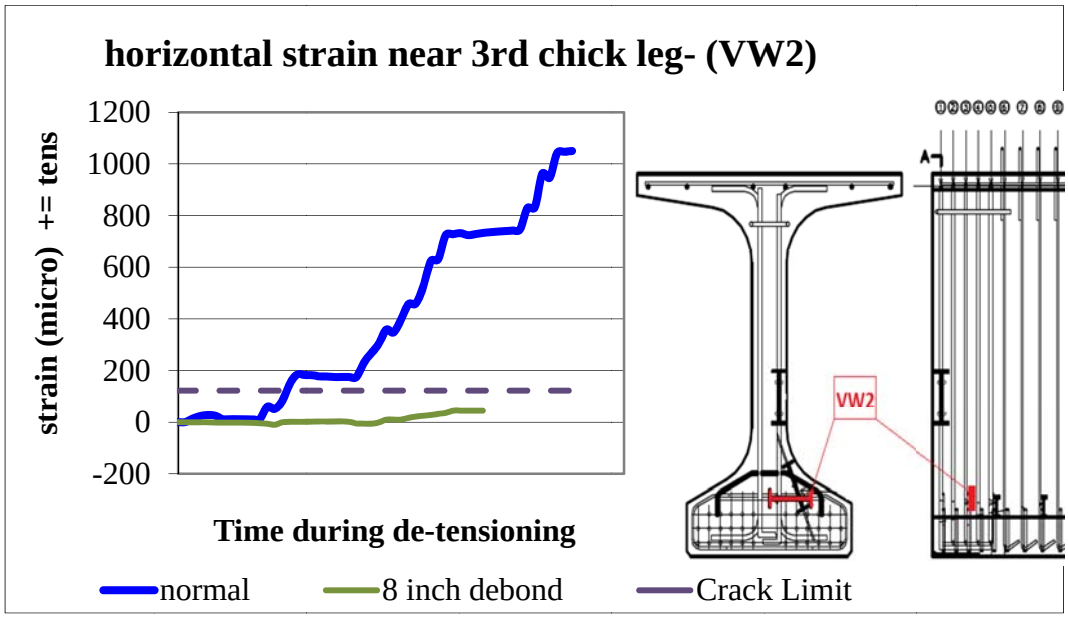

Figure 6-22. Strain Results for Vibrating wire gauge VW2. *(positive = tension)*

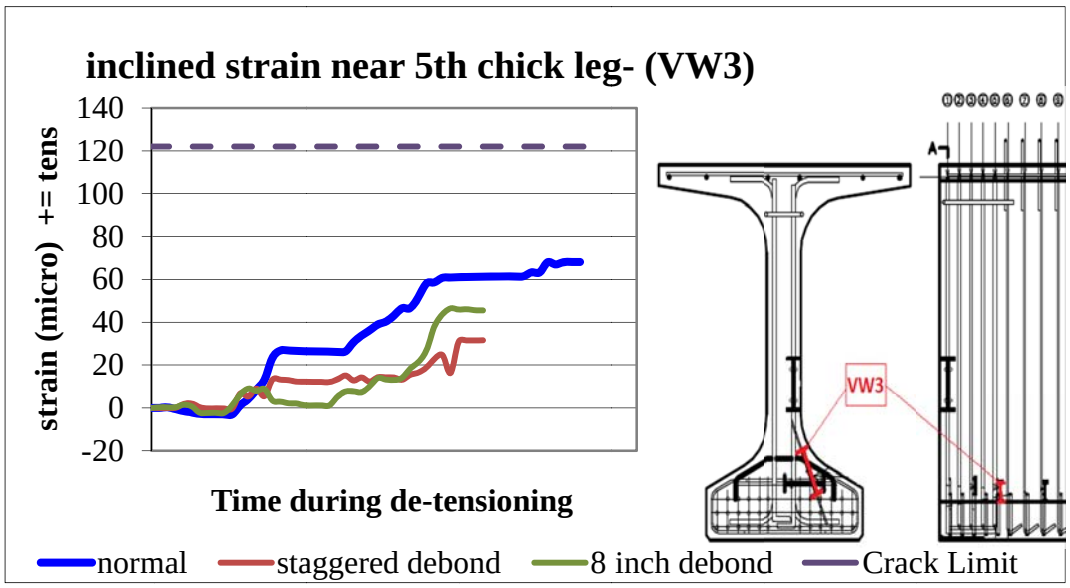

Figure 6-23. Strain Results for Vibrating wire gauge VW3. *(positive = tension)*

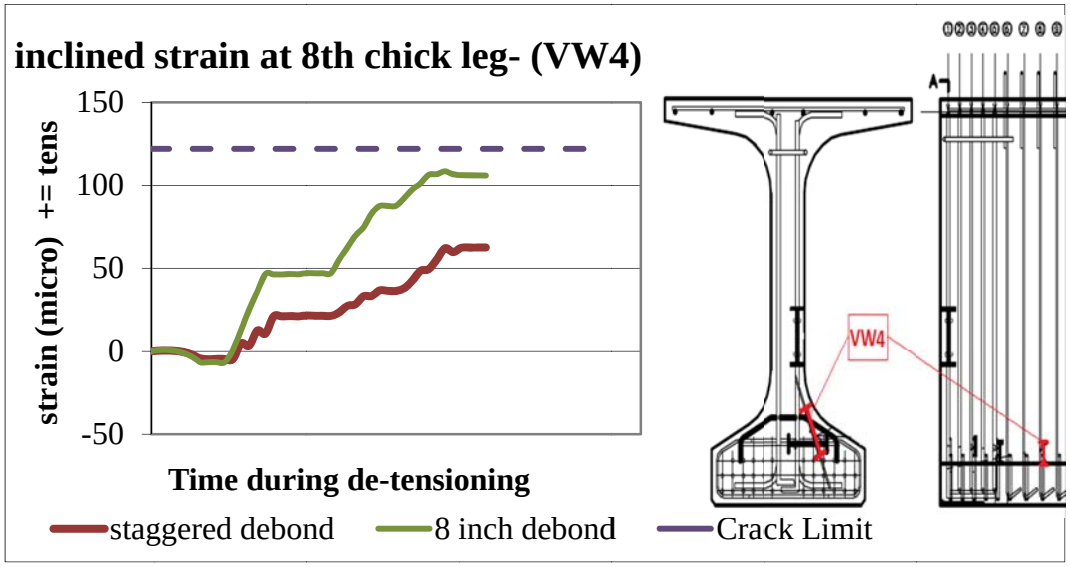

Figure 6-24. Strain Results for Vibrating wire gauge VW4. *(positive = tension)*

The plots of Figure 6-21 through Figure 6-24 will be examined individually, starting from the top plot with the VW1 gauge. VW1 is vertically located at 30in. from top center of the first longitudinal top flange bar. This gauge was placed to detect horizontal cracks in the

web and at the location where the predicted web tension strains were the highest. The gauge in the 8in. debonded beam did not work. The results for both the normal girder and the 38% debonded seem to indicate that cracking did occur, probably after the strands of the middle bottom row were released. The average strain over the 6in. gauge length reached 166 micro strain in the normal girder and 134 micro strain in the 38% debonded girder. The predicted cracking strain was 122 micro strain. It is unfortunate that the VW1 gauge of the 8in. debonded girder was broken. From the measured strains horizontal cracking of the web might be expected in both girders.

The VW2 gauges were placed horizontally at the top of the bottom flange and 8in. from the end of the girder – where a Y crack might occur. The gauge was inoperable in the 38% staggered debonded girder. Strains in the normal girder jumped after the middle bottom row of strand was detensioned and indicated likelihood of a Y crack having developed with an average peak of 1050 micro strain. The girder with 8in. debonding only developed 45 micro strain at the same location, which is below the cracking limit. Therefore, the 8in. debonding showed a 96% decrease in tension strain compared to the normal girder.

Luckily all three inclined vibrating wire gauges in the bottom flange worked at the location of VW3, approximately 14in. in from the girder end, so that the effect of debonding patterns could be compared. The resulting strains in all three beams were low and indicating that Y cracking was unlikely this far into the beam. The normal girder showed an average of 68 micro strain over the 2in. gage length, the 38% debonded reached 32 micro strain and the 8in. debonded developed 46 micro strain. Debonding did provide a small decrease in strains: 53% in staggered pattern and 32% in the 8in. debonded girder.

Further into the girder, in the VW4 location approximately 26in. from the end, the gauge in the bonded girder was inoperable. Therefore, only a comparison of the two debonded girders can be made. Both the strains in the debonded girders are below the cracking limit, however, so Y cracking was not expected at this location in either girder. The peak strain value of the 8in. debonded girder is 108 micro strain whereas it is 65 micro strain for the staggered debonded girder.

6.2 Cracks in Girders

Concrete is a heterogeneous mixture of an aggregate, sand, cement and water. However, the distribution of these components are not even throughout the body depending on many factors like casting position of concrete member, vibration, etc. so locating cracks by modelling concrete bodies is a challenging job. As mentioned before, the location of all gauges were positioned inside the concrete according where high strains were predicted by Abaqus models with nonlinear material properties. Figure 6-25 shows the general location of vibrating wire gauges in each girder. This is made to see how close the gauges were placed to the visible cracks.

It seems that except for the vibrating wire gauge labelled as VW1, cracks did not cross the other vibrating wire gauges. The VW 1 gages were very near to, or possibly crossing a crack.

Figure 6-25. The location of vibrating wire gauges in bonded (top left), 38% debonded (top right), and the girder that is debonded 8 in. from end (bottom).

Figure 6-26. Close-up picture of bottom flange for bonded (top), 38% de-bonded (middle), and 8in. debonded (bottom) girders.

Right after de-tensioning, it was observed that Y cracks in the instrumented ends did not develop or show a vertical leg through the bottom flange as in Figure 6-26. While the 8 inch debonded beam showed the start of top legs of a Y crack, the VW2 gage was parallel to the cracks and would not provide any measurement. The VW3&4 gages might have crossed the cracks if the cracks extended far enough in from the end of the girder.

Surprisingly, a severe Y crack did not occur in the bonded girder as predicted analytically. There may be a partial explanation for this. Workers at the plant put two uncoated #4- 30”x36” U bars beneath the top row of strands and above the bottom row strands as in Figure 6-27 even though this was not in the standard WisDOT plans. The U bars likely resisted some of the flange tension stresses and reduced the Y crack formation or reduced the crack width so it was not visible. However, further study might be needed to conclude that this is an effective method to prevent Y cracks at the bottom flange.

Figure 6-27. U bars beneath the top row of strands and above the bottom row of strands in side view (top) and in top view (bottom).

One of the good measures to compare effectiveness of the debonding is to compare the total length of cracks at the ends of girders. Below, in Table 6-3 and Figure 6-28, crack lengths of the instrumented end, the other end, and total of these two ends are shown. An end wise comparison is preferred because Y crack lengths in each girder are fairly small. Therefore, a bigger percentage of total lengths of cracks are in a combination of horizontal and inclined cracks.

	Bonded	38% De-bonded	De-bonded 8in. from end
Instrumented End	132	42	174
Other End	194	14	88
Total	326	56	261

Table 6-3. Total end crack lengths of each girder. All measures are in inches.

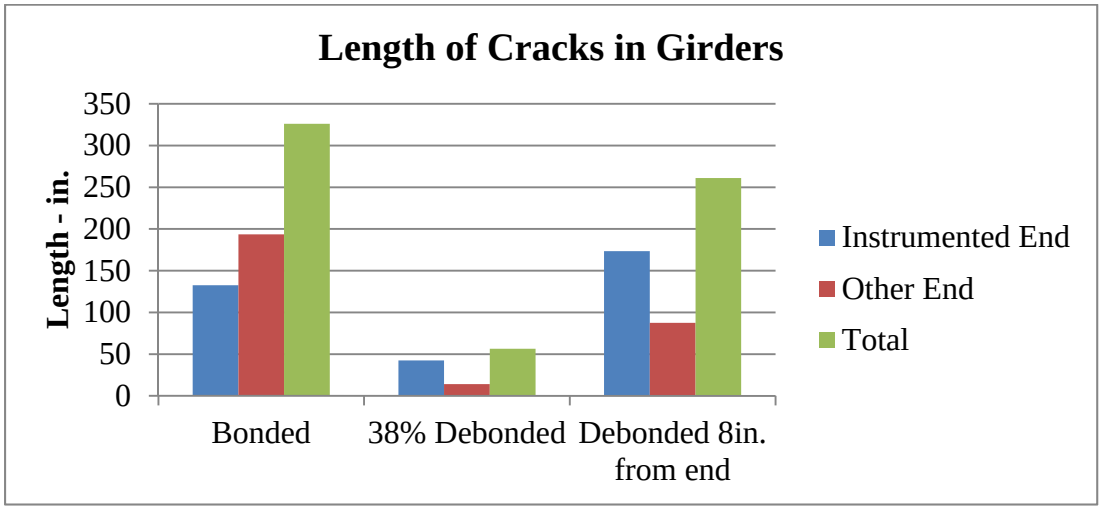

Figure 6-28. Total crack lengths of girders.

The bonded girder was cast in a different bed and a different day than the debonded girders. The debonded girders were in the same casting bed as in Figure 6-29 and the instrumented ends were facing each other in the middle. The “X” in the “top view” of Figure 6-29 represents the places that the strands were flame cut. There was approximately 4 feet between the faces of the girders at the middle.

In cutting strands the free length, outside of the beam, stores strain energy that is abruptly released when a strand is cut. The longer the free distance, the larger the energy and dynamic effect on the girder concrete at the initial bond point. An end of the girder with a long free strand would be expected to be susceptible to more cracking than an end with a short free length.

In the present case the normal girder was the end girder in the casting bed and our instrumentation was placed at the end with hydraulic jacks, rather than at the girder end between two girders, that is at the right side of the girders shown in Figure 6-29.

The instrumentation for the debonded girders was placed in the gap betwee the two girders, rather than at the bed end where the hydraulic jacks were. This would be at the middle joint shown in Figure 6-29.

When strands were cut between two girders there was a longer free strand length than when the strands were cut at the end of the bed. The 38% debonded girder had a free strand length of approximately 10 inches while the 8in. debonded girder had a free strand length of nearly 38 inches.

It is possible that the layout of the girders in the bed affected the end cracking. Looking at the other end of the normal girder, as in Figure 6-30, the top horizontal legs of a Y crack were apparent just as in the 8 inch debonded girder.

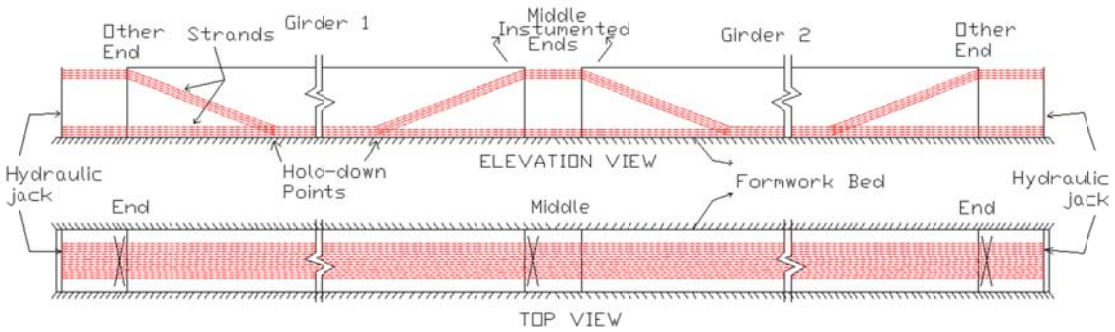

Figure 6-29. Plan of de-bonded girders in the same formwork bed.

Figure 6-30. Other end of normal girder which was in the middle of the bed.

In respect to total cracking, both debonding patterns worked well for reducing the length of cracks but 38% debonding seems to be more effective than full debonded by 8 in. The data from gauges supports this conclusion.

6.3 Bonded Girder Comparison with the Results of Finite Element Models

Finite element models were created in Abaqus for the girders tested. The basic structure of the models used the same procedures as described in Chapter 4 but some changes were necessary for each girders' properties such as concrete strength, etc. to simulate the test conditions. The transfer length of the strands in all girders was taken as 36in. based on the data obtained from strain gauges and the AASHTO guideline..

6.3.1 Bonded Girder Crack Locations

The average initial concrete strength of the bonded girder was measured as 7820 psi from cylinder tests before de-tensioning of strands. Using this information, the cracking strain was

calculated as 126 με. The concrete strains from both test and models were compared with this cracking limit. Reinforcing bar strains were compared with 690 με corresponding to the 20 ksi limit on splitting zone reinforcement of AASHTO LRFD BDS Section 5.10.10.1.

A first comparison is between the real girder end of the bonded girder and the model built for this girder. In Figure 6-31, the real horizontal crack locations are almost at the same height and position as predicted in the model (evidenced by light blue at 236με, green or orange contours at higher strains).

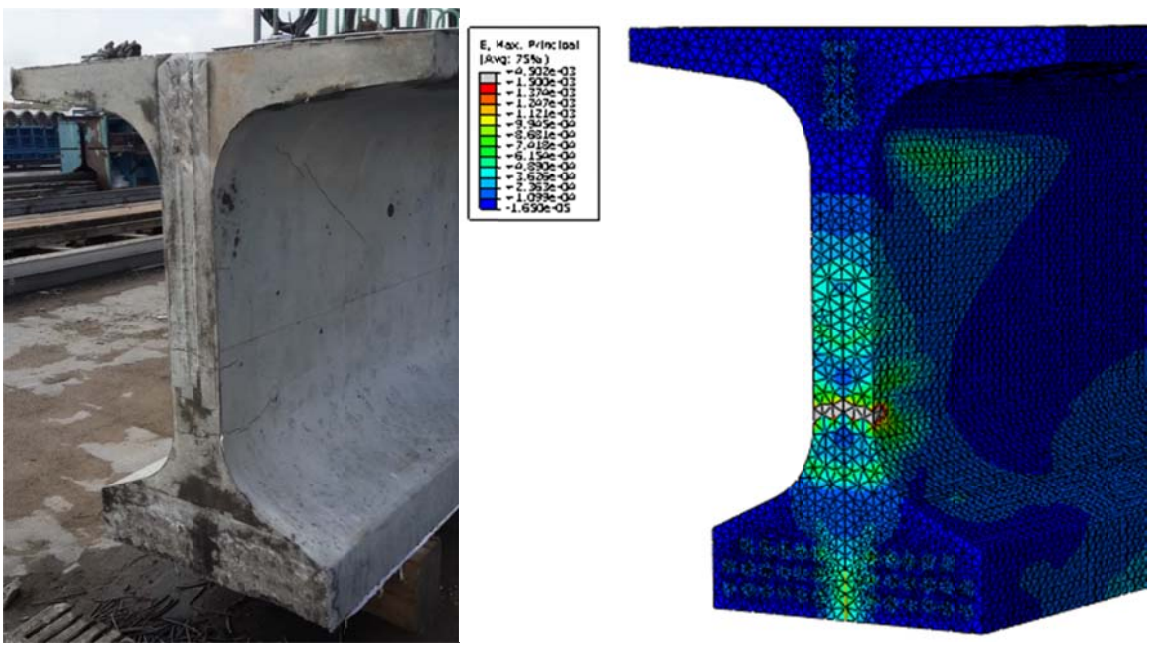

Figure 6-31. The comparison of bonded girder ends in reality and in model.

6.3.2 Bonded Girder: Strain Results at Vibrating Wire Gauges

The strains predicted near the vibrating wire gauge were obtained from the finite element models by averaging the element strains near the caps of the gages. The vibrating wire gauges measure the average strain over the full gage length while the FEM gives strain at a

point. Figures 6-32 to 6-34 show strains are in microstrain and the graphs were plotted as the prestressing force was transferred to the concrete. The results from VW 4 were omitted because it was damaged during release.

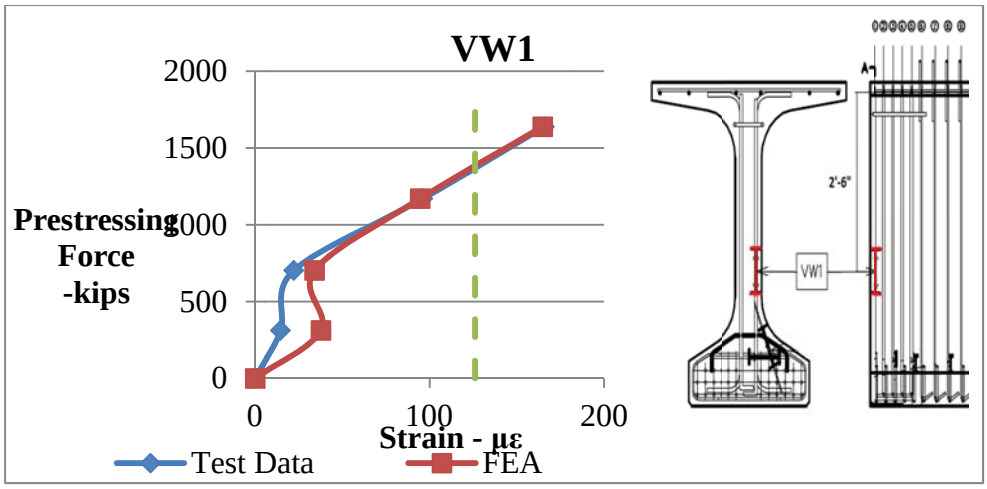

Figure 6-32. Concrete strain comparison between data obtained by VW gauge 1 and finite element model during prestress release for bonded girder. *(positive = tension)*

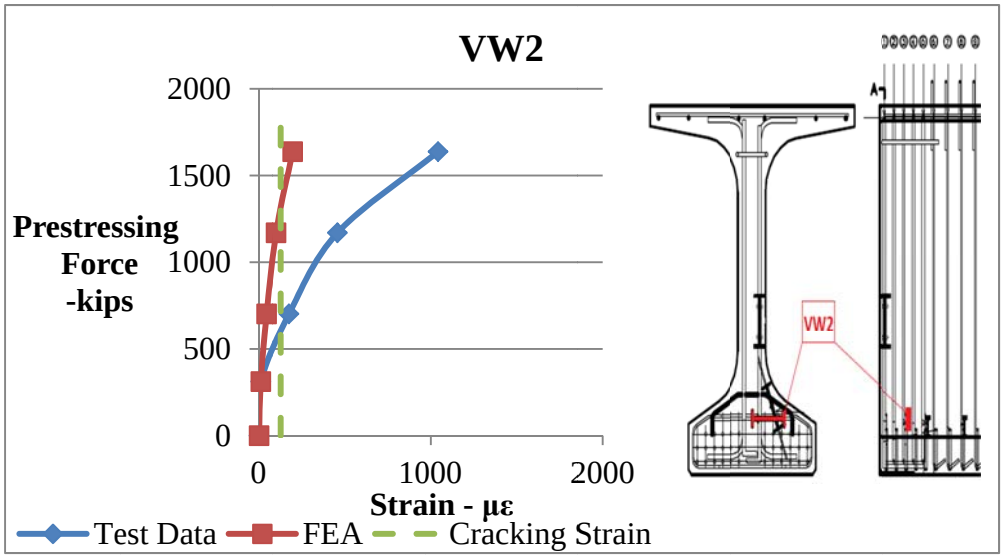

Figure 6-33. Concrete strains comparisons between data obtained by VW gauge 2 and finite element model during prestress release for bonded girder. *(positive = tension)*

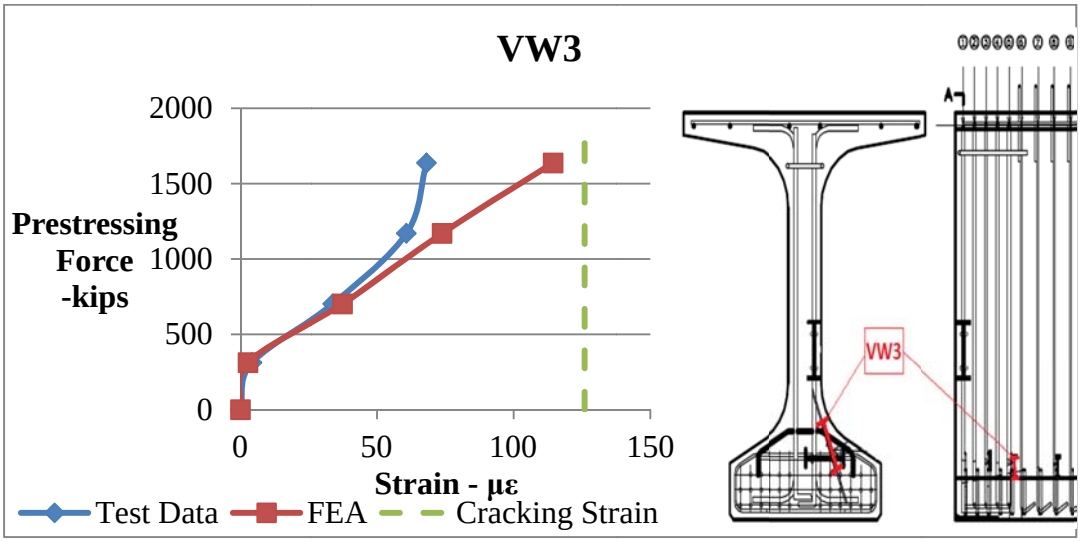

Figure 6-34. Concrete strains comparisons between data obtained by VW gauge 3 and finite element model during prestress release for bonded girder. *(positive = tension)*

VW1 was expected to be under high tension based on the finite element model, which predicted a potential location for cracking. Figure 6-32 shows that the gage indicated tension and had good agreement with the finite element model. The final measured strain nearly coincided with the FEA model prediction. They are both over the cracking limit.

Likewise, tension was expected in the location of VW2. The maximum principal direction in the FEM model was almost horizontal, therefore, the gage was placed horizontally. The model seems to match measured strain well until the top row of bottom flange strands were cut, which correspond to approximately 700 kips of prestressing force. After that, the difference increases rapidly with the gauge results indicating a likely crack intercept by the gauge. The predicted strains are then significantly lower. Both results, however, are over the cracking limit so there must be cracking inside of the girder. Though

the strains were larger than the cracking limit, during end zone observations no Y cracks were visible.

Test and model results at the VW3 location indicate that strains are smaller than the expected concrete cracking limit, which means that cracks probably did not extend to that location. The agreement between the the model and the data is good until the middle strand row in the bottom flange was cut. From there the FEM predicted strains continued to increase but the measured strains stayed relatively constant. The behavior of the measured strains seems to indicate that there may have been a crack nearby, limiting an increase in stress, but strains in adjacent concrete stayed constant. Since the strains were below the cracking limit defined for the FEM model the behavior continued as elastic without cracking. It is likely that cracking started in the girder at a strain lower than expected by the AASHTO equation for cracking stress/strain used in the FEM model.

6.3.3 Bonded Girder: Strain Results at Strain Gauges

All strain values in the reinforcing bars were below the AASHTO LRFD limit of 20 ksi, which corresponds to 690 $\mu\varepsilon$, so the limit was not included in Figures 6-35 to 6-39. Since re-bars are homogeneous and remain elastic, the correlation between measured and predicted strains should be close. The strains in the figures are for gages S1-S3 on the vertical web bars, S4 on the bottom flange banana bar and S5 on a bottom stirrup.

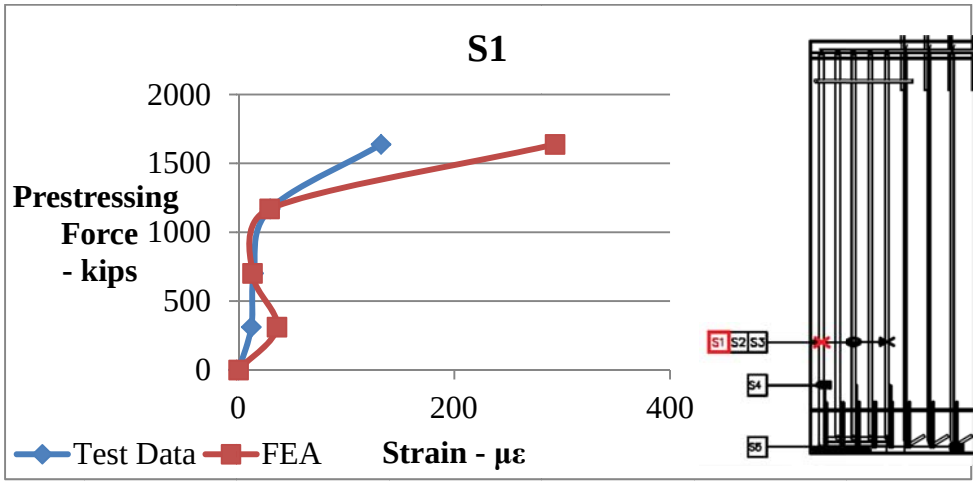

Figure 6-35. Re-bar strain comparisons between data obtained from strain gauge 1 and finite element model during prestress release for bonded girder. *(positive = tension)*

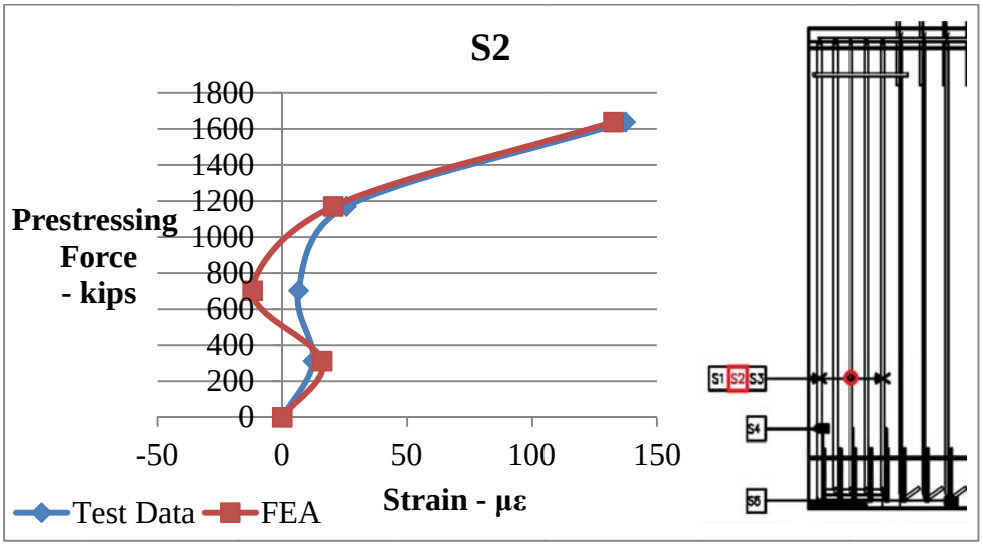

Figure 6-36. Re-bar strain comparisons between data obtained from strain gauge 2 and finite element model during prestress release for bonded girder. *(positive = tension)*

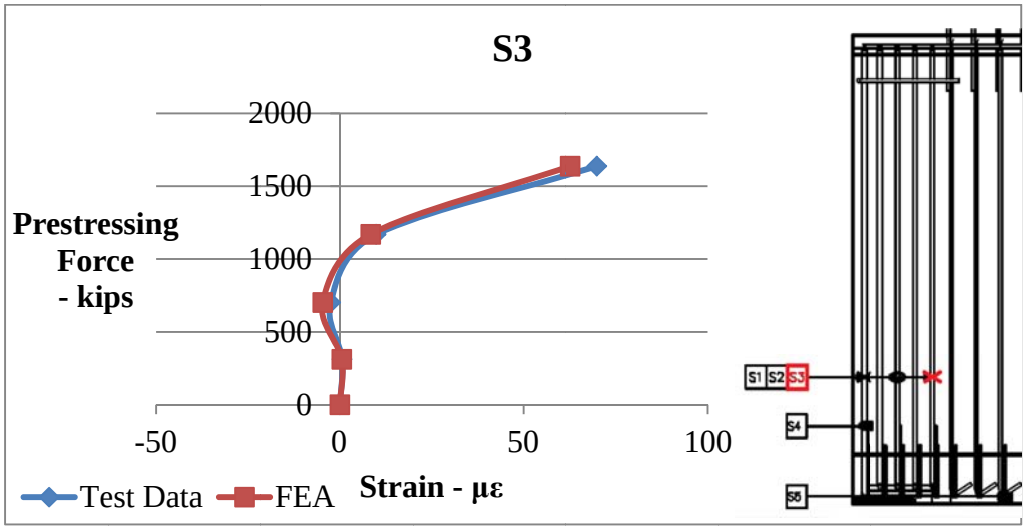

Figure 6-37. Re-bar strain comparisons between data obtained from strain gauge 3 and finite element model during prestress release for bonded girder. *(positive = tension)*

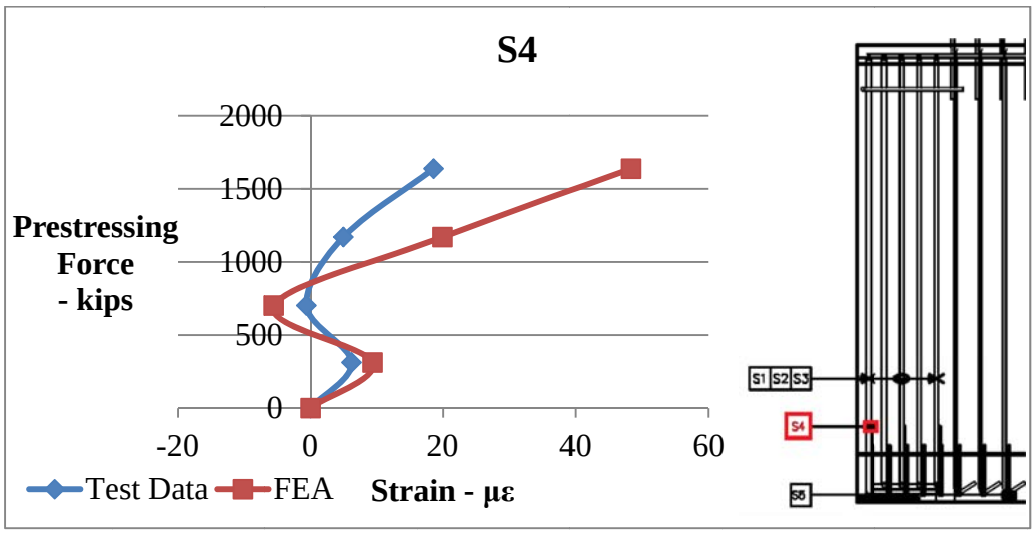

Figure 6-38. Re-bar strain comparisons between data obtained from strain gauge 4 and finite element model during prestress release for bonded girder. *(positive = tension)*

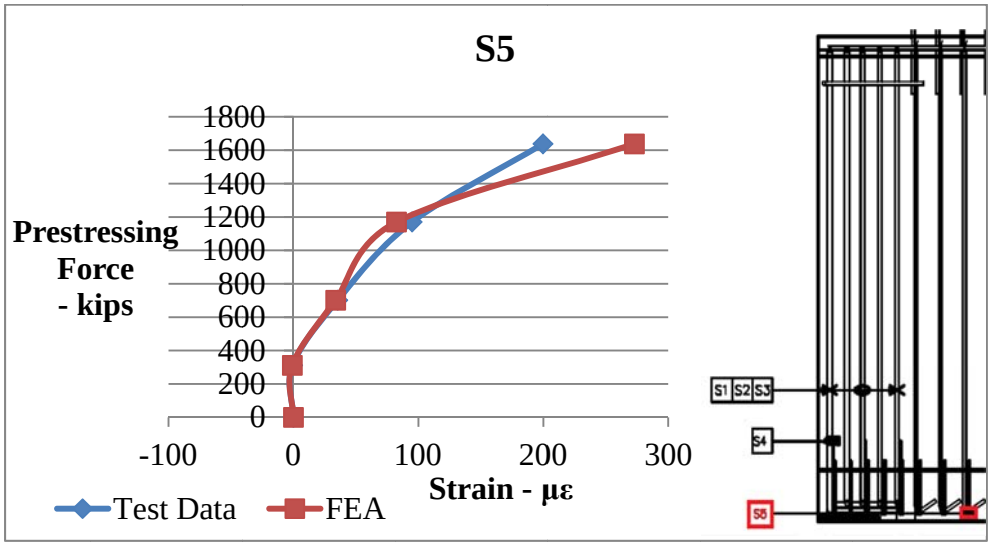

Figure 6-39. Re-bar strain comparisons between data obtained from strain gauge 5 and finite element model during prestress release for bonded girder. *(positive = tension)*

The correlations for gauges S2, S3 and S5 were very good. The final FEM predicted value for the strain at gauge S1 was nearly double the actual measured strain, though the correlation was good until the bottom strand row was released. This difference could have occurred if the actual girder had cracked slightly above or below the gauge location, allowing the bar stress and strain to remain constant at the gauge. This may be corroborated by the rapid variation in concrete strains shown by the contours in Figure 6-31.

The predicted strain at gauge S4 was also nearly double the measured strain after the middle strand layer in the bottom flange was released. Neither of the strains are significant – being between 20 and 48 με, well below the concrete cracking strain. The 28 με error is well within the bound of accuracy expected in measuring and prediction of strains in reinforced concrete members.

6.4 38% De-bonded Girder With Strands Bonded in Staggered Lengths

The initial concrete strength for the girder with 38% debonding was 8140 psi from cylinder tests before de-tensioning of strands. This information was used to calculate the cracking strain of concrete, which is 126 με. The concrete strains from both test and models were compared with this cracking limit. Again, reinforcing bar strains were compared with 690 με corresponding to the 20 ksi limit on splitting zone reinforcement of AASHTO LRFD BDS Section 5.10.10.1.

Comparison of ends showed good correlation in visible and predicted crack locations. The model showed the region where cracks will occur, based on the 126 με limit, in Figure 6-40 as light blue or green in contour color. No cracking clearly appeared in the model, except possibly in the bottom flange, but limited web cracking did occur in the girder.

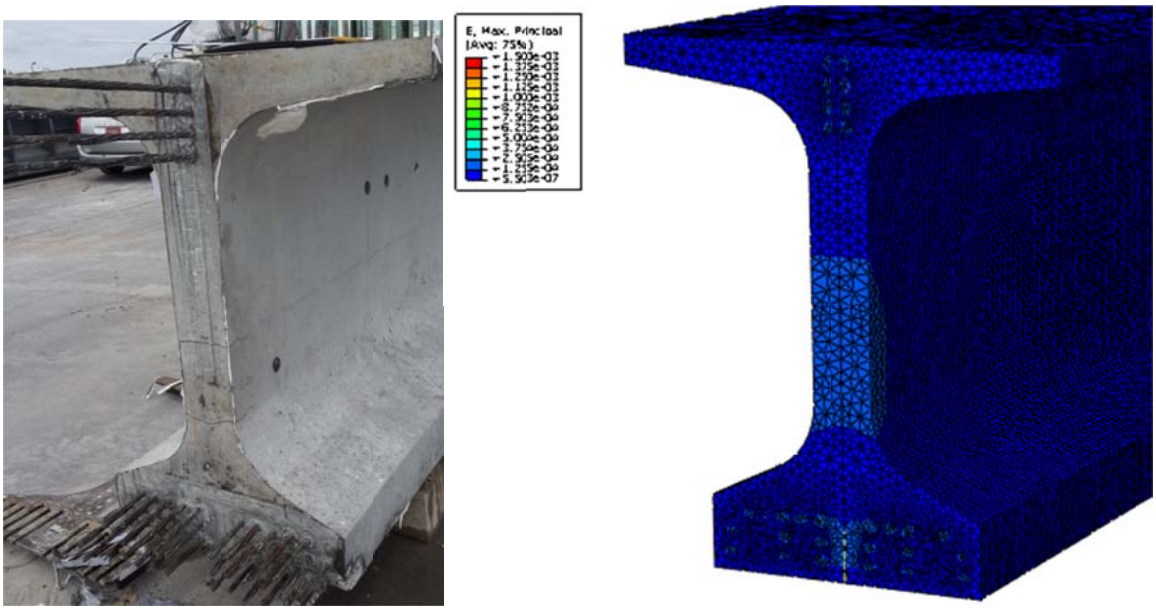

Figure 6-40. The comparison of 38% de-bonded girder ends in reality and in model.

6.4.1 38% Debonding: Strain Results at Vibrating Wire Gauges

The following Figure 6-41 through Figure 6-43 are comparisons between test data and finite element model strain predictions in the concrete. The graphs were plotted as prestressing force was transferred to the concrete (time along x-axis) versus strain. The results from VW2 were omitted because it was damaged during release.

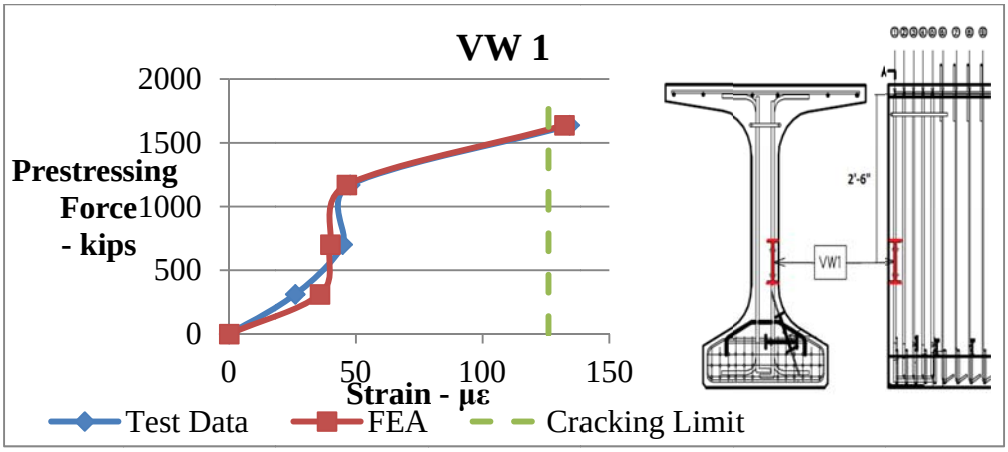

Figure 6-41. Concrete strain comparison between data obtained by VW gauge 1 and finite element model during prestress release for 38% de-bonded girder. *(positive = tension)*

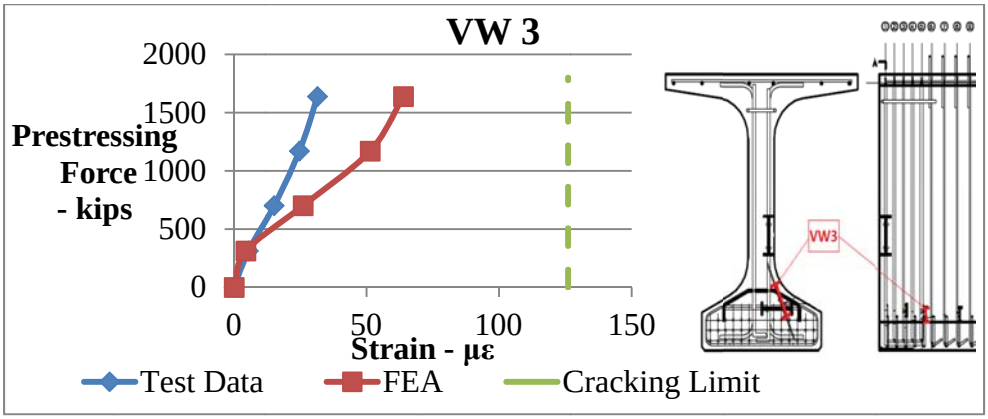

Figure 6-42. Concrete strain comparison between data obtained by VW gauge 3 and finite element model during prestress release for 38% de-bonded girder. *(positive = tension)*

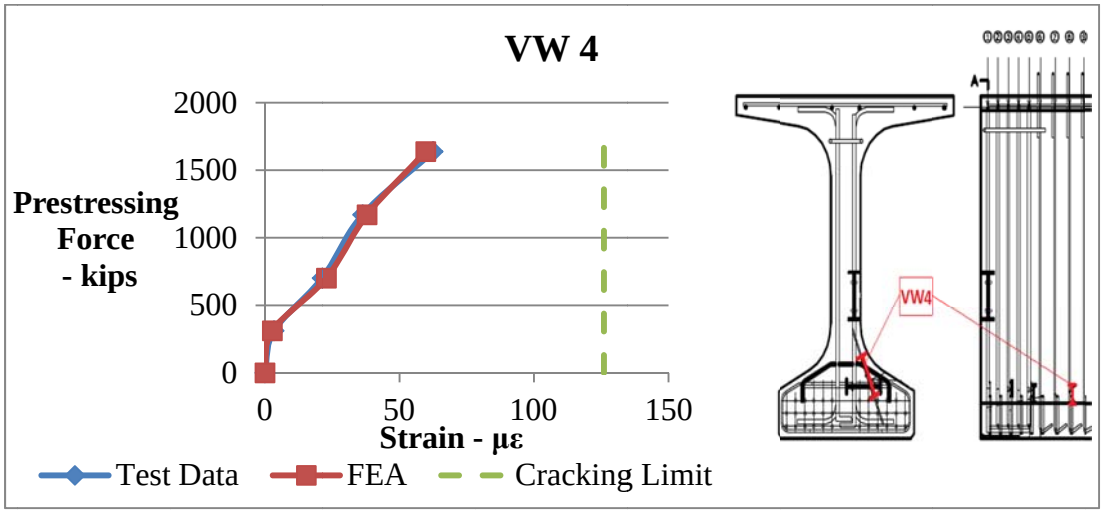

Figure 6-43. Concrete strain comparison between data obtained by VW gauge 4 and finite element model during prestress release for 38% de-bonded girder. *(positive = tension)*

Good correlation is apparent at the VW1 gauge location as shown in Figure 6-41. In Figure 6-25, the horizontal crack just reached the VW1 location, so it is logical that the strains are over the cracking limit. The results at the VW4 location are also good, although the strains are quite low.

The strains at VW3 did not exhibit a good correlation after the bottom strands started being released. The FEA model predicted double the tensile strain measured, though the strain was less than 60με.

6.4.2 38% Debonded Girder: Strain Results at Strain Gauges

In the 38% de-bonded girder, the S1 and S3 gauges were broken so their plots are not shown. S2 and S3 results are from the vertical web bars, S4 and S5 are from the bottom flange.

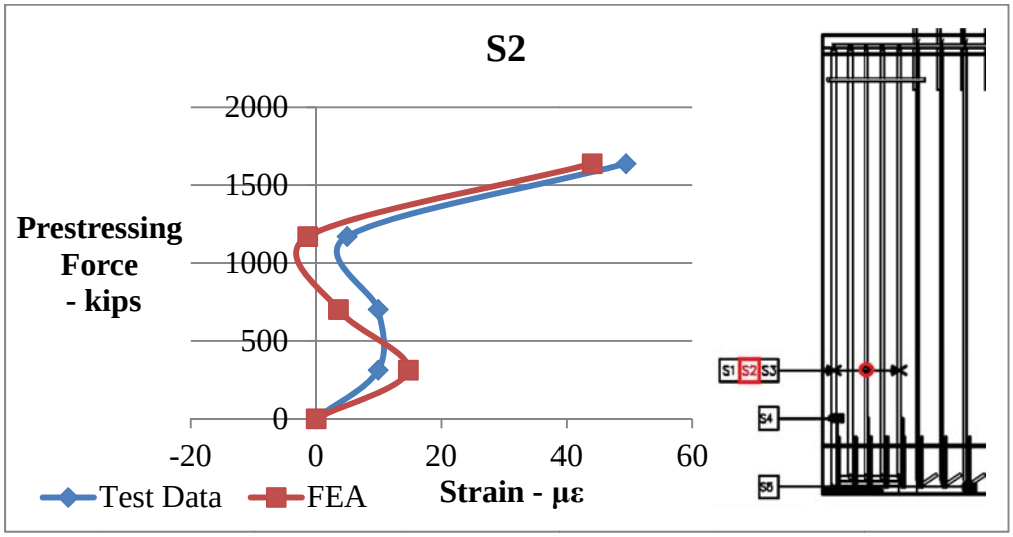

Figure 6-44. Re-bar strain comparisons between data obtained from strain gauge 2 and finite element model during prestress release for 38% de-bonded girder. *(positive = tension)*

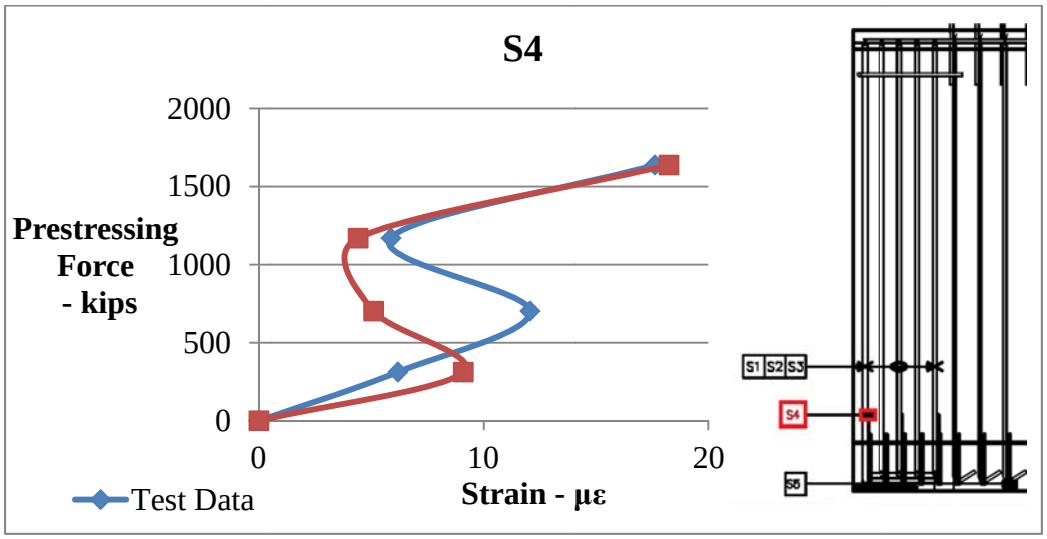

Figure 6-45. Re-bar strain comparisons between data obtained from strain gauge 4 and finite element model during prestress release for 38% de-bonded girder. *(positive = tension)*

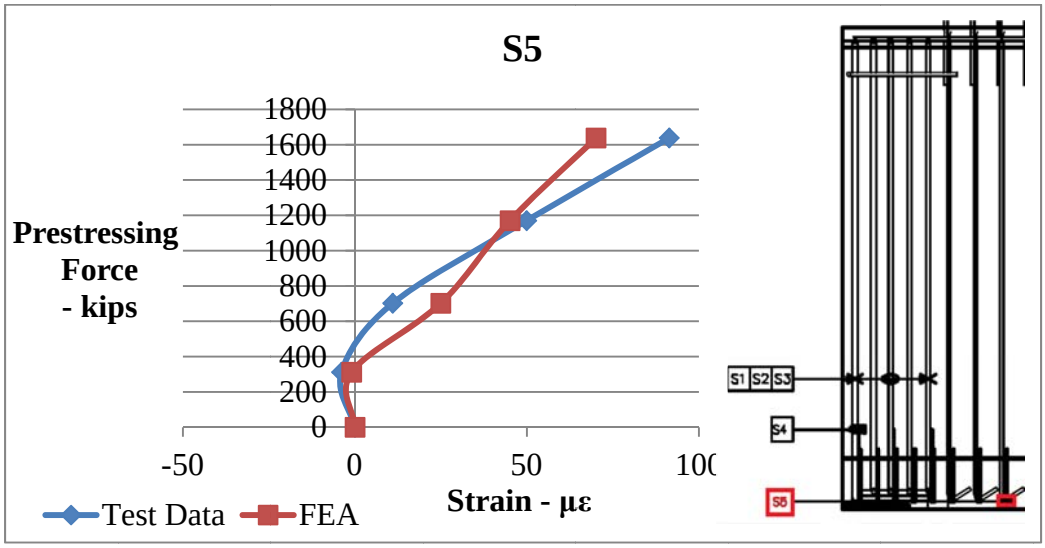

Figure 6-46. Re-bar strain comparisons between data obtained from strain gauge 5 and finite element model during prestress release for 38% de-bonded girder. *(positive = tension)*

All of the rebar strain results in Figures 6-44 to 6-46 show good correlation between measured strains and the predicted values, validating the accuracy of the FEM analysis.

6.5 62% De-bonded Girder With Strands Bonded at 8in. From End

The initial concrete strength of the 62% de-bonded girder was 7975 psi from cylinder tests before de-tensioning of strands. Again, the cracking strain of concrete is 126 με and is used to compare the concrete strains from both test and models to predict cracking.

Comparing the ends, the FEM model seems to capture all cracks except one horizontal crack at the top close to the inclined crack. The model did not predict any Y cracks. The actual beam did have the beginning of a Y crack with partial top arms that did not extend into the flange. A possible reason for the difference is that on release the dissipated energy of the

free strands beyond the girder end created an addition dynamic force that might have created that crack. No dynamic effects were simulated in the model. Model cracks are expected where the color contours are light blue, green or orange in Figure 6-47.

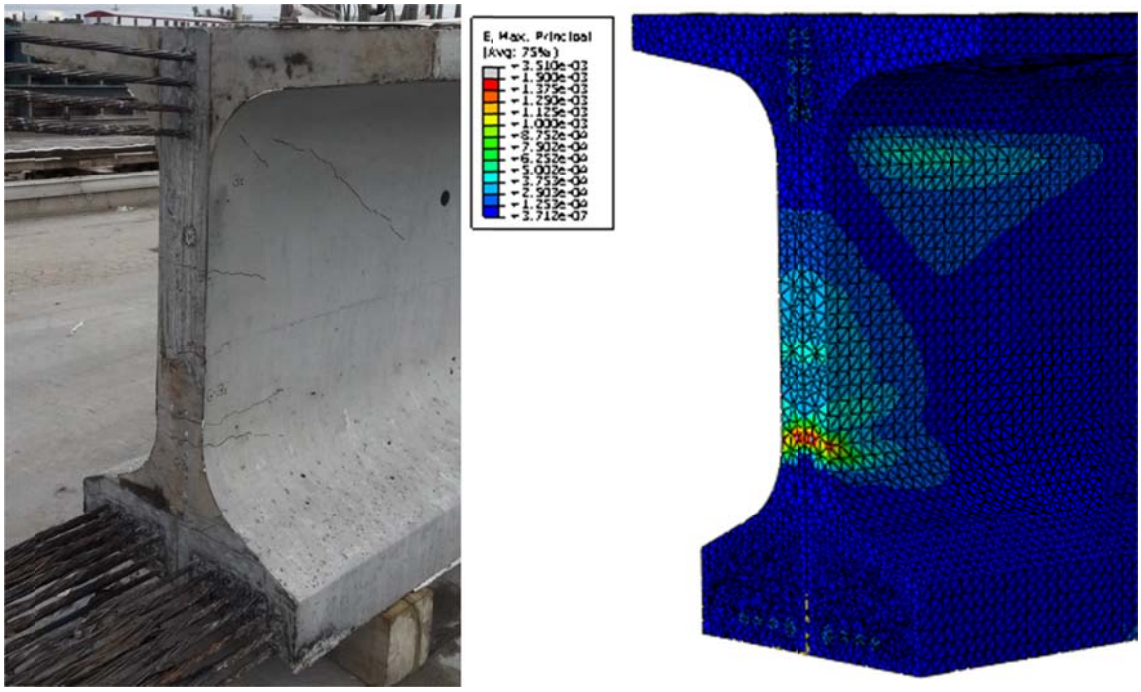

Figure 6-47. The comparison of 62% de-bonded girder ends in reality and in model.

6.5.1 <u>62% Debonded: Strain Results at Vibrating Wire Gauges</u>

From viewing Figure 6-25, the formation of the Y crack did not visibly reach to the location of VW2 gauge on the banana bar of the bottom flange. The predicted concrete strain however, was nearly twice the measured strain though staying below the assumed cracking level. Strains at VW3 also did not reach cracking based on both Figure 6-25 visual indications and the concrete cracking strain limit. The model correctly predicted that cracking should not occur. Again, the FEM predicted higher strains than measured, but in

both cases the measeured strains were small and the errors were not significant. Strains at VW4 were in good agreement.

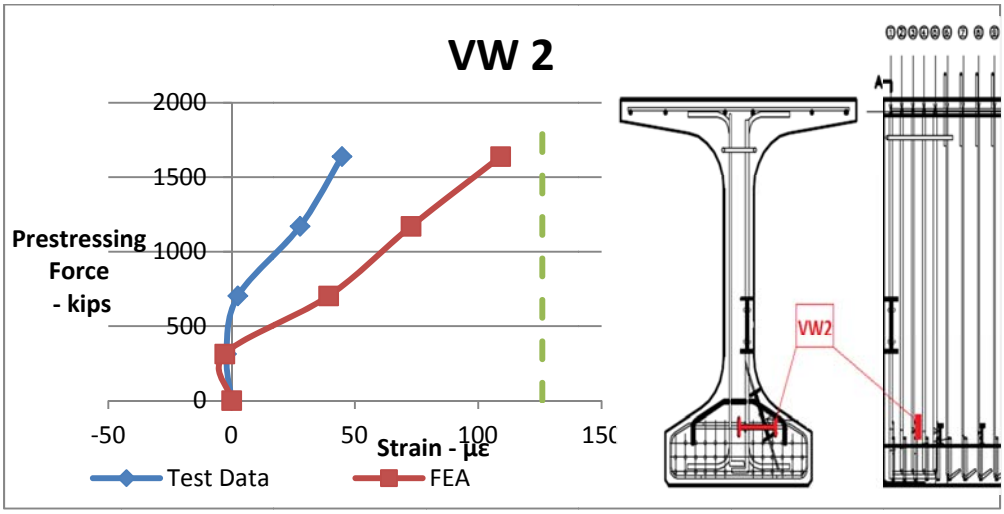

Figure 6-48. Concrete strains comparisons between data obtained via VW gauge 2 and finite element model during prestress release for 62% de-bonded girder. *(positive = tension)*

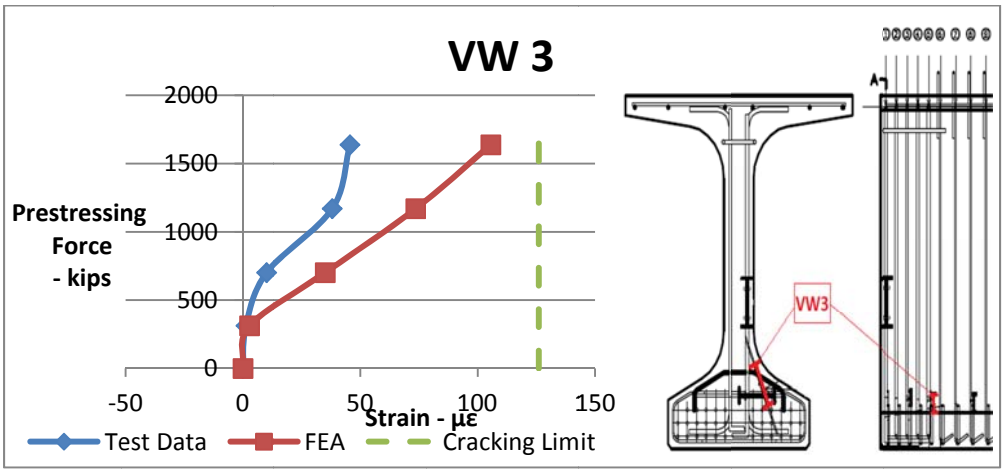

Figure 6-49. Concrete strains comparisons between data obtained via VW gauge 3 and finite element model during prestress release for 62% de-bonded girder. *(positive = tension)*

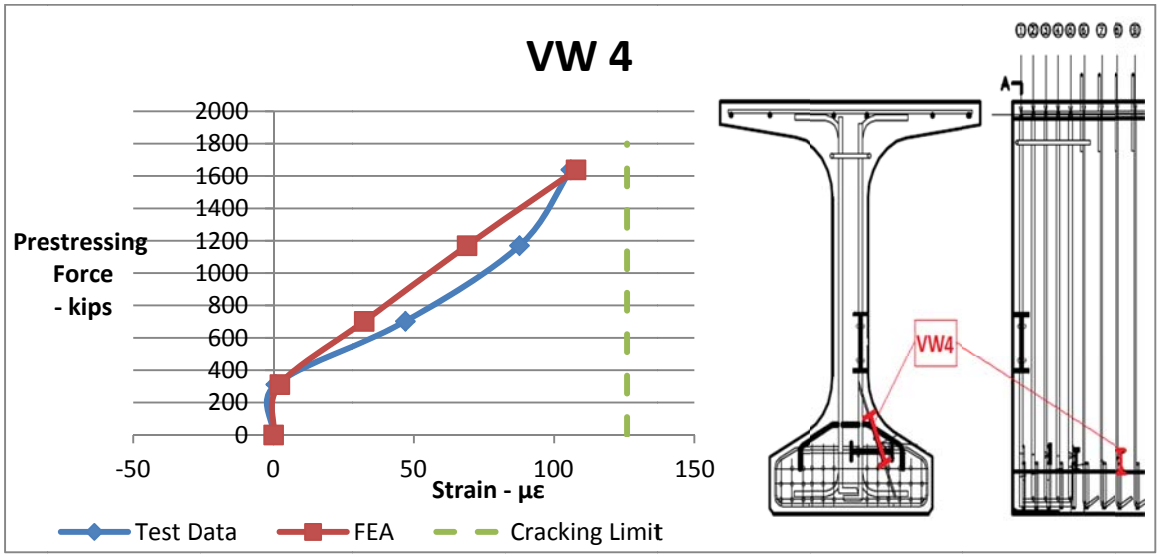

Figure 6-50. Concrete strains comparisons between data obtained via VW gauge 4 and finite element model during prestress release for 62% de-bonded girder. *(positive = tension)*

6.5.2 <u>62% Debonded: Strain Results at Strain Gauges</u>

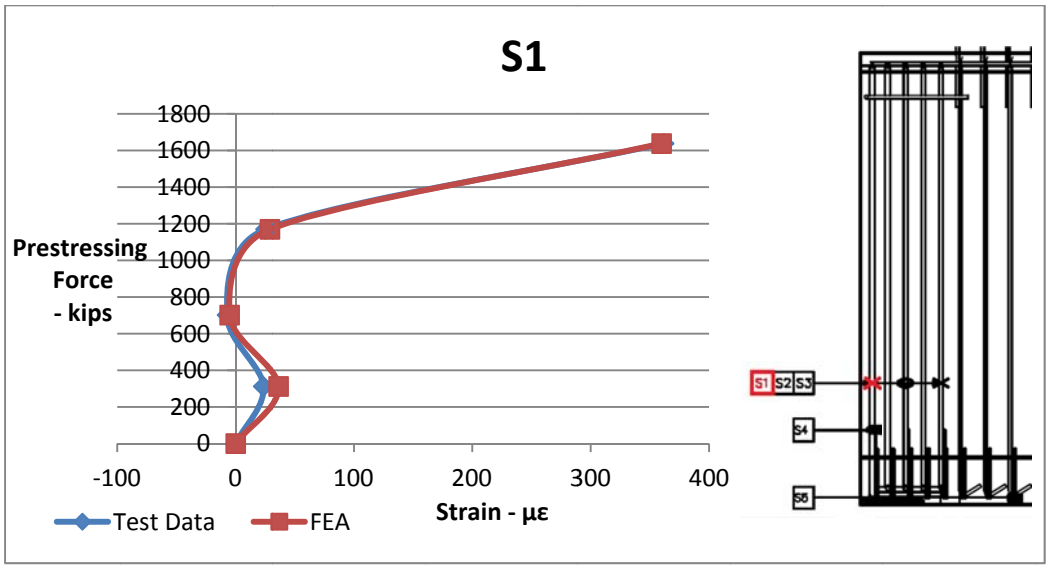

Figure 6-51. Re-bar strain comparisons between data obtained from strain gauge 1 and finite element model during prestress release for 62% de-bonded girder. *(positive = tension)*

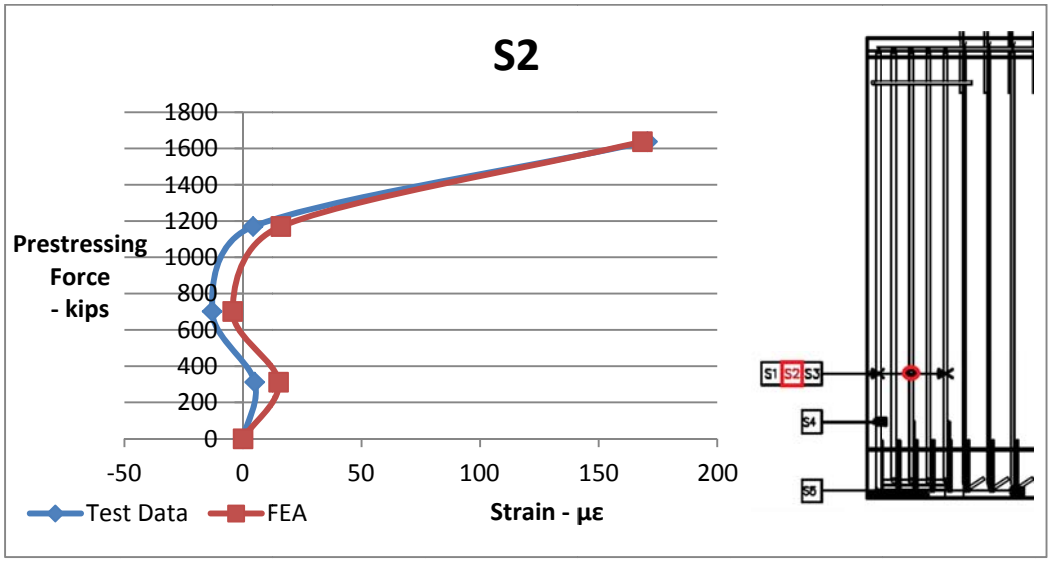

Figure 6-52. Re-bar strain comparisons between data obtained from strain gauge 2 and finite element model during prestress release for 62% de-bonded girder. *(positive = tension)*

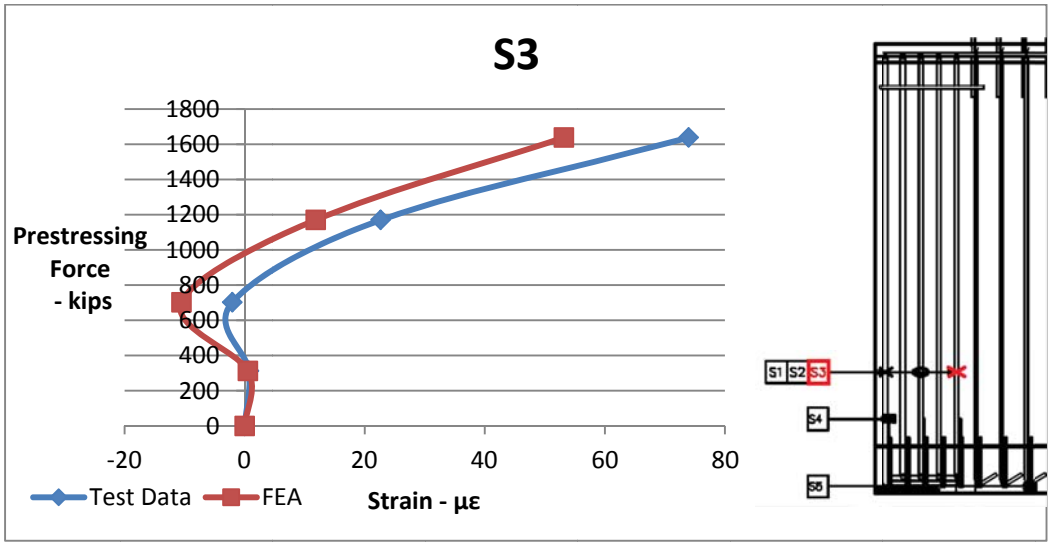

Figure 6-53. Re-bar strain comparisons between data obtained from strain gauge 3 and finite element model during prestress release for 62% de-bonded girder. *(positive = tension)*

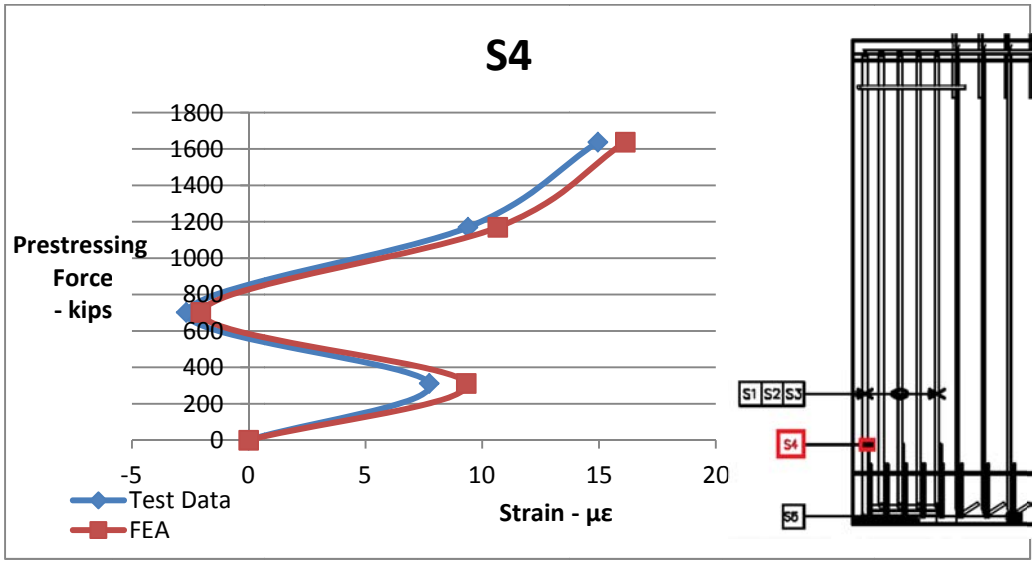

Figure 6-54. Re-bar strain comparisons between data obtained from strain gauge 4 and finite element model during prestress release for 62% de-bonded girder. *(positive = tension)*

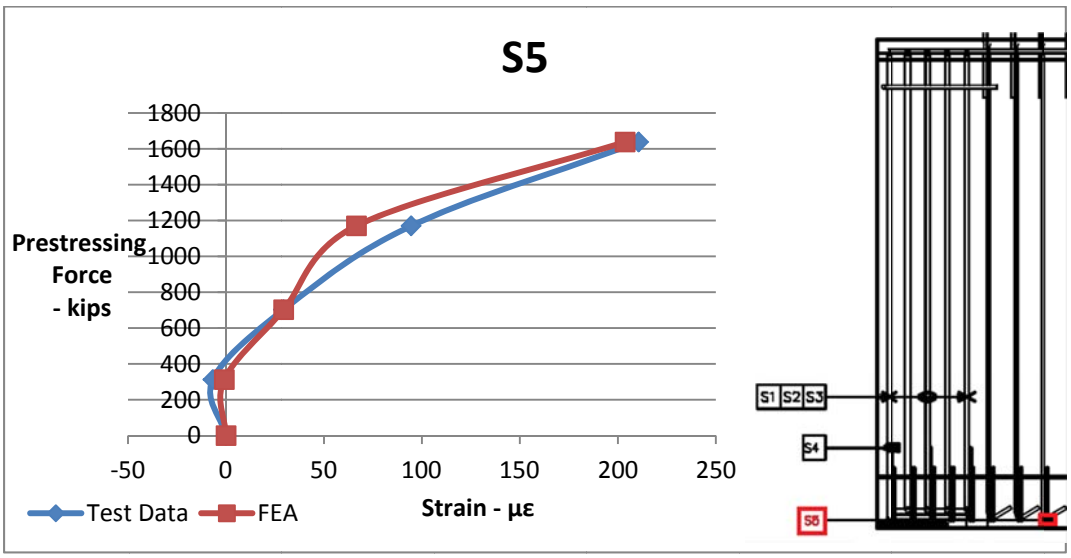

Figure 6-55. Re-bar strain comparisons between data obtained from strain gauge 5 and finite element model during prestress release for 62% de-bonded girder. *(positive = tension)*

All the comparisons of strains at locations S1 to S5 obtained from the FEA model and the test data are in good agreement. Therefore, the FEM model seems to predict reinforcing bar strains accurately.

6.6 Observations and Summary

The results from some strain gauges in the instrumented end of the girder with strands debonded 8in. from the end gave higher strains than found in the bonded girder end. The strain gauge in the first vertical web steel re-bar increased by 182%, and by 35% in the third web rebar. The strain gauge on the fifth web bar was fairly far from the cracking zone and therefore the bar strains were small. Debonding the strand for 8in. apparently can be expected to increase horizontal web cracking. This is not a serious consequence since the web cracks are not near strand and cracks will not likely cause strand corrosion. The web cracks also tend to close as additional dead and live load is applied to the girder.

Since the strain gauges were mounted on more uniform material (re-bars) than concrete, the results of a measured and predicted comparison are good.

The results of a vibrating gauge used to indicate horizontal web crack (VW1) showed a decreased of 19% in tensile strain in the 38% debonded girder compared to the fully bonded girder. The results from the vibrating wire gauges on the first web bar (VW1), used to detect horizontal web cracking, had a good agreement in both bonded and 38% de-bonded girders with the analytic predicted strains. The results were over the concrete cracking limit because that gauge had apparently crossed one of the horizontal cracks.

The S5 strain gauge on a bottom flange tie bar was placed to indicate the degree of bursting stresses developing in the girders. 38% debonding with a staggered pattern decreased these bursting strains by 53% compared to the bonded girder. The strains at the same location were not changed compared to the fully bonded girder when the bottom strands were debonded 8 inches.

Possible cracking of the concrete in the bottom flange was judged by measured concrete strains. Though the concrete tensile cracking strain is not well known, a value suggested by AASHTO was assumed as a limit to gage possible crack formation. The VW2 gauge (used to measure possible Y cracks) showed that debonding 8in. from the end decreased the horizontal strains across the bottom flange by 96% at the end of the beam compared to the fully bonded case. Results from the other two other vibrating wire gauges showed that strains were decreased with both debonding patterns, compared to the fully bonded case.

Also, the final value of the strain gauge on the banana bar below the first web bar (S4) showed poor correlation with predicted results in the bonded girder. The reason is that this re-bar was epoxy coated so there might not be enough bond between concrete and steel.

6.7 Conclusion

Debonding 38% of the strands in the bottom flange at the girder end of 54W girders considerably decreases strains both in reinforcing bars and in the concrete as compared to a

bonded girder. Y cracking can be eliminated with staggered debonding and sufficient strands debonded. The staggered debonding also reduced horizontal web cracking. The reason is that 38% debonding, with staggered debonded strands, gradually transfers the prestress over a long distance with less stress concentration.

Debonding the bottom strands for an 8 inch distance from the girder end is also an effective technique for controlling Y cracking. The 8 inch debonding actually increases horizontal web cracking slightly compared to a normal girder. This is not a serious effect, however, since the horizontal web cracks close under added dead and live loads. Y cracks tend to open with added loading and are of prime concern.

Debonding works well for decreasing the total length of cracks, but the 38% debonded girder showed the least cracking.

The effect of placing U bars horizontally in the bottom flange, as County Precast did in the 54Ws, might be be investigated as an added aid in reducing girder end crack widths.

Strain data measured from the vertical web reinforcing bars allows a conclusion that the first three bars from the end of the girder work to control cracking. The extra two bars used in the WisDOT standard designs are ineffective and could be removed.

7 CAUSE OF CRACKING & DESIGN OF GIRDERS

FEA is a very important tool to get full response information for a wide domain of differing girders while conventional experiments can only provide information at discrete gage locations. The response of many loadings in any direction can easily be examined with the FEA models. Examination of strain and stress information from the FEA models may also be used to explain the possible cause of cracks at the girder ends.

The primary explanation for cracking is that high principal tensile strains are crack prone locations of the girder. In this chapter the response of concrete and reinforcing steel, due to prestress loading at the end of pretensioned girders, will be examined and discussed. For this, the strain fields in the bonded 54W girder models will be used since they were in good agreement with measured data and the 72W bonded girder gave similar trends.

In Chapter 0, concrete behavior was defined: “after attaining the tension cracking strain limit, concrete elements undergo plastic deformations and cannot carry further loads (cracks occurs). In these locations, stresses drop while the strains increase”. For this reason, using concrete strains makes sense for a cracking investigation because they grow rapidly once a crack forms. The behavior of steel reinforcement bars, however, were modeled as linear elastic since no yielding was expected. The effects in the re-bars can be presented as stresses or strains.

The comparison of the finite element model results and test results agreed well, so the models are assumed acceptable for use in explaining the behavior of the girder end zone and

to examine the required percentage of debonding needed to prevent all cracks. Because of variations in fabrication, concrete strength, non-homogeneity, etc., FEA should not be anticipated to simulate the behavior of every girder with perfect accuracy. It is, however, sufficient to represent the typical girder cracking behavior. After explaining causes of cracks, the percentage of strands needed to control cracking will also be discussed in this chapter.

7.1 Concrete Response & Causes of Cracks

Figure 7-1 shows the maximum principal strains in a fully bonded 54W girder with 42 strands. The principal strains are shown by various colors and go up to 4500 $\mu\varepsilon$ (with positive strain indicating tension) and light blue indicating possible start of cracking. The red, green and yellow colors are for high strains, indicating the locations of cracks. For this girder, a cracking strain was calculated as 132 $\mu\varepsilon$ based on the compression strength of the girder, which is 7820 psi. However, 150 $\mu\varepsilon$ (or $1.50*10^{-4}$ strain) was assumed to be an initial cracking strain based on the observations between test data and model data.

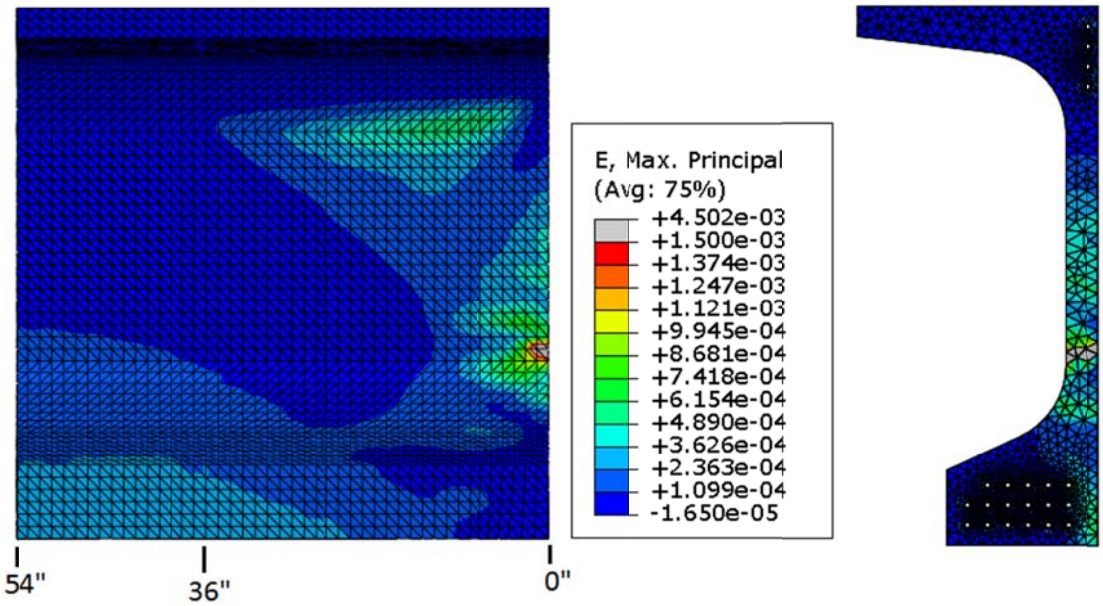

Figure 7-1. Principal tensile strains in concrete, elevation view (left) and cross section view at the end (right). *(positive = tensile)*

There are three regions which show high strains, and as expected most of these regions are the same locations where cracks are observed in the field. The first region is around the inclined crack region visible in the elevation view near the top. This region is close to draped strands. The concrete elements near the strands experience increased compression strains compared to their surroundings, and tension strains develop perpendicular to the compression direction - causing cracks.

The second region is near 1/3 the girder depth up from the bottom and visible in the web from the elevation view of Figure 7-1. This is where horizontal cracks form in the webs of the girders, and the strains are high. There are some locations where strains are especially high (red and yellow contours) and the highest of these peaks is at the lower portion of the

web just above the bottom flange-web junction. Again, the locations of these high web strains coincide with the observed locations of horizontal web cracks.

The last region where high strains are observed is in the bottom flange; near the middle of the width of the flange as evident in the cross section view of Figure 7-1. High strains seem to initiate near the bottom of the girder, and extend upwards to meet the horizontal crack right at the web junction, creating the Y-cracks as observed in the field.

7.1.1 Cause of Inclined Crack & Horizontal Crack

Figure 7-1 only shows the maximum principal strain values but it does not give any information about the direction of these strains. Figure 7-2 shows the principal tensile strain directions to further support the previous discussion. Cracks are likely to form perpendicular to the direction of these tensile strains. The strains are indicated by lines with arrows and the lengths of these lines indicate the size of strains.

By looking at Figure 7-2, the inclined cracks probably initiate 2-3 inches in from the girder end and near the top of the web where the strain lines are longest in length = high strains. Then the cracks extend downward with an inclination while remaining perpendicular to the principal tension. Concrete tensile strains predicted in the inclined crack region reached 718 $\mu\varepsilon$, which is well above the expected concrete cracking limit of the 54W bonded girder.

The inclined cracks are caused by the draped strands in the thin web section. Basically, once the stresses in the draped strands transfer to the concrete, the principal

compression stresses increase, causing an increase in the principal tensile strains in the concrete. After exceeding the concrete tensile strain limit, cracks occur.

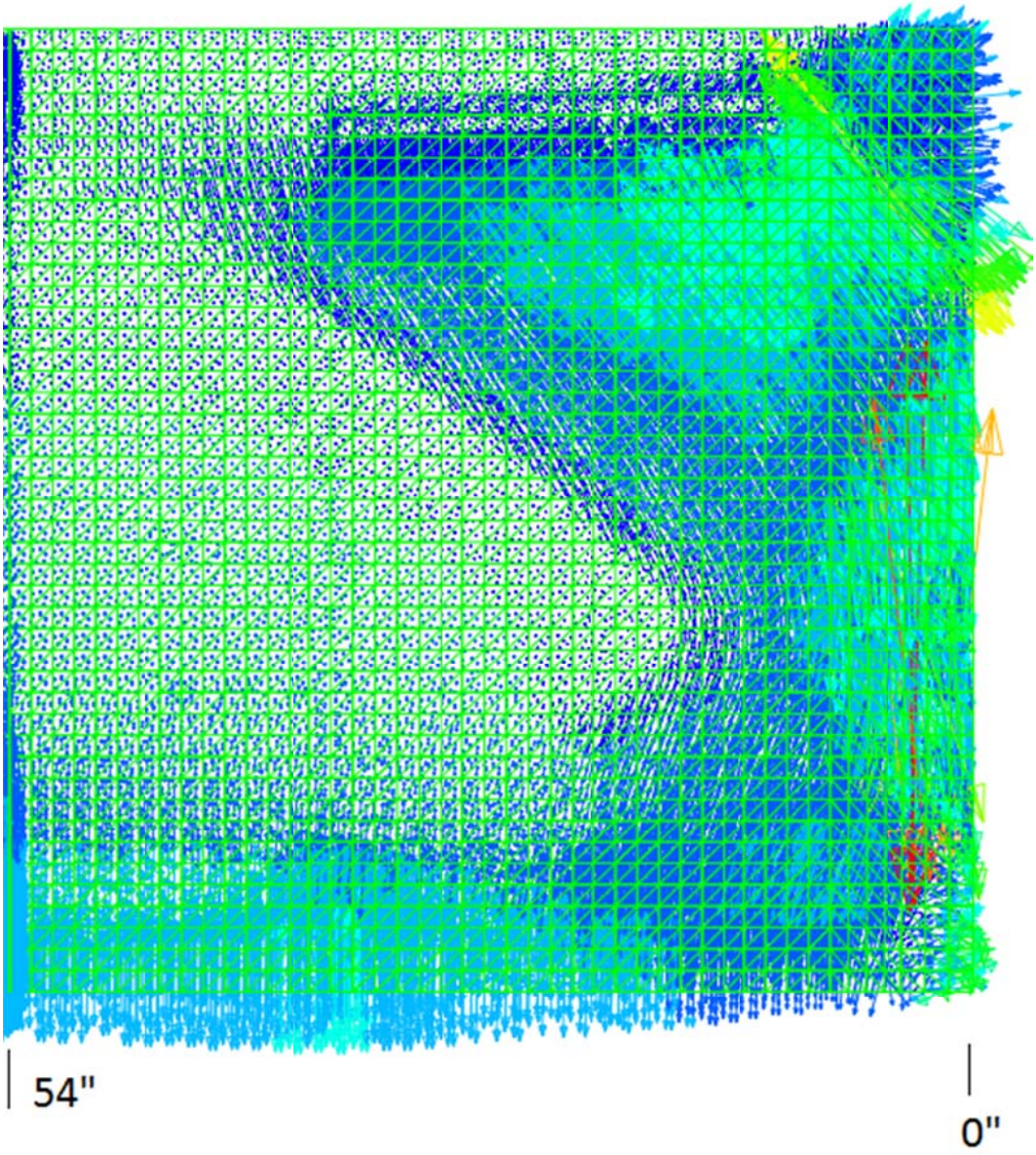

Figure 7-2. Principal tensile strains directions – 0” is the girder end.

Figure 7-2 shows that the directions of tensile strain lines are vertical in the web near the end of the beam. Web cracks may occur because of the eccentricity between the bottom

straight and upper draped strands. Two prestressing force resultants are applied to the concrete at the different depth locations. The force resultants from the draped strands and straight strands effectively create a moment in the web. The top concrete, near the draped strands, is compressed inward longitudinally. Concrete near the middle of the depth, between the strand locations, is relatively uncompressed. Concrete in the bottom flange is highly compressed inward longitudinally. The effect of the differing compression is to cause a bending effect with the end of the girder web developing vertical tension. The web at the girder end, therefore might crack under this bending. With heavier prestressing, more crack opening will be prone to occur.

7.1.2 Cause of Y Cracking

To predict the Y cracks, the principal tension strain directions in the cross section of the bottom flange at 0, 6, 12, 18, 24, 36, 42, and 48 inches in from the girder end are shown in Figure 7-3. If the strains on the cross section are all in the same or similar direction, and their sizeis large enough, a crack is likely. Otherwise, it is unlikely to occur.

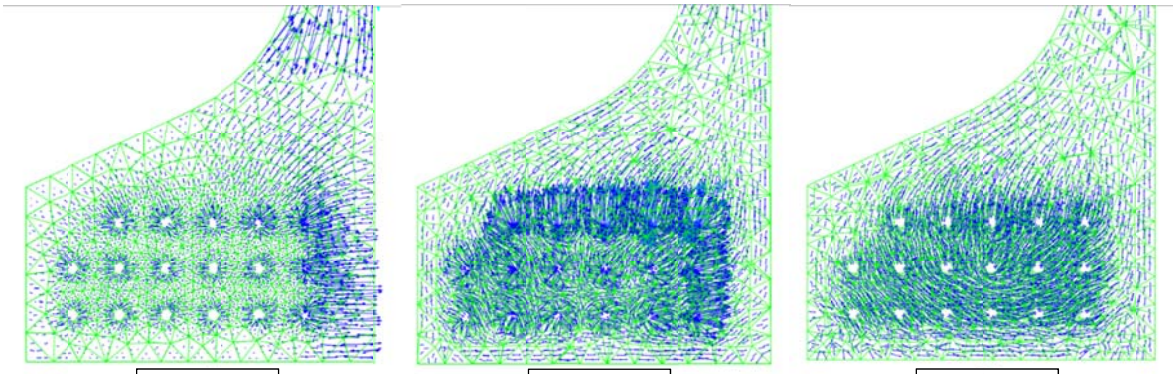

0 in. ***6 in.*** ***12 in.***

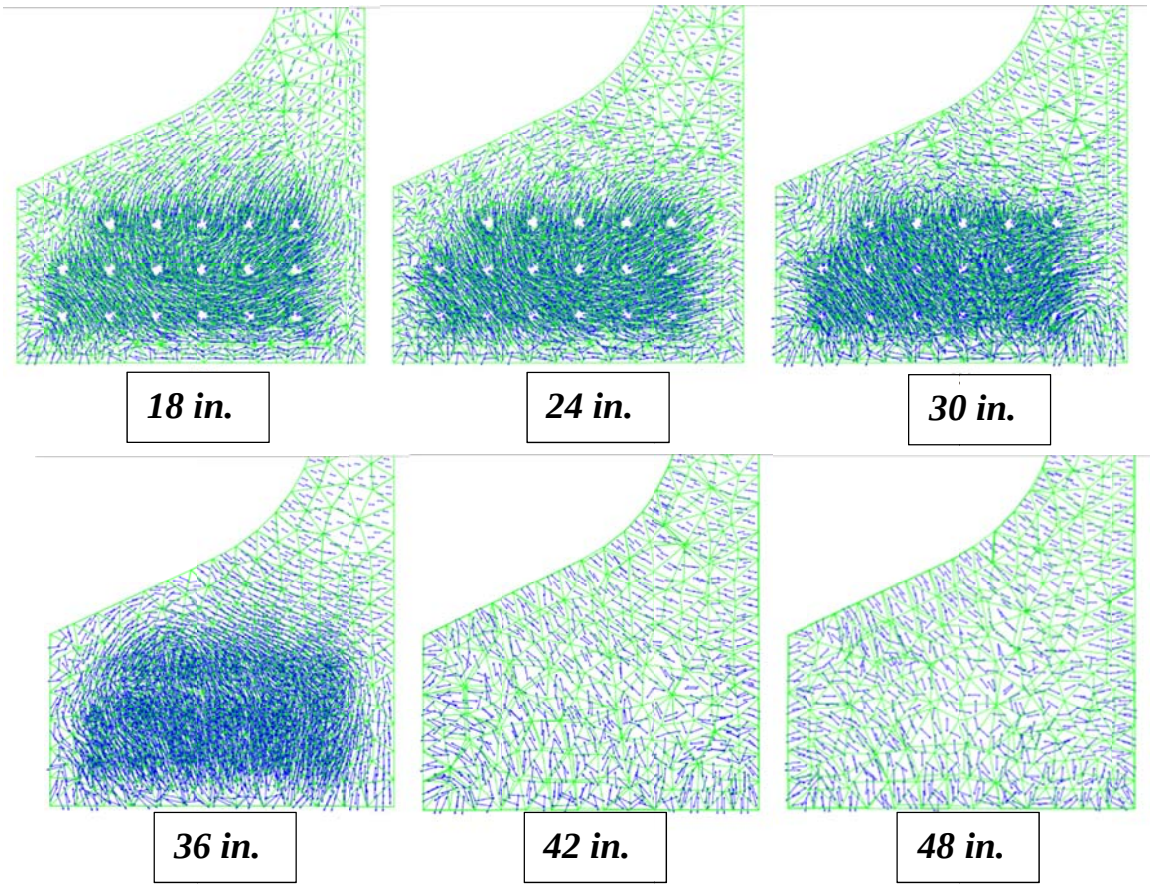

Figure 7-3. Principal tensile strains directions on the cross section of bottom flange at various distances in from the girder end.

In Figure 7-3, the principal tensile strain directions at the girder end (0 in.) are large and all horizontal in the middle of the flange, which could lead to the formation of the vertical leg of a Y crack at the bottom. Those strain lines in Figure 7-3 at 0 in. are actually larger (strain magnitude) than any other lines in the bottom flange.

From 0in. to 18in. the strain lines in the web-to-flange joint region are also all parallel and appear to run tangent to the girder surfaces. At 0in., just above the flange, the strain lines are again particularly large – indicating high tension strains that could cause horizontal or

slightly angled cracks at that interface. The initial vertical flange crack might turn toward both web faces with these second strains that are tangent to the radius of the web-to-flange joint.

From 18 in. to 36 in. (at the end of transfer length), the tension strain lines tend to encircle the strands, indicating a bursting effect. Therefore, the confinement stirrups in this region of the flange may be useful. After 36 inches, no particular trend in tension strain direction is observed. Tension strains are in random directions and much smaller. So cracks should not be anticipated.

The vertical leg of the Y crack that forms at the girder end may be caused by the eccentricity of strand force to each side of the mid flange section. Similar to web cracking, the resultant force of strands on each side of the bottom flange, with no force at the center – due to the absence of the draped strands, creates a bending effect in the flange section, causing the crack. The outsides of the flange are both compressed inward, while the mid-section is uncompressed and restrained by the stress-free web. Once the vertical crack forms at the girder end it tends to meet the lower web cracks, forming a Y crack. Releasing outer strand first accentuates this eccentricity and cracking.

7.2 Steel Response

As described in Chapter 0, the reinforcing bars are modeled as linear elastic truss elements in the FEM analysis. Once the nonlinear concrete elements pass the cracking limit,

a stress redistribution takes place. When the concrete softens in tension due to cracking, the resistance will be provided by adjacent reinforcing bar elements.

The longitudinal stress change in reinforcing bars of the 72W model is shown in Figure 7-4. The colors represent the stress level; ranging from dark blue for low stress (i.e.-compression) to red for high tension stress. The maximum vertical web bar stresses are in the same locations as horizontal web cracks are predicted to occur, indicating that the re-bars were engaged and stress distribution took place after the concrete cracked. This high tension rebar strain and stress can be seen in the red portion of vertical web rebar approximately 1/3 the depth up from the girder bottom at the girder end. Vertical bars close to the end developed the highest stresses with a value of 22 ksi, which is below the yield stress of re-bars. Other bars have lower stresses. Therefore, the reinforcing bars are in the linear elastic range.

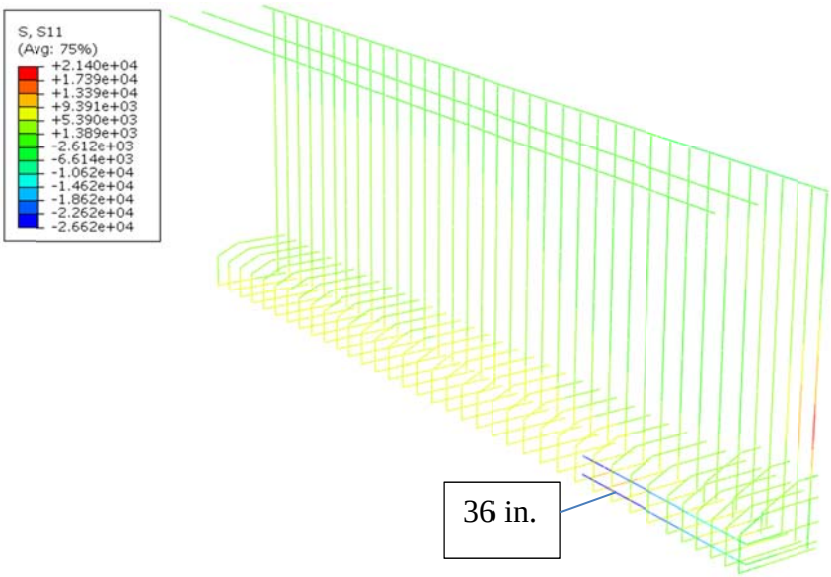

Figure 7-4. Longitudinal stresses – S11 (psi) of reinforcing bars in 72W girder.

The stresses in bottom flange stirrups are low at the girder end but reach 17 ksi at the end of the transfer length because of the bursting effect, as was discussed with sections between 18 and 36in. of Figure 7-3.

The largest peak stresses predicted in the 54W and 72W girders are presented in Table 7-1. Note that the vertical bar stresses should be limited to 20 ksi for crack control by AASHTO LRFD Bridge Design Specifications. The girders, however, exceed these limits by 10 and 15 percent, respectively. Also, all the maximum stresses are below yield stress of steel, which proves that the assumption of modelling the steel elements with a linear elastic property is a correct approach.

Maximum Stresses in Reinforcing Bars - ksi			
54W		72W	
Vertical Web Bar	Bottom Stirrup	Vertical Web Bar	Bottom Stirrup
22	10	23	49

Table 7-1. Maximum stresses observed in 54W and 72W models.

In conclusion, the FEA model of a 54W bonded girder is used to explain cracking at the ends by looking at the distribution and direction of the tensile strains. The inclined cracks were thought to be caused by the bursting pressure due to the draped strands. The web cracks were due to the eccentricity of the straight and draped strands over the depth. Finally, the Y cracks were triggered by the eccentricity of the strands over the width of the girder. Debonding is an effective method to control the cracking because it reduces the resultant prestressing force coming from strands, lessening the internal concrete tension stresses. Debonding strands close to the flange edges at the bottom flange, reducing the eccentricity of

the resultant prestress force from the section center, is useful to reduce the tensile strains causing the Y cracking.

8 RECOMMENDED DEBONDING WITH DIFFERENT NUMBERS OF STRANDS IN WISCONSIN 54W AND 72W GIRDERS

Debonding reduces the concentration of prestressing force applied to the concrete in the girder end region by moving the transfer lengths of some strands further into the girder. Since cracking has been shown to be induced by high concentrated concrete prestress force, debonding seems to be a logical solution for controlling cracking.

Finding the necessary number and locations of strands that should be debonded for both 54W and 72W girders, with different standard strand contents, required special investigations based on debonding length, debonding percentage, strands to debond, the prestressing force, material properties, and the length of the girders. These investigations involved looking analytically at numerous possible designs for each girder with a particular strand content. The best debonding patterns were found by modelling both 54W and 72W girders with different numbers of strands.

What it is meant by best debonding pattern is a design that reduced the concrete tensile strains to a value near or below 150 $\mu\varepsilon$. The true cracking limit is actually thought to be larger than the value calculated from the AASHTO rupture equation (130 $\mu\varepsilon$) and 150 $\mu\varepsilon$ was assumed. Since it is important to control the eccentricity of resultant prestress forces across the width of the bottom flange, the inner most strand column was left bonded. The AASHTO LRFD BDS does not allow debonding of the outermost strand columns so that requirement was also followed. AASHTO also limits debonding to 25% of the strand, but

the commentary in C5.11.4.3 acknowledges that states have had success with greater percentages of debonded strands. Texas has used debonding percentages over 50%. No limit is placed on the number of unbonded strands in the designs examined here.

In the analyses, a uniform stress was applied to the concrete over the strand transfer length to simulate the strand concrete bond. The uniform stresses transferred from prestressing steel to concrete were calculated from the jacking stresses of strands ($0.75*f_{PU}$=202.5 ksi). However, since elastic losses were considered, a value which is smaller than that was applied to models with elastic loss estimated. Again, to be consistent, the concrete strength was taken as 7000 psi, which is slightly larger than the normal WisDOT specified value of 6800 psi, - the minimum required concrete strength that should exist before strand release. Finally, the assumed girder lengths (used for elastic loss and girder weight) were chosen from the WisDOT Bridge Manual (14). The maximum girder lengths allowed by this manual for 72W and 54W girders with a specific number of strands were used as assumed extreme cases.

8.1 Best Debonding Percentage for Each Girder

FEA was used to study the debonding pattern needed for each girder with different numbers of strands. The maximum number of strands with 72W girders is 48 strands. Therefore, exploration of different debonding patterns for the 72W girder with 48 strands will be shown here but the same procedures were used to find the best debonding patterns for other strand quantities and for 54W beams.

Six debonding patterns were tried for the 72W girder with 48 strands. Results with one fully bonded strand pattern is also shown for comparison. In the following discussion “DB” represents debonding and the number next to it is the percentage of total strands that are debonded. Finally, the letters A and B are for the same debonding percentage but different debonding patterns. The debonding patterns examined were as follow.

- DB 0: All strands are bonded at the girder end. 8 strands were draped. (Figure 8-1a)
- DB 38: 38 % of all strands were debonded. They start to get bonded after 3ft., 6ft. and 9ft. from the girder end. 8 strands were draped. (Figure 8-1b)
- DB 42_A: 42 % of all strands were debonded. They start to get bonded after 3ft., 6ft. and 9ft. from the girder end. 8 strands were draped. (Figure 8-1c)
- DB 42_B: 42 % of all strands were debonded. They start to get bonded after 3ft., 6ft. and 9ft. from the girder end. 6 strands were draped. (Figure 8-1d)
- DB 46: 46 % of all strands were debonded. They start to get bonded after 3ft., 6ft. and 9ft. from the girder end. 8 strands were draped. (Figure 8-1e)
- DB 50_A: 50 % of all strands were debonded. They start to get bonded after 3ft., 6ft. and 9ft. from the girder end. 8 strands were draped. (Figure 8-1f)
- DB 50_B: 50 % of all strands were debonded. They start to get bonded after 3ft., 6ft. and 9ft. from the girder end. No strands were draped. (Figure 8-1g)

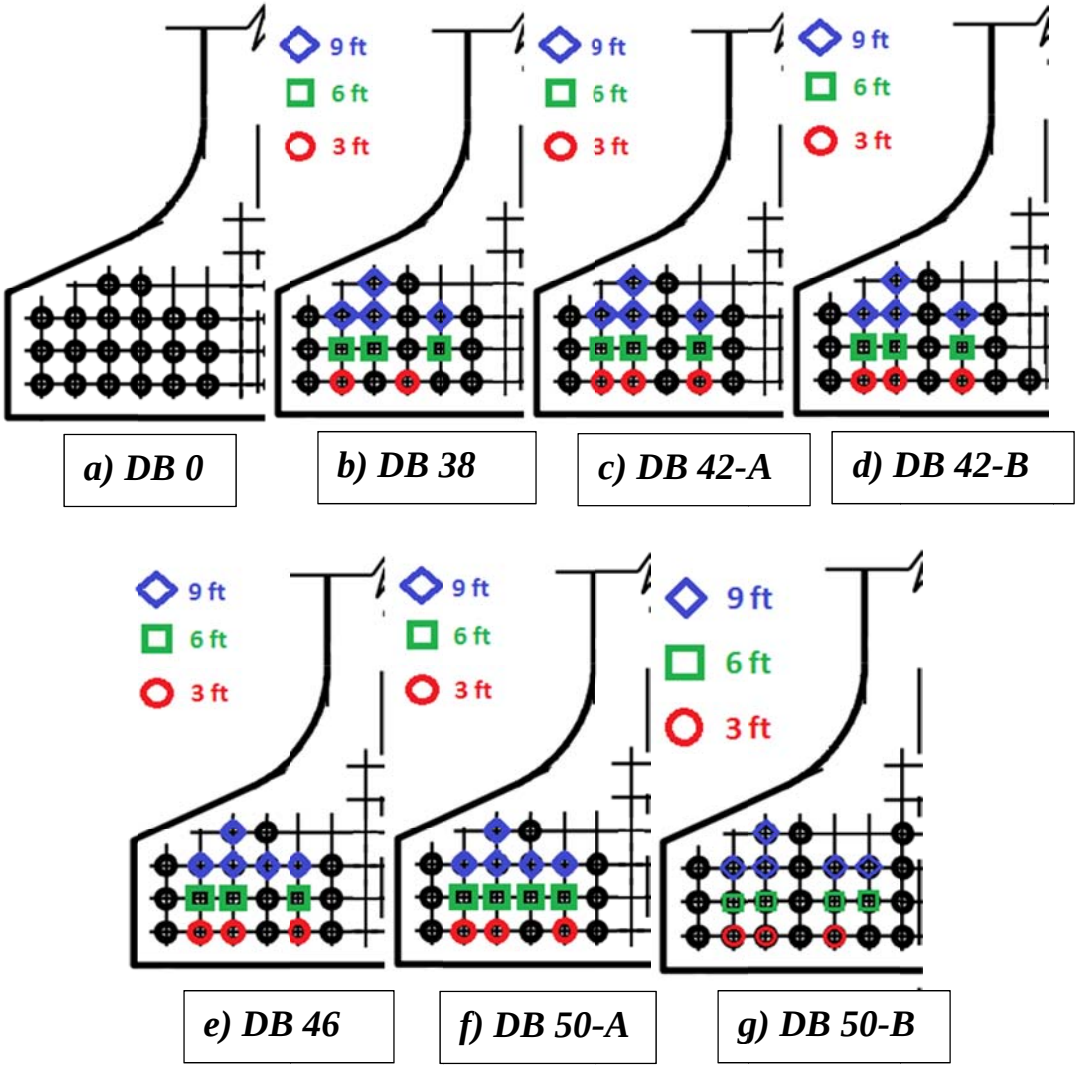

Figure 8-1. Strand patterns at the ends of girders. Distances denoted are locations where those strands start bonding.

The contour plots of principal tensile strain for the girders with different debonding cases, and maximum principal strains at horizontal and Y crack regions for each girder are shown in Figure 8-2, and Figure 8-3, respectively. The contour maximum tension strain was set to 500 με in each figure to visually compare the strain changes in the girder models. The girder with no debonding predicted crack locations at the end and the tension strain values

are large. The effect of debonding can be immediately seen by comparing the contour plots of the DB 0 and DB 38 girders. The strains in DB 38 were reduced to 215 με for the Y crack region and 280 με for the horizontal crack region, from bonded values of 2734 με and 1243 με respectively. The 38% debonding reduced Y crack strains by 92% but cracking is still expected so further debonding is needed.

Draping six strands instead of eight actually helped to eliminate Y cracks in the DB 42-B girder, as compared to 42-A with 8 draped strands, but horizontal web cracking is still expected. The DB 50-A girder is another option for the 72W girder with 48 strands since the Y crack strain of 151 με was the lowest of all the patterns. A design with no draped strands and 50% debonding (DB50-B) is again effective for Y crack elimination but not for horizontal web cracks. Since horizontal web cracks will normally close as dead and live load are added, the 42A or no drape 50B are acceptable alternatives. Maximum principal tension strains for all the girder patterns are shown in Figure 8-3.

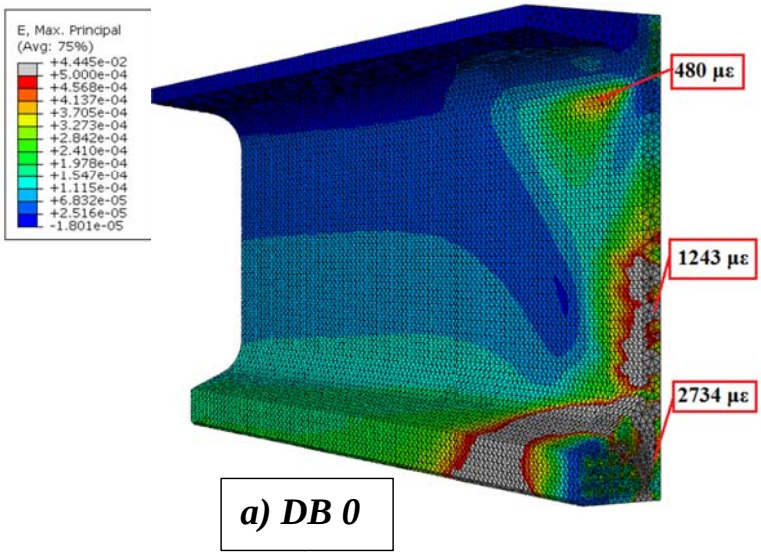

a) DB 0

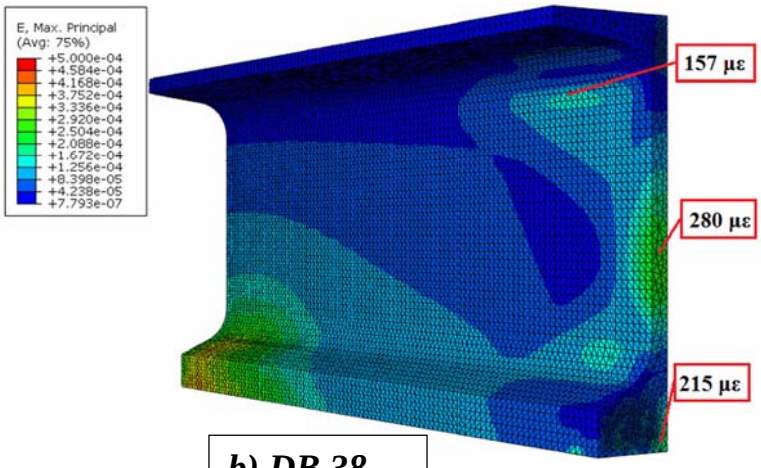

b) DB 38

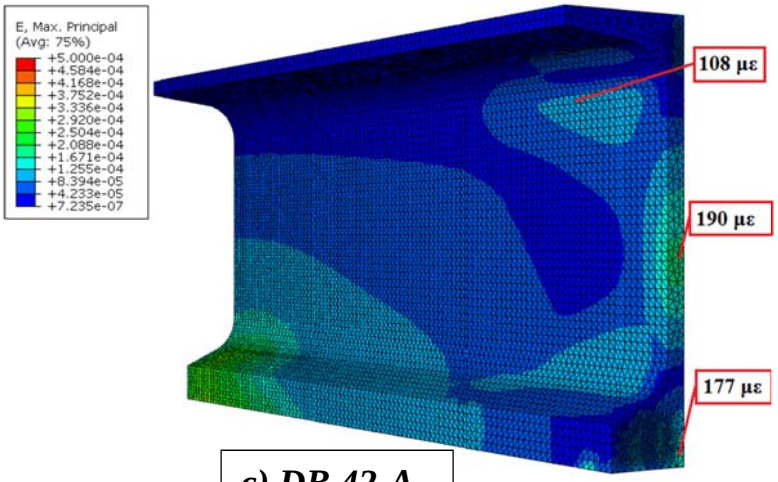

c) DB 42-A

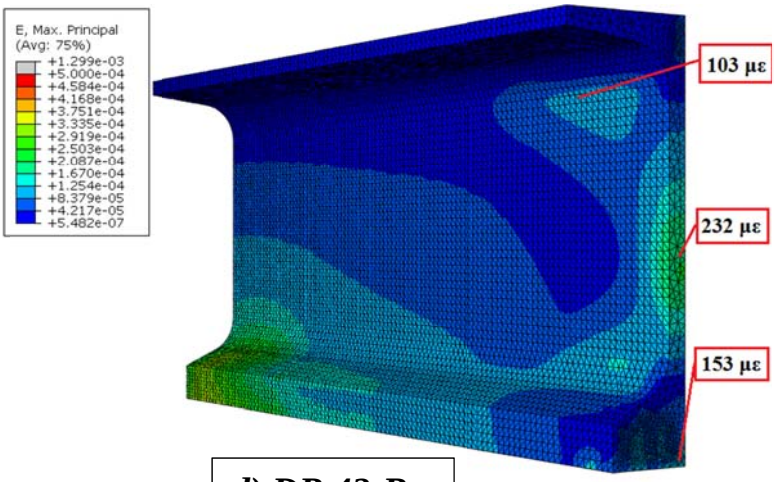

d) DB 42-B

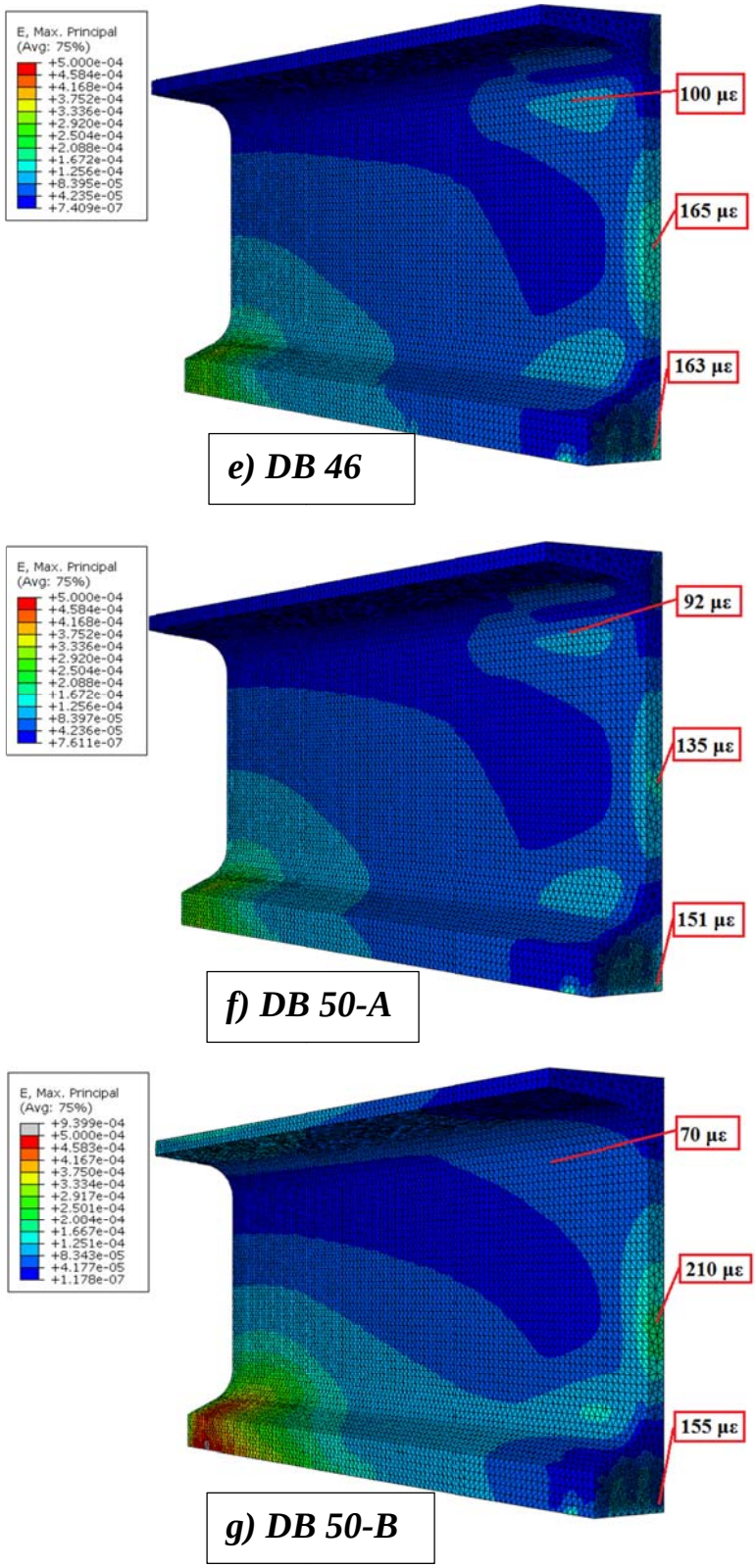

Figure 8-2. Contour plots of bonded and debonded 72W girders with 48 strands.

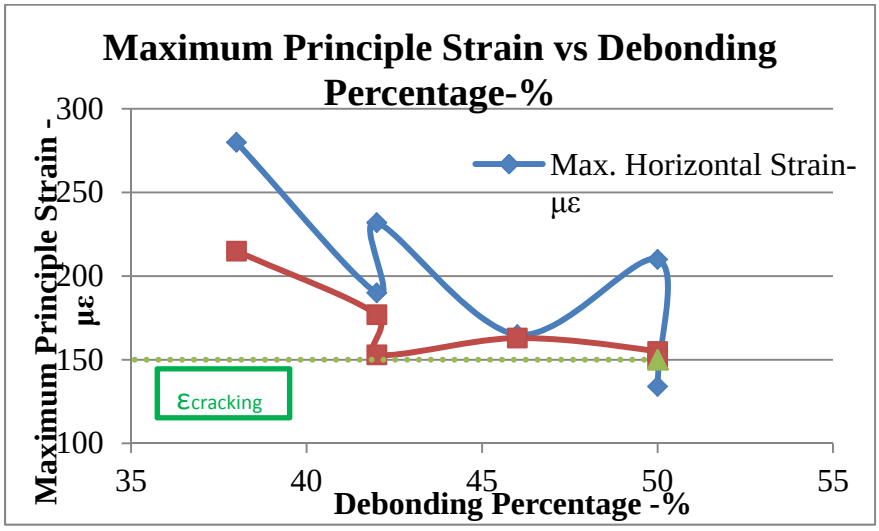

Figure 8-3. Maximum principal strain at horizontal and Y crack region from each girder. *(Note: A fully bonded strand pattern resulted in maximum horizontal and Y-crack strains of 1243 and 2734$\mu\varepsilon$ respectively.)*

Since inclined cracks are a result of draped strands, reducing the number of draped strands (DB42A to 42B) helped to get of these cracks. Also, strain around the Y crack region decreased with fewer draped stands because of the increase in compression in the mid-region of the bottom flange with strands present that otherwise would have been draped. On the other hand, the larger bottom flange resultant prestress force increased the tensile strains in the horizontal web cracking region.

In the web zone, higher levels of debonding reduced the maximum tensile strains. This result is anticipated because bonding fewer strands close to the end will reduce the moment magnitude in the web region induced by combined eccentric draped and straight strands. Likewise, debonding the strands close to the bottom flange edges decreases the eccentricity about the flange mid- cross section, leading to have smaller Y crack inducing

tensile strains. If this strategy is not followed, the strains causing Y cracking will increase by the range of 200-250 με.

Following these procedures, effective debonding patterns were tried and found for other 72W strand amounts and for 54W girders. In all cases the aim was to limit the concrete tension strains to 150 με, but some of the values are just above that limit, which was deemed acceptable.

It was found that the desired debonding percentage is the same for different girders (72W and 54W) when the same number of strands are used. This is logical because both girders have the same size bottom flanges and web widths.

Table 8-1 and Figure 8-4 show the best debonding percentages for 72W and 54W girders with different numbers of strands and their maximum tensile strains at horizontal and Y cracking regions; and the best debonding patterns, respectively. The work for determining these other debonding patterns is shown in the Appendix. Drawings of each of these selected patterns are also in Figure 8-4 and could serve as a basis for creating alternative WisDOT Bridge Manual Standards 19.16 and 19.18.

		72W Girder		54W Girders	
Number of Strands	Debonding Percentage- %	Max. tension strain in web region - με	Max. tension strain in Y-crack region- με	Max. tension strain in web region - με	Max. tension strain in Y-crack region- με
48	50	135	151	-	-
46	48	151	157	-	-
44	45	150	142	-	-
42	43	156	100	145	125
40	40	154	123	129	130
38	42	132	130	119	135
36	39	133	142	130	140
34	29	156	143	152	144
32	31	142	102	131	94
30	33	133	104	133	90
28	29	140	135	142	121
26	23	138	141	149	140

Table 8-1. Best debonding percentages for 72W and 54W girder with different number of strands and their maximum values in horizontal and Y crack cracking locations.

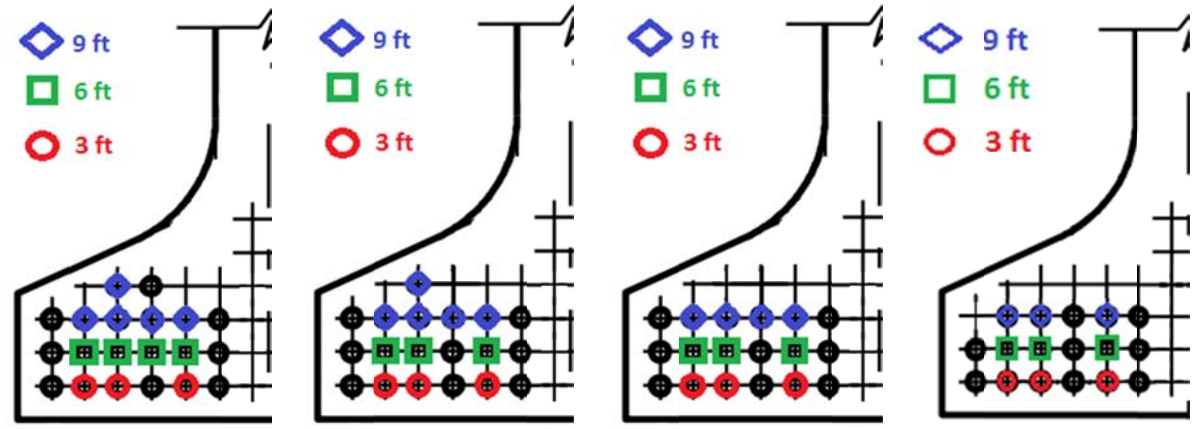

a) 48 DB 50% *b) 46 DB 48%* *c) 44 DB 45%* *d) 42 DB 43%*

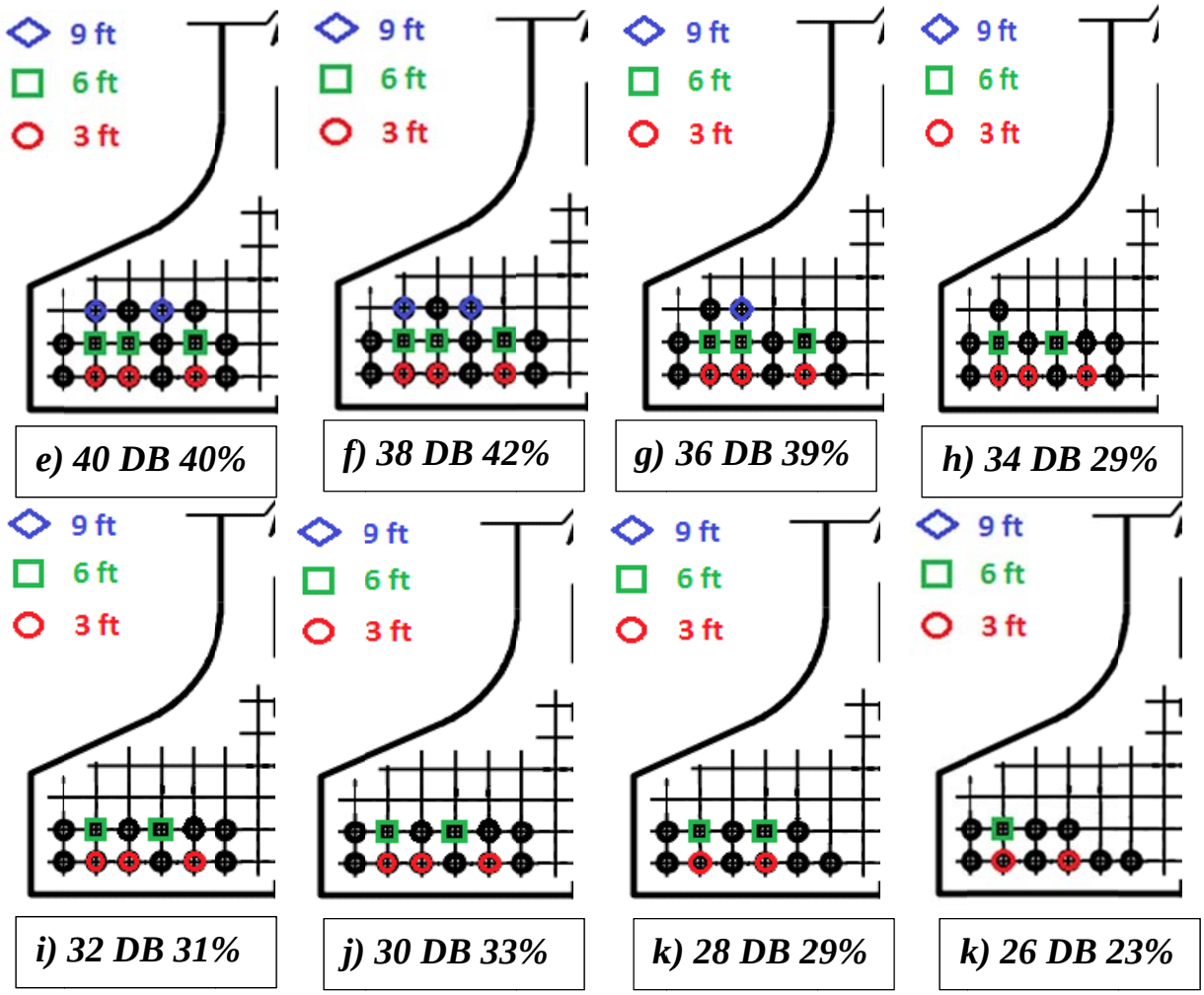

Figure 8-4. Recommended debonding patterns for 72W and 54W girders with different number of strands.

(The designation "32DB31%" represents 32 total strands with 31% debonded.)

Debonding many strands might reduce the shear capacity at the ends where critical sections are located for shear. Shear strength, therefore, must be checked at critical end locations. Since the project details for the debonded girder designs in Chapter 5 & Chapter 6 were known, the shear capacity at the ends were checked. However, the bridge spans and

girder spacing for the other girders analyzed were not known and the shear capacities could not be checked.

The results of the debonding study showed that debonding patterns, with careful selection, brought the concrete tension strains below the elastic cracking limit for the crack prone zones. Draping six strands instead of eight helped to eliminate Y cracks but the strains around the horizontal web crack region increased. Also, a no draped strand girder design with 50% debonding is effective for Y crack elimination but not for horizontal cracks. Since the horizontal web cracks are not as critical as Y cracks, the no draped strand design may be preferred. Under added vertical loading, over the girder weight alone, the web cracks tend to close but the Y-cracks actually widen. Since the Y crack is in the critical region where strand corrosion occurs, their elimination is essential.

Placement of shielding over strand during fabrication, to create debonding, adds some difficulty to the construction process. Long lengths of shielding sleeve (over 10 ft.) are more difficult to place than short lengths. Hence it is desirable from a construction viewpoint, as well as for shear strength, to keep debonded lengths short. Placing sleeves over interior strands is more difficult than exterior, but AASHTO requires that exterior strand in each row should not be debonded. Limited wicking of cement paste into the sleeves may occur, but the bond developed is usually broken when the strand is released with careful sleeve placement and sealing.

In this Chapter, recommended debonding patterns for each girder were presented. Debonding affects the shear capacity at critical end locations so when debonding is used, shear capacities should be checked for the specific span and girder loading pattern to insure sufficient shear capacity.

9. SUMMARY and CONCLUSIONS

The main objective of this research was to recommend a method to control cracking at the ends of pretensioned girders, right after detensioning the strands, for the Wisconsin Department of Transportation (WisDOT). These cracks can cause durability problems in the long term and discourage engineers from designing deep and heavily prestressed girders.

The girder ends should be modelled with nonlinear behavior due to cracks occurring and force redistribution. In most other studies on this topic, however, the anchorage zone materials were treated as linear. Accurate stress and strain distributions in this nonlinear cracked region were not found in the literature descriptions.

The process in this study was to identify the strain pattern at the girder ends using nonlinear FEA and find strand debonding patterns that would likely eliminate bottom flange cracking. The verification of the nonlinear FEA was done by using test data and the quantitative correlation of the FEA results with field data was found satisfactory. The ability to predict crack locations analytically was good for both girders that were actually tested. Then, the FEA was utilized to examine the causes of cracking. After verifying that debonding eliminates cracking by examining the cause of cracks at the ends of the girders, recommended debonding patterns were found for 54W and 72W girders with different number of strands. The ability of debonding to reduce the strains below or close to the theoretical cracking limit was shown.

FEA models of the 54W bonded girder were used to explain cracking at the ends by looking at the distribution and direction of the tensile strains. The inclined cracks were thought to be caused by the bursting pressure due to the draped strands. The web cracks were due to the eccentricity of prestress forces caused by the straight and draped strands over the girder depth. Finally, the Y cracks were triggered by the eccentricity of the prestress force induced by the bottom flange strands arranged over the width of the flange.

Debonding is an effective method to eliminate cracks because it reduces the resultant prestressing force coming from strands, lessening the moment across the web and the transverse bending of the bottom flange. The web cracks and the bottom flange Y cracks can be eliminated by the debonding. The stresses of reinforcing bars used to control cracking at the girder end remain below the yield level when prestress forces are applied. Vertical web re-bars within 12 in. from the girder end are the only bars effective in controlling the width of web cracks when debonding is not used. The bursting stirrups placed around the bottom flange strands are ineffective in controlling the Y crack widths, without debonding, because the epoxy coatings reduce the concrete to steel bond.

The results of the debonding study showed that debonding patterns, with careful consideration of selection, greatly reduce concrete tension strains to below the elastic cracking limit for the crack prone zones. Draping six strands instead of eight aids in eliminates Y cracks. Designing with no draped strands and debonding 50% of the strand is effective for eliminating Y cracks in the girders with the largest number of strands. The recommended debonding patterns for Wisconsin 54W and 72W girders, with various strand

content are identified. Debonding can affect the shear capacity at the girder end so when debonding is used, shear capacities should be carefully checked.

REFERENCES

1. Okumus P. Nonlinear analysis of pretensioned bridge girder ends to understand and control cracking at prestress release: PhD Thesis, University of Wisconsin-Madison,; 2012.
2. Crispino, Ed., Anchorage Zone Design for Prestensioned Precast Bulb-T Brige Girders in Virginia, 2009
3. American Association of State Highway and Transportation Officials, LRFD Bridge Design Specifications, Washington, DC: American Association of State Highway and Transportation Officials. 7th Ed., 2014.
4. Code M. International Federation for Structural Concrete, Vol. 1-Bulletin 55, Vol. 2-Bulletin 56. Lausanne; 2010.
5. American Concrete Institute, Building Code Requirements for Structural Concrete (ACI 318-14) and Commentary, American Concrete Institute, 2014
6. Kannel J, French C, Stolarski H., Release Methodology of Strands to Reduce End Cracking in Pretensioned Concrete Girders, Journal PCI, 42(1):42-54, 1997
7. Carroll JC, Cousins TE, Roberts-Wollmann CL,. A Practical Approach for Finite-Element Modeling of Transfer Length in Pretensioned, Prestressed Concrete Members Using End-slip Methodology, Journal PCI, 59(3), 2014
8. Janney JR., Nature of Bond in Pre-tensioned Prestressed Concrete, Portland Cement Association, Research and Development Laboratories; 1954.
9. Arab A, Badie SS, Manzari MT, Khaleghi B, Seguirant SJ, Chapman D., Analytical Investigation and Monitoring of End-zone Reinforcement of the Alaskan Way Viaduct Super Girders, Jouranl PCI, 59(2), 2014
10. Gergely P, Sozen MA., Design of Anchorage-zone Reinforcement in Prestressed Concrete Beams, University of Illinois; 1967.
11. Castrodale R, Lui A, White C, editors., Simplified Analysis of Web Splitting in Pretensioned Concrete Girders, Proceedings PCI/FHWA/NCBC Concrete Bridge Conference; 2002.

12. Tuan CY, Yehia SA, Jongpitaksseel N, Tadros MK., End Zone Reinforcement for Pretensioned Concrete Girders, Journal PC, 49(3):68, 2004

13. Ayoub A, Filippou FC., Finite-element Model for Pretensioned Prestressed Concrete Girders, Journal of Structural Engineering, ASCE 136(4):401-9, 2009

14. Bureau of Structures Wisconsin DOT, "Highway Structures - WisDOT LRFD, Standard Detail Drawings," 2016.

15. Tokyo Sokki Kenkyujo Co, Ltd. Products: Strain Gauge. Available at : http://www.tml.jp/e/product/productindex/strain_gauge.html. 2016.

16. Bureau of Structures Wisconsin DOT, Highway Structures - WisDOT LRFD, Standard Detail Drawings. Wisconsin Department of Transportation. 2016.

17. Toupin R.., Saint-Venant and a Mateter of Principle, Transactions of The New York Academy of Sciences. 28(2 Series II):221-32, 1965

18. Allam SM, Shoukry MS, Rashad GE, Hassan AS., Evaluation of Tension Stiffening Effect on the Crack Width Calculation of Flexural RC Members, Alexandria Engineering Journal, 52(2):163-73, 2013

19. Abaqus 6.12 Analysis User's Manual, Volume III: Materials. 2012.

20. Lubliner J, Oliver J, Oller S, Onate E., A Plastic-damage Model for Concrete, International Journal of Solids and Structures. 25(3):299-326, 1989

21. Lee J, Fenves GL., Plastic-damage Model for Cyclic Loading of Concrete Structures, Journal of Engineering Mechanics, ASCE, 124(8):892-900, 1998

22. Hillerborg A, Modéer M, Petersson P-E., Analysis of Crack Formation and Crack Growth in Concrete by Means of Fracture Mechanics and Finite Elements, Cement and Concrete Research, 6(6):773-81, 1976

23. Lubliner J., Plasticity Theory, Courier Corporation, 2008

24. H. Bae, M. Oliva, L. Bank, "Obtaining Optimal Performance with Reinforcement-free Concrete Highway Bridge Decks," Engineering Structures, Elsevier, V32, 2300-2309, 2010

25. Briere V, Harries KA, Kasan J, Hager C., Dilation Behavior of Seven-wire Prestressing Strand–the Hoyer Effect, Construction and Building Materials, 40:650-8, 2013

26. Mirza J, Tawfik M., End Cracking in Prestressed Members During Detensioning, Journal PCI, 23(2):66-77, 1978

27. Geokon. Concrete Embedment Strain Gages, 4200 Series. , 2016Available from:<http://www.geokon.com/products/datasheets/4200.pdf>.

9. APPENDIX

CHAPTER 4 Appendix:

- Compression Behavior for bonded 72W girder:

Compression by FIB 2010 (Inelastic range) and AASHTO (elastic range)

INPUT: Specified design strength or cylinder strength, f'_c =		**7808**	**psi**
Characteristic strength, cylinder, f_{ck} =		45.8	MPa
Closest concrete grade corresponding to f_{ck}	**C**	**50**	
Error between fck and concrete grade, % =		-8.3	

		US Units		SI Units	
Mean value of Compressive Strength, fck + Δf,	f_{cm} =	7808	psi	58.0	MPa
Characteristic strength (cylinder) or Concrete grade number,	f_{ck} =	7252	psi	50	MPa
Strain at maximum compressive stress, Table 5.1.8,	ε_{cl}=	-0.0026		-0.0026	
$\eta = \varepsilon_c / \varepsilon_{cl}$,	η =	variable		variable	
Plasticity number, E_{ci}/E_{cl}, or Table 5.1.8,	k =	1.73		1.73	

Tangent Modulus, $E_{co}\alpha_E[f_{cm}/10]^{1/3}$, or Table 5.1.8,	E_{ci} =	5602676	psi	38629	MPa
Constant,	E_{co} =	3118311	psi	21500	MPa
Aggregate type factor, (1 for quartzite aggregates),	α_E	1		1	
Secant Modulus from origin to the peak, fcm/εc1, or Table 5.1.8	E_{cl} =	3235457.4	psi	22308	MPa
Ultimate strain,	ε_{clim} =	-3.40E-03		-3.40E-03	
Δf, constant	Δf =	1160	psi	8	MPa
Strain,	ε_c =	variable		variable	
Stress, -fcm $[(k\eta - \eta^2)/(1+(k-2)\eta)]$ for $\varepsilon_c < \varepsilon_{clim}$	σ_c =	variable		variable	

Table 0-1. Compression Behavior for bonded 72W girder.

Input for Abaqus:

ABAQUS INPUT

1. Assume concrete behaves elastic up to 40% of ultimate strength

Input: use linear Ec (AASHTO) up to σc = 3123.2 psi and ε = -5.86E-04

Abaqus input:
Linear E = 5239994 psi

2. Assume concrete behaves inelastic above the strain corresponding to 40% of ultimate strength

Input: εinelastic = εtotal - εelastic for ε > -5.86E-04

εctotal	**σ_c (psi)(yield stress)**	**$\varepsilon_{cinelastic}$**	
0.00E+00	0		Linear -Elastic Range based on AASHTO E
1.17E-04	614		
2.34E-04	1229		
3.52E-04	1843		
4.69E-04	2457		
5.86E-04	3072	0.0000	

7.03E-04	3586	0.0001	Nonlinear - Inelastic Range based on FIB Model
8.21E-04	4108	0.0002	
9.38E-04	4606	0.0004	
1.06E-03	5079	0.0005	
1.17E-03	5527	0.0006	
1.29E-03	5947	0.0007	
1.41E-03	6340	0.0008	
1.52E-03	6703	0.0009	
1.64E-03	7035	0.0011	
1.76E-03	7336	0.0012	
1.88E-03	7603	0.0013	
1.99E-03	7835	0.0014	
2.11E-03	8031	0.0015	
2.23E-03	8188	0.0016	
2.34E-03	8305	0.0018	
2.46E-03	8380	0.0019	
2.58E-03	8411	0.0020	
2.70E-03	8396	0.0021	
2.81E-03	8332	0.0022	
2.93E-03	8217	0.0023	
3.05E-03	8047	0.0025	
3.17E-03	7821	0.0026	
3.28E-03	7535	0.0027	
3.40E-03	7185	0.0028	

Table 0-2. Input for compression behavior for bonded 72W girder.

- Tensile Behavior of the same girder:

Tension by FIB 2010 (inelastic range) and AASHTO (elastic range)

Direct Tensile Strength, AASHTO, C.5.4.2.7 =	**643**	**psi =**	**4.43**	**Mpa**
Uniaxial Tensile Strength, FIB 2010, Equation 5.1.3 =	589	psi =	4.1	Mpa
$f_{ct\ AASHTO}/f_{fct\ FIB\ 2010}$ =	1.09		1.09	

	US Units		SI Units	
Mean tensile strength of concrete, fctm =	643	psi	4.43	Mpa

Tangent Modulus, $E_{co}\alpha_E[f_{cm}/10]^{1/3}$, or Table 5.1.8,	E_{ci} =	5602676	psi	38629	MPa
0.9 x mean tensile strength of concrete,	*0.9*fctm* =	578	psi	3.99	Mpa
0.15 x mean tensile strength of concrete,	*0.20*fctm* =	129	psi	0.89	Mpa
Crack opening for σck = $0.20*f_{ctm}$, G_F/f_{ctm},	*wl=*	0.00132912	in	0.034	mm
Crack opening for σ_{ct} = 0, $5G_F/f_{ctm}$,	*wc =*	0.00664558	in	0.169	mm
Mean value of Compressive Strength,	f_{cm} =	7808	psi	53.8	MPa
Fracture energy, $73f_{cm}^{0.18}$,	*GF =*	0.854	Lbf in/in^2	150	Nm/m^2
Tensile strain,	*εct =*	variable	-	variable	-
Crack opening,	*w =*	variable	in	variable	mm
Tensile stress for w<wl, fctm(1-0.8w/wl),	*σct =*	variable	psi	variable	MPa
Tensile stress for wl<w<wim, fctm(0.25-0.05w/wl),	*σct =*	variable	psi	variable	MPa

Table 0-3. Tensile behavior for bonded 72W girder.

Abaqus input:

1. Assume concrete behaves elastic under ultimate tensile strength
Input: use linear Ec
(AASHTO) up to σ = 643 psi and

Abaqus input: Linear E =	**5239994**	**psi**

2. Assume tension softening beyond the ultimate tensile strenght

Input: displacement = w

σc (psi)(yield stress)	**Displacement (in)**
643	0.000000
591	0.000133
540	0.000266
488	0.000399
437	0.000532
386	0.000665
334	0.000797
283	0.000930

231	0.001063
180	0.001196
129	0.001329
116	0.001861
103	0.002392
90	0.002924
77	0.003456
64	0.003987
51	0.004519
39	0.005051
26	0.005582
13	0.006114

Table 0-4. Input for tensile behavior for bonded 72W girder.

CHAPTER 8 Appendix:

Different Debonding work done for 54W and 72W girders.

		72W Girder		54W Girders	
Number of Strands	Strand debonding percentage -%	Max. tension strain in web region - με	Max. tension strain in Y-crack region- με	Max. tension strain in web region - με	Max. tension strain in Y-crack region- με
48	38	280	215	-	-
48	42	190	177	-	-
48	42	232	153	-	-
48	46	165	163	-	-
48	50	210	155	-	-
48	50	134	151	-	-
46	43	173	171	-	-
46	43	213	154	-	-
46	48	236	128	-	-
46	48	151	157	-	-
44	41	173	155	-	-
44	41	214	154	-	-

44	45	150	142	-	-
44	50	225	147	-	-
42	38	176	134	219	125
42	43	156	100	145	125
40	35	-	-	135	324
40	40	154	123	128	130
38	37	-	-	140	169
38	43	132	130	119	135
36	33	161	150	163	147
36	39	133	142	131	140
34	29	156	143	153	144
34	29	-	-	153	144
34	35	134	135	125	136
32	31	142	102	131	94
32	25	-	-	182	119
32	31	-	-	129	123
32	25	-	-	180	129
32	25	-	-	179	123
32	25	-	-	177	152
32	25	166	108	182	99
32	31	-	-	145	94
30	33	133	104	133	90
30	26	-	-	176	115
30	33	-	-	133	119
30	26	-	-	176	125
30	26	-	-	176	118
30	26	-	-	175	149
30	26	167	108	178	95
30	33	-	-	144	91
28	29	140	135	142	121
28	36	113	129	108	115
26	23	138	141	149	140
26	31	113	131	117	128

Table 0-5. Debonding patterns tried on different girders.

The debonding patterns are described by following half picture of 72W girder with 48 strands. The draped strands were not shown in the picture as it belongs to the end of the

girder but there are 8 draped and 40 straight strands in this girder. The letter “S” stands for strands in the girder and first and second numbers following that letter are the row and column axis in Figure 0-1. After these numbers, another numbers were written right after dash. These numbers are for the length of debonding shield at strands. As the number of strand decrease in the girder, NS (No Strand) letter was used to account for removed strand in the picture and the number after these letters again represent the axis number. Finally, the number of draped strands reduces to 6 after girders with 30 strands and for that ODSR (one draped strand was reduced- consider half of girders) was used.

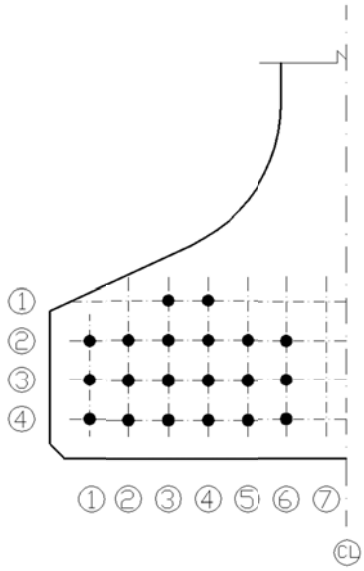

Figure 0-1. Half of 72W girder with 48 strands.

Number of Strands	Strand Debonding Percentage-%	Debonding Description
48	38	(S13-9ft),(S22-9ft),(S23-9ft),(S25-9ft),(S32-6ft),(S33-6ft),(S35-6ft),(S42-3ft),(S44-3ft)
48	42	(S13-9ft),(S22-9ft),(S23-9ft),(S25-9ft),(S32-6ft),(S33-6ft),(S35-6ft),(S42-3ft),(S43-3ft),(S45-3ft)
48	42	(S13-9ft),(S22-9ft),(S23-9ft),(S25-9ft),(S32-6ft),(S33-6ft),(S35-6ft),(S42-

		3ft),(S43-3ft),(S45-3ft),(S47-0ft)
48	46	(S13-9ft),(S22-9ft),(S23-9ft),(S24-9ft),(S25-9ft),(S32-6ft),(S33-6ft),(S35-6ft),(S42-3ft),(S43-3ft),(S45-3ft)
48	50	(S13-9ft),(S22-9ft),(S23-9ft),(S25-9ft),(S26-9ft),(S32-6ft),(S33-6ft),(S35-6ft),(S36-6ft),(S42-3ft),(S43-3ft),(S45-3ft),(S17,S27,S37,S47-0ft)
48	50	(S13-9ft),(S22-9ft),(S23-9ft),(S24-9ft),(S25-9ft),(S32-6ft),(S33-6ft),(S34-9ft),(S35-6ft),(S42-3ft),(S43-3ft),(S45-3ft)
46	43	(S13-9ft),(S22-9ft),(S23-9ft),(S25-9ft),(S32-6ft),(S33-6ft),(S35-6ft),(S42-3ft),(S43-3ft),(S45-3ft), (NS14)
46	43	(S13-9ft),(S22-9ft),(S23-9ft),(S25-9ft),(S32-6ft),(S33-6ft),(S35-6ft),(S42-3ft),(S43-3ft),(S45-3ft),(S47-0ft),(NS14)
46	48	(S13-9ft),(S22-9ft),(S23-9ft),(S25-9ft),(S26-9ft),(S32-6ft),(S33-6ft),(S35-6ft),(S36-6ft),(S42-3ft),(S43-3ft),(S45-3ft),(S17,S27,S37,S47-0ft),(NS14)
46	48	(S13-9ft),(S22-9ft),(S23-9ft),(S25-9ft),(S26-9ft),(S32-6ft),(S33-6ft),(S35-6ft),(S42-3ft),(S43-3ft),(S45-3ft),(NS14)
44	41	(S22-9ft),(S23-9ft),(S25-9ft),(S32-6ft),(S33-6ft),(S35-6ft),(S42-3ft),(S43-3ft),(S45-3ft), (NS13,NS14)
44	41	(S22-9ft),(S23-9ft),(S25-9ft),(S32-6ft),(S33-6ft),(S35-6ft),(S42-3ft),(S43-3ft),(S45-3ft),(S47-0ft),(NS13,NS14)
44	45	(S22-9ft),(S23-9ft),(S25-9ft),(S26-9ft),(S32-6ft),(S33-6ft),(S35-6ft),(S42-3ft),(S43-3ft),(S45-3ft),(NS13,NS14)
44	50	(S22-9ft),(S23-9ft),(S25-9ft),(S26-9ft),(S32-6ft),(S33-6ft),(S35-6ft),(S36-6ft),(S42-3ft),(S43-3ft),(S45-3ft),(S17,S27,S37,S47-0ft),(NS13,NS14)
42	38	(S23-9ft),(S25-9ft),(S32-6ft),(S33-6ft),(S35-6ft),(S42-3ft),(S43-3ft),(S45-3ft), (NS13,NS14,NS21)
42	43	(S22-9ft),(S23-9ft),(S25-9ft),(S32-6ft),(S33-6ft),(S35-6ft),(S42-3ft),(S43-3ft),(S45-3ft), (NS13,NS14,NS21)
40	35	(S23-13.5ft),(S32-9ft),(S34-9ft),(S36-9ft),(S42-4.5ft),(S44-4.5ft),(S46-4.5ft), (NS13,NS14,NS21,NS26)
40	40	(S22-9ft),(S24-9ft),(S32-6ft),(S33-6ft),(S35-6ft),(S42-3ft),(S43-3ft),(S45-3ft), (NS13,NS14,NS21,NS26)
38	37	(S23-9ft),(S32-6ft),(S33-6ft),(S35-6ft),(S42-3ft),(S43-3ft),(S45-3ft), (NS13,NS14,NS21,NS25,NS26)
38	43	(S22-9ft),(S24-9ft),(S32-6ft),(S33-6ft),(S35-6ft),(S42-3ft),(S43-3ft),(S45-3ft), (NS13,NS14,NS21,NS25,NS26)
36	33	(S23-9ft),(S32-6ft),(S34-6ft),(S42-3ft),(S43-3ft),(S45-3ft), (NS13,NS14,NS21,NS24,NS25,NS26)
36	39	(S23-9ft),(S32-6ft),(S33-6ft),(S35-6ft),(S42-3ft),(S43-3ft),(S45-3ft), (NS13,NS14,NS21,NS24,NS25,NS26)
34	29	(S32-6ft),(S34-6ft),(S42-3ft),(S43-3ft),(S45-3ft), (NS13,NS14,NS21,NS23,NS24,NS25,NS26)
34	29	(S32-6ft),(S34-6ft),(S42-3ft),(S43-3ft),(S45-3ft), (NS13,NS14,NS21,NS23,NS24,NS25,NS26)
34	35	(S32-6ft),(S33-6ft),(S35-6ft),(S42-3ft),(S43-3ft),(S45-3ft), (NS13,NS14,NS21,NS23,NS24,NS25,NS26)
32	31	(S32-6ft),(S34-6ft),(S42-3ft),(S43-3ft),(S45-3ft), (NS13,NS14,NS21,NS22,NS23,NS24,NS25,NS26)
32	25	(S32-6ft),(S34-6ft),(S43-3ft),(S45-3ft), (NS13,NS14,NS21,NS22,NS23,NS24,NS25,NS26)
32	31	(S33-6ft),(S35-6ft),(S42-3ft),(S43-3ft),(S45-3ft), (NS13,NS14,NS21,NS22,NS23,NS24,NS25,NS26)
32	25	(S33-6ft),(S35-6ft),(S42-3ft),(S44-3ft),

		(NS13,NS14,NS21,NS22,NS23,NS24,NS25,NS26)
32	25	(S33-6ft),(S34-6ft),(S42-3ft),(S45-3ft), (NS13,NS14,NS21,NS22,NS23,NS24,NS25,NS26)
32	25	(S33-6ft),(S35-6ft),(S43-3ft),(S45-3ft), (NS13,NS14,NS21,NS22,NS23,NS24,NS25,NS26)
32	25	(S32-6ft),(S34-6ft),(S42-3ft),(S44-3ft), (NS13,NS14,NS21,NS22,NS23,NS24,NS25,NS26)
32	31	(S32-6ft),(S33-6ft),(S35-6ft),(S42-3ft),(S43-3ft), (NS13,NS14,NS21,NS22,NS23,NS24,NS25,NS26)
30	33	(S32-6ft),(S34-6ft),(S42-3ft),(S43-3ft),(S45-3ft), (NS13,NS14,NS21,NS22,NS23,NS24,NS25,NS26)& ONDS
30	26	(S32-6ft),(S34-6ft),(S43-3ft),(S45-3ft), (NS13,NS14,NS21,NS22,NS23,NS24,NS25,NS26) & ODSR
30	33	(S33-6ft),(S35-6ft),(S42-3ft),(S43-3ft),(S45-3ft), (NS13,NS14,NS21,NS22,NS23,NS24,NS25,NS26) & ODSR
30	26	(S33-6ft),(S35-6ft),(S42-3ft),(S44-3ft), (NS13,NS14,NS21,NS22,NS23,NS24,NS25,NS26) & ODSR
30	26	(S33-6ft),(S34-6ft),(S42-3ft),(S45-3ft), (NS13,NS14,NS21,NS22,NS23,NS24,NS25,NS26) & ODSR
30	26	(S33-6ft),(S35-6ft),(S43-3ft),(S45-3ft), (NS13,NS14,NS21,NS22,NS23,NS24,NS25,NS26) & ODSR
30	26	(S32-6ft),(S34-6ft),(S42-3ft),(S44-3ft), (NS13,NS14,NS21,NS22,NS23,NS24,NS25,NS26) & ODSR
30	33	(S32-6ft),(S33-6ft),(S35-6ft),(S42-3ft),(S43-3ft), (NS13,NS14,NS21,NS22,NS23,NS24,NS25,NS26) & ODSR
28	29	(S32-6ft),(S34-6ft),(S42-3ft),(S44-3ft), (NS13,NS14,NS21,NS22,NS23,NS24,NS25,NS26,NS36) & ODSR
28	36	(S32-6ft),(S34-6ft),(S42-3ft),(S43-3ft),(S45-3ft), (NS13,NS14,NS21,NS22,NS23,NS24,NS25,NS26,NS36)& ODSR
26	23	(S32-6ft),(S42-3ft),(S44-3ft), (NS13,NS14,NS21,NS22,NS23,NS24,NS25,NS26,NS35,NS36) & ODSR
26	31	(S32-6ft),(S34-6ft),(S42-3ft),(S44-3ft), (NS13,NS14,NS21,NS22,NS23,NS24,NS25,NS26,NS35,NS36) & ODSR

Table 0-6. Description of debonding patterns tried on different girders.